MODIFICATIONS OF POLYURETHANE SHAPE MEMORY POLYMERS FOR MEDICAL DEVICES

A Dissertation

by

GRACE KIELY FLETCHER

Submitted to the Graduate and Professional School of
Texas A&M University
in partial fulfillment of the requirements for the degree of

DOCTOR OF PHILOSOPHY

Chair of Committee,	Duncan Maitland
Committee Members,	Daniel Alge
	Balakrishna Haridas
	David Staack
Head of Department,	Michael McShane

December 2021

Major Subject: Biomedical Engineering

ABSTRACT

Shape memory polymers (SMPs) are materials with the ability to undergo geometric change in response to a stimulus, also known as the shape memory effect. This shape memory behavior enables minimally-invasive delivery of medical devices, making SMPs of interest to biomedical researchers. Our group has extensively studied thermoset polyurethane SMP foams and modifications thereof to improve device performance. These gas-blown, low-density foams demonstrate high volumetric recovery and rapid hemostasis, making them particularly desirable for embolic applications. Another SMP thermoplastic polyurethane (TPU) material was previously developed by Hearon et al. This SMP system is currently underutilized, but it is highly tunable and processable, enabling control over polymer properties and architecture.

This research provides a foundation for expanded future use of both polyurethane SMP systems (thermoset and thermoplastic) by addressing their major limitations for biomedical applications. There is a lack of inherent X-ray and MRI visibility with these polymeric materials, which can hinder device delivery and monitoring; therefore, a major goal was to modify the thermoset systems to achieve adequate visualization on X-ray and MRI modalities. Similarly, the TPU material system was modified to improve the X-ray visibility on molded parts. Drug delivery from a SMP matrix was explored for the intended use in breast cancer recurrence after tumor resection. Antimicrobial foams with modified antimicrobial triols and direct incorporation of antimicrobial agents were explored for use in hemostatic devices. Finally, *in vivo* use of the thermoset material is limited by its susceptibility to oxidation. Thus, the last goal was to improve the biostability of SMP thermoset foams.

DEDICATION

My dissertation is dedicated to my uncle Page Fletcher, whose untimely death from a ruptured aneurysm in Spring 2015 when I was deciding where to attend graduate school led me to the Biomedical Device Laboratory.

ACKNOWLEDGEMENTS

There are so many people who helped get me to this point that I am almost certain I will leave someone out (although I hope I do not). It is fitting that I thank my early mentors first, whose support and early investment led me to graduate school. Dr. Peppas is my "academic grandfather" and is responsible for introducing me to the wide world of research as an undergraduate at UT. Kim and Bill have been wonderful mentors, scientific role models, and always fit me into their exceptionally busy schedules.

My family has been a wonderful support for me and I truly would not have made it through my Ph.D. without them. My parents have been there every step of the way to cheer me on, cheer me up, or cheers to finally being done. My brothers and friends in Houston and Austin have lifted me up when I really needed it and provided extracurricular activities that kept me sane and gave me fun excuses to get out of College Station. My BCS support crew of Bianca, Andrew, and (of course) Toby have been there for me every time I needed any support or time to decompress. Bianca, thank you for embracing my love of bad TV and Lindt chocolates and for letting me practice my presentations for you. Andrew, thank you for supporting me through a Ph.D. that lasted much longer than I thought it would when we first started dating – I can't wait to marry you and see what our future holds!

My BDL colleagues that I had the pleasure of working with throughout my years have been instrumental in support and development into a scientist. Mary Beth, thank

you for patiently mentoring me through the beginning of my Ph.D. and being a wonderful role model both personally and professionally. Marziya, thank you for teaching me the art of foaming and helping me on my journey of become more self-assured. Landon, thank you for being my personal Ph.D. cheerleader who wouldn't let me doubt myself and seemed to know exactly when I needed a "hang in there" text. Scott, I really lucked out that you started in the BDL the same time as me – thanks for all the technical help (both with my research and Fantasy Football) and for hanging until 1pm. I can't wait to turn one of our crazy ideas into a company someday! Maddy, collaborating with you and then becoming real friends was one of the highlights of graduate school for me and I actually wouldn't have survived without our Writing Wednesdays. Every member of BDL (Marziya, Landon, Tony, Todd, Mark, Rachael, Andrew, Adam, Scott, Nick, Lance, Lindy, Sam, Tyler, and Achu) that I have worked with has been wonderful and I can't wait to follow your great careers. I have also appreciated all of the help I received throughout the years from undergraduate assistants: Garrett, Alexa, Ashley, Kedar, Kendal, and Katarina.

The BwoMEN group and the professors who supported its inception – Dr. Mary McDougall, Dr. Kristen Maitland, Dr. Melissa Grunlan, and Dr. Elizabeth Cosgriff-Hernandez, had a profound effect on my graduate career. I have valued the camaraderie and the encouragement of that group and I hope it has been valuable to others as well.

The BMEN staff members helped with all of the behind the scenes. Maria Lyons, Ashlyn Montgomery, Barb Slusher, Amanda Myatt, Jacob Clough, and Stormy

Kretschmar have all been assets to my graduate experience. I also appreciate the leadership of Dr. Mike McShane and his vision for the department.

All of my committee members have provided incredible guidance and support through my graduate school experience. Dr. Staack always checked in on the status of my publications when we met, Dr. Haridas taught me to think like an entrepreneur and asked the practical questions, and Dr. Alge played a large role in my decision to come to A&M and helped me become a better polymer chemist. Their input has been invaluable to my work and personal development.

Finally, I would like to thank my Ph.D. advisor, Duncan Maitland, whose strength (after many seasons as a Browns fan) is sticking with you through the worst and the best. I am extremely fortunate to have had you as my advisor these past 6 years. Thank you for giving me a non-traditional Ph.D. path and encouraging me to believe in myself, find my strengths, and get experiences outside the lab. I truly would not have finished without your encouragement and support. Thank you for caring about us as people, catering to us as individuals, and inspiring us to think in new ways.

CONTRIBUTORS AND FUNDING SOURCES

Contributors

This work was supervised by a dissertation committee consisting of Professor Duncan Maitland [advisor] of the Department of Biomedical Engineering and Professors Balakrishna Haridas and Daniel Alge, also of the Department of Biomedical Engineering and Professor David Staack of the Department of Mechanical Engineering.

I consulted with Dr. Landon Nash on development of synthetic protocol for both material systems in Chapter II. Data collection for Chapter II was conducted in part by my undergraduate assistant, Ana Katarina Sweatt. Lance Graul assisted with preparing polymers for MR imaging and MR images were obtained by Matt Wilcox. Drs. Steven Wright and Mary McDougall advised on parameters for MR imaging. X-Ray images were taken by Tyler Touchet. All authors provided edits on the manuscript, which was published in 2020. ICP-MS data acquisition and analysis was conducted by Dr. Bryan Tomlin from the Elemental Analysis Laboratory at Texas A&M University.

Chapter III was conducted with assistance from Tyler Touchet and Achu Byju. Tyler Touchet captured the X-ray images of the TPU compositions and assisted with mechanical testing protocol development. Sam Briggs and Dr. David Truong at the Soft Matter Facility at Texas A&M University helped with GPC sample preparation and runs. Dr. Balakrishna Haridas and Achu Byju provided valuable insights on the mechanical behavior of these materials.

Data collection for Chapter IV was completed in collaboration with Shreedevi Arun Kumar. She completed all cellular and drug delivery studies. Dr. Jonathan Bova

and Kelsey Johnson from the Comparative Medicine program assisted with the protocol for our planned animal study (IACUC 2020-0295).

The National Center for Electron Beam Research Facility at Texas A&M performed sterilization on materials in Chapters III and IV. Sara Parsons was the dosimetrist who ran all samples and provided reports.

The antimicrobial foams in Chapter V were initially conceived by Dr. Mary Beth Monroe. Data collection for Chapter V was completed with the assistance of Calla Boyer, Dr. Mary Beth Monroe, Alexa Easley, and Ashley Rook. Drs. Marziya Hasan and Andrew Weems consulted on method development for degradation study.

Biorender.com was used for figure generation throughout my dissertation and is cited in the caption of those figures.

Funding

Graduate study was supported in part by the Texas A&M University College of Engineering Doctoral Fellowship (2015-2016). The department of Biomedical Engineering also awarded an Enrichment Fellowship in 2015.

NOMENCLATURE

AA	Allyl alcohol
AM	Antimicrobial SMP
ATIPA	5-amino-2,4,6-triiodoisphthalic acid
BAPO	Bis-acyl phosphine oxide
E-beam	Electron beam
CA	Cinnamic acid
CFU	Colony forming unit
Dox	Doxorubicin
DI H_2O	Deionized water
DMPD	Dimethyl pentanediol
DSC	Differential scanning calorimetry
G	Glycerol (chemical) OR Gauge (needle)
GBCA	Gadolinium-based contrast agent
Gd	Gadolinium
GPA	Gadopentetic acid
GPC	Gas permeation chromatography
HCA	Modified cinnamic acid triol
HD	Hexanediol
HDI	Hexamethylene diisocyanate
HDPE	High density polyethylene

HIPE	High internal phase emulsion
HLB	Hydrophile-lipophile balance
HPED	N,N,N',N'-Tetrakis(2-Hydroxypropyl)ethylenediamine
ICP-MS	Inductively coupled plasma mass spectroscopy
IPA	Isopropyl alcohol
Ir	Irradium
MAM	Modified antimicrobial SMP
MPD	Methyl propanediol
MRI	Magnetic resonance imaging
NCO	Isocyanate
OH	Hydroxyl
PA	Phenolic acid
PD	Polyvinyl alcohol/doxorubicin mixture OR Propanediol
PETMP	Pentaerythritol tetrakis(3-mercaptopropionate)
PolyHIPE	Polymerized high internal phase emulsion
Pt	Platinum
PU	Polyurethane
PVA	Polyvinyl alcohol
SEM	Scanning electron microscopy
SME	Shape memory effect
SMP	Shape memory polymer
TE	Echo time (in MR imaging)

TEA	Triethanolamine
THF	Tetrahydrofuran
TIP	Triiodophenol
T_g	Glass transition temperature
TMHDI	Trimethyl hexamethylene diisocyanate
TMPAE	Trimethylol propane allyl ether
TPU	Thermoplastic polyurethane
T_{trans}	Transition temperature
UV	Ultraviolet
µm	Micron
W	Tungsten

TABLE OF CONTENTS

Page

LIST OF FIGURES

Page

LIST OF TABLES

Page

CHAPTER I

INTRODUCTION

Shape memory polymers (SMPs) are materials with the ability to undergo geometric change in response to a stimulus, also known as the shape memory effect. This shape memory behavior enables minimally-invasive delivery of medical devices, making SMPs of interest to biomedical researchers. Polyurethanes (PUs) are commonly used in biomedical applications due to material performance, biocompatibility, and capacity for modification. Our group has extensively studied thermoset polyurethane SMP foams and modifications thereof to improve device performance.[1-10] These gas-blown, low-density foams demonstrate high volumetric recovery and rapid hemostasis, making them particularly desirable for embolic applications.[11-13] However, this thermoset material platform has limitations in device geometries, feature precision, and process repeatability. Thermoplastic materials are widely used in industry and are amenable to a variety of processing techniques (extrusion, injection molding, additive manufacturing, etc.) that can enable precise and complex geometries. A SMP thermoplastic polyurethane (TPU) material was previously developed by Hearon et al.[14-16] This SMP system is currently underutilized, but it is highly tunable and processable, enabling control over polymer properties and architecture.

This work will provide a foundation for expanded future use of both PU systems (thermoset and thermoplastic) by addressing some of their major limitations for biomedical applications. There is a lack of inherent X-ray and magnetic resonance imaging (MRI) visibility with these polymeric materials, which can hinder device delivery

and monitoring; therefore, one goal is to modify the thermoset system to achieve adequate visualization on multiple medical imaging modalities. Similarly, the TPU system will be modified for X-ray visibility. Adding functionality such as drug-eluting and antimicrobial behavior expands the utility of the SMP foam platform. *In vivo* use of the thermoset material is limited by its susceptibility to oxidation. Thus, another goal is to improve the biostability of SMP thermoset foams.

This work is significant because it improves existing materials and methods and will therefore provide a foundation for expanded future use of both polymer systems. The modifications to the thermoset and thermoplastic SMP systems developed in the Biomedical Device Laboratory enable enhanced biostability, processability, and X-ray visibility of these materials to improve and expand their potential for clinical translation (Figure I-1).

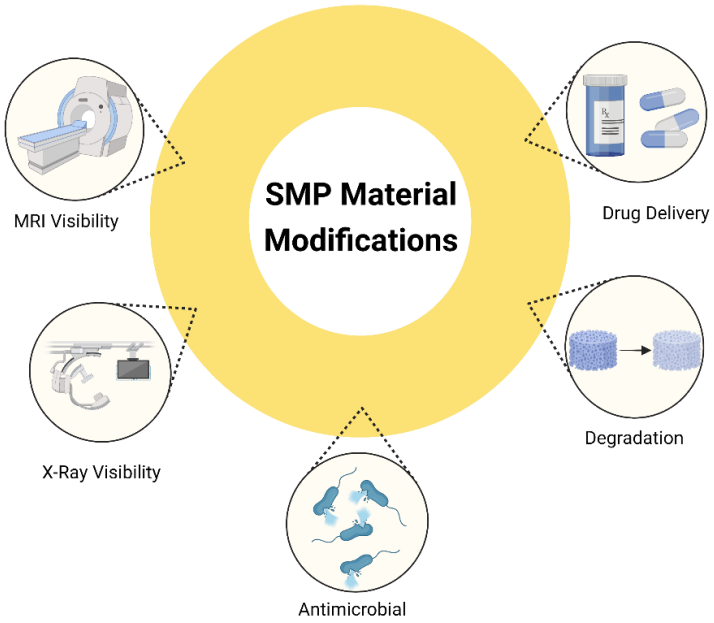

Figure I-1. Summary figure of shape memory polymer material modifications to improve material utility in medical devices that are explored in this dissertation. (*Created with BioRender.com*)

Background and Motivation

Shape Memory Polymers in Biomedical Applications

Shape memory polymers (SMPs) are a class of polymeric materials that undergo shape change in response to some external stimulus. Thermally-actuated SMPs are the most common class of SMP materials, wherein the shape change relies on a characteristic transition temperature (T_{trans}) that allows for movement of the switching segments.[17] The shape memory effect is utilized when a material is brought above T_{trans} to plasticize the polymer, allowing for chain movement, where it can be deformed into a secondary geometry. As it cools in this secondary geometry, the chains align to obtain shape fixity,

and they remain in that state until exposed to temperatures above the T_{trans} again, upon which they return to their primary shape. The shape memory effect is shown on a radially crimped SMP foam scaffold in Figure I-2. This is an entropy-driven process because the polymer chains want to recover to an equilibrium state with random conformation. SMPs have been investigated for use in a variety of medical devices including bone scaffolds, self-closing sutures, and neural probes. [11, 18-21]

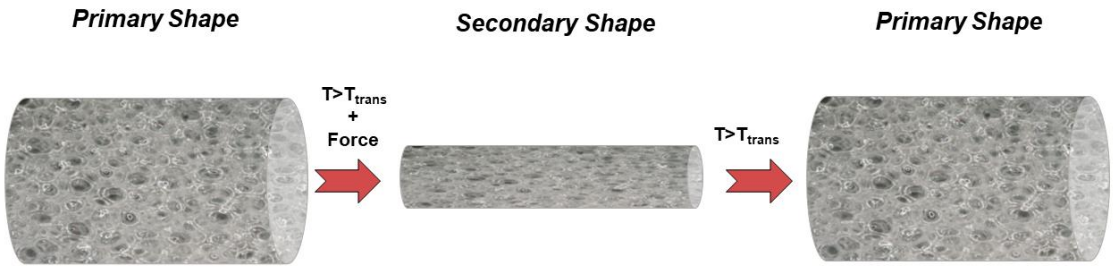

Figure I-2. The shape memory effect shown with an example of a radially crimped SMP foam that is thermally actuated. When the temperature is raised above the transition temperature, it can be deformed into a secondary geometry. It will return to the primary shape when heated above the transition temperature again.

Polymers fall into two basic categories: thermosets and thermoplastics. Thermosets are covalently crosslinked networks that maintain a 3-dimensional shape without melting, whereas thermoplastics are linear chains that can be dissolved or melted into intricate geometries. There are benefits to each system, and material choice depends on the application or processing conditions. For example, thermoset materials are useful in high temperature applications because they cannot be melted; thermoplastic materials are beneficial in applications requiring feature precision.

Thermoset SMP Foams

The primary polymer system that our lab utilizes for device fabrication is a thermoset SMP polyurethane (PU) foam synthesized from aliphatic isocyanates and polyols originally developed by Wilson et al. These ultra-low-density foams with properties desired for embolic applications were further optimized by Singhal et al.[1] The polymers' interconnected porous morphology and large surface area encourage clot organization. Polyurethanes are commonly used in medical device fabrication due to established biocompatibility. Use of this SMP material platform in medical applications is limited by its oxidative degradation behavior and inconsistencies in the foaming process. Furthermore, the SMP foams have potential as a conformal wound dressing and a drug eluting matrix. Therefore, adding these functionalities to the SMP foams will expand the utility of the porous SMP scaffolds in medical applications.

Thermoplastic Polyurethane (TPU)

While improving the functionalities of the thermoset SMP system is valuable, its application range is still limited by its processability. TPUs are widely used in industry due to their tunable, elastomeric behavior. It is possible for TPU resins to achieve a wide range of material performance between hard thermoplastics and flexible elastomers. TPUs are melt-processable and can therefore be used with traditional melt-processing techniques, like injection molding, as well as newer methods, such as additive manufacturing. Their versatility stems from the ability of TPUs to be produced with a range of mechanical properties, controlled primarily by the ratio of hard and soft segments.

Other polymeric properties, such as molecular weight, crystallinity, and hydrophobicity, can also alter thermoplastic processability. Previously Hearon et al. developed a highly tunable and processable thermoplastic polyurethane (TPU) material platform,[14-16] and despite its many benefits, it is currently underutilized in our lab. Due to its unique architecture, this material has advanced processing capabilities as a thermoplastic and can be crosslinked into a thermoset SMP post-processing. Thermoset materials have superior shape fixity and recovery in shape memory, so this post-process crosslinking enables a system where the benefits of each material system are realized. Synthesis and characterization of tunable TPU scaffolds in consideration of processing requirements using this previously developed system will enhance their potential use in biomedical applications.

Another benefit of this material system is its versatility of crosslinking. This material has been used for crosslinking via thiol-ene click chemistry[14] and electron beam (e-beam) irradiation.[15-16] Figure I-3 shows the two methods of crosslinking utilized with the TPU material system. As previously discussed, the pendant C=C groups control crosslink density in both crosslinking schemes. The thiol-ene crosslinking provides a method for rapid crosslinking that is unaffected by the presence of water, which is useful in polyHIPE fabrication due to concerns about emulsion stability. However, E-beam crosslinking offers a greener process that can be used in industrial scale operations.

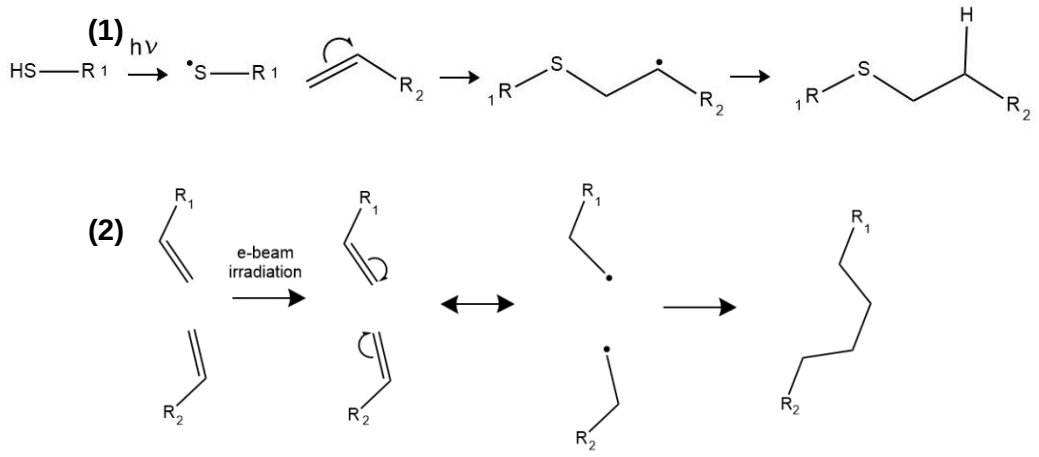

Figure I-3. Schematic of potential crosslinking mechanisms via (1) thiol-ene "click" chemistry hydrothiolation or (2) e-beam irradiation radical formation.

"Click chemistry" is terminology originally defined by Sharpless and colleagues used to describe a set of reactions that are "*modular, wide in scope, give very high yields, generate only inoffensive byproducts…, and… stereospecific.*"[22] The thiol-ene reaction in particular has been of interest across scientific disciplines because it is simple, yet versatile.[23] Multiple groups have used thiol-ene reactions to synthesize materials proposed for biomedical applications ranging from drug delivery to tissue engineering.[24-27]

Crosslinking of thermoplastic polymers via E-beam irradiation is performed for many thermoplastic systems. Depending on the dosage of irradiation, E-beam processing can result in either bond formation or chain scission; it is also reported that undesired changes to polymer microstructure and crystallinity can occur with excessive irradiation, which highlights the important of optimizing crosslinking parameters.[28]

Applications

Medical Imaging of Shape Memory Polymers

To provide further value to both SMP systems, visualization under X-ray is desired because it enables delivery guidance and monitoring capabilities. Fluoroscopy guided delivery is used in many interventional procedures, particularly those that are minimally invasive. Since polymers lack the high density required for radiopacity, there has been extensive work to achieve X-ray visibility through a variety of methods.[29-31]. Previous work in our lab has explored both nanoparticle and microparticle fillers to improve opacity in thermoset SMP foams,[2, 5, 7, 32-33] but these methods can alter bulk thermal and mechanical properties. Barium sulfate is a common additive to medical grade TPUs for X-ray visualization that can also enhance mechanical properties, such as toughness and tensile strength.[34-35] Nash et al. achieved adequate visualization of the thermoset SMPs by chemically incorporating iodine-containing motifs that are commonly used in injectable contrast solutions.[8] This approach was superior to the physical additive incorporation because it did not compromise bulk properties of the material. To expand the use of this approach, translating it to the TPU system and combining it with MRI visibility of the thermoset system were explored.

MRI visibility in SMPs was previously explored in thermoset SMP foams by Weems et al through incorporation of gadolinium chelates.[36] The gadolinium chelates are also used clinically in injectable contrast solutions like Magnevist, Gadavist, Omniscan, and Eovist where the dose administered is dependent on patient body mass. Gadolinium based contrast agents (GBCAs) are generally considered safe, and chelation averts some

of the toxicity concerns that exist with free gadolinium ions. There have also been recent FDA safety communications about retention of gadolinium, which concluded that the benefits outweighed the risks for patients without normal renal function and not currently pregnant.[37]

Drug Eluting Polymeric Devices

Polymers have been used in many drug delivery applications and can be tailored to achieve a variety of desired release profiles. The desired release profile may depend on the application, the drug used, or a combination of the two. For example, in zero-order drug release there is a linear rate of release, but it may take too long to reach adequate concentration for therapeutic efficacy. Conversely, in burst release a large amount of the drug is released initially, but is not sustained. Therefore, strategies have included incorporating both of these release behaviors to get the best of both worlds. There are also instances where release should be triggered by a specific event, such as pH or temperature change. All of these functionalities can be delivered through polymer architecture.

The intended use of the SMP drug-coated foam system is as an adjunct to surgery where it is placed in the resected tissue void to provide local drug delivery and prevent tumor recurrence. Gliadel wafers are a similar, approved device currently used clinically in glioblastoma treatment and deliver the chemotherapeutic agent carmustine. The polymer used in Gliadel is a polyanhydride, which is degradable and delivers the drug payload over about 5-6 days. Similar approaches have been explored for brain cancers[38], unresectable solid tumors[39], and liver cancer, but have not yet been translated successfully to clinical use.

The SMP drug-coated foams in the chosen approach are tuned by coatings of varied concentrations of polyvinyl alcohol mixed with drug. Polyvinyl alcohol (PVA) is also a common component of drug delivery systems and has historically provided drug delivery benefits in mucoadhesive applications.[40]

Antimicrobial Shape Memory Polymers

SMPs have been proposed for use as a hemostat due to their ability to initiate clots quickly and fill irregular spaces. The ability to prevent hemorrhage remains a major concern for the United States military. This has been an area of interest for our lab for many years and explored approaches from composite hemostats with hydrogels with povidone to hemostats that would degrade over time.[20, 41] Tuning the materials to be amenable to a deployed environment is another goal of this project.

There are also growing fears about the difficulty of treating antibiotic-resistant bacterial strains in traumatic wound healing. To address this issue, antimicrobial phenolic acids (PAs) will be chemically incorporated into the bulk foam. These PAs naturally contain antimicrobial and antifungal properties, and have even proven to be active against multi-drug resistant organisms without exposing them further to drug. Finally, depending on the chemical structure of the PA chosen, there is the ability to directly incorporate them into the PU SMP foam chemistry. Therefore, a library of potential modifications using PAs exists.

Shape Memory Polymer Degradation

Use of the current thermoset SMP material platform in medical applications could be limited by its oxidative degradation behavior. Degradation is a chemical change resulting in bond cleavage and is tied to structure-property relationships of the polymer. Previous work by Weems et al. determined that the degradation mechanism of the thermoset SMP materials was oxidation due to scission at the site of tertiary amines.[42] From a medical device material perspective, degradation is undesirable due to diminished device performance. Additionally, FDA clearance requires extensive testing to demonstrate safety and efficacy throughout the device lifetime. *In vitro* tests are required to approximate mass loss and degradative behavior by exposing polymers to oxidative or hydrolytic degradation solutions. To address the challenges associated with degradation, I hypothesized that a reduction in tertiary amine-containing monomers in the system would provide a system with improved biostability and reduced complications for commercialization.

This work replaces TEA with glycerol, thereby removing the oxidatively-susceptible amine linkages to provide increased biostability to the polymer system. After synthesis and characterization of glycerol-based SMP foams, accelerated *in vitro* degradation studies to confirm that the synthetic changes have improved the material biostability.

Summary

The modifications discussed in this dissertation will improve the performance and utility of the SMP material systems in medical devices. This work is significant because it improves existing materials and methods and will therefore provide a foundation for expanded future use of both polymer systems. Direct modification of the SMP systems' chemistry were made that enable enhanced X-ray and MRI visibility, processability, antimicrobial activity, and biostability of these materials to improve their potential for clinical translation. Additionally, a composite approach for adjuvant drug delivery was explored.

CHAPTER II

CHEMICAL MODIFICATIONS OF POROUS SHAPE MEMORY POLYMERS FOR ENHANCED X-RAY AND MRI VISIBILITY[1]

Introduction and Background

Shape memory polymers (SMPs) are a class of polymeric materials with an ability to change geometry in response to external stimuli. Thermoresponsive SMP materials actuate across a characteristic transition temperature (T_{trans}) that is based on polymeric structure. Temperature elevation above the polymer's T_{trans} enables deformation into a secondary geometry. Maintaining the deformation while cooling below T_{trans} temporarily programs this secondary shape. The unconstrained material will return to the primary geometry when heated back above the T_{trans}. This behavior enables a variety of biomedical applications such as conformal bone defect grafts, self-tightening sutures, and devices for minimally-invasive procedures.[18-19, 21]

Porous polymeric scaffolds are useful in a variety of applications, particularly those requiring tissue ingrowth, as the porous network and large surface area promote cellular infiltration, attachment, and rapid clot formation.[11-13] A class of biocompatible thermoset polyurethane SMPs using aliphatic isocyanates that can be gas-blown into low density, porous morphologies was originally envisioned for use in biomedical

[1] Reprinted with permission from "Chemical Modifications of Porous Shape Memory Polymers for Enhanced X-ray and MRI Visibility" by Fletcher, G.K.; Nash, L.D.; Graul, L.M.; Jang, L.K.; Herting, S.M.; Wilcox, M.D.; Touchet, T.J.; Sweatt, A.K.; McDougall, M.P.; Wright, S.M.; Maitland, D.J., 2020. Molecules, 25(20), 4660, Copyright retained by author [2020]. Published by MDPI.

applications.[1, 43] To utilize these properties, these foams and modifications thereof have been implemented in variety of embolic device designs.[12-13] In this case, the shape memory behavior coupled with the porous foam morphology enables minimally-invasive delivery of medical devices as the foams can be compressed to low diameters for catheter-guided delivery.[44] However, a major limitation of the SMP materials is that they are not visible on medical imaging modalities.

Many medical procedures are guided by or monitored using X-ray fluoroscopy. Since polymers lack the high density required for radiopacity, there has been extensive work to achieve X-ray visibility through a variety of chemical and physical additive approaches.[29-31] Use of nanoparticle and microparticle fillers to improve opacity in the SMP foams has been explored,[2, 5, 7, 32-33] but these composite methods can alter bulk thermal and mechanical properties. Another possible approach is chemically incorporating a radiopaque monomer. Recently, Lex et al. reported on polyesters with enhanced X-ray contrast derived from custom iodinated monomers.[45]

This work will build upon previous work by Nash et al. who achieved adequate visualization of thermoset SMP foams by chemically incorporating iodine-containing motifs.[8] The radiopaque monomer used in this work is 5-amino-2,4,6-triiodoisphthalic acid (ATIPA) which contains a triiodobenzene ring with an amine group and two carboxylic acid groups for incorporation into the polyurethane network. Triiodobenzene iodine motifs are commonly used in biomedical contrast agents such as Iohexol and Iopamidol due to their absorption of X-rays. While X-ray is a common medical imaging modality, it does necessitate patient exposure to ionizing radiation which can be a

concern for pediatric populations and patients requiring imaging often. Furthermore, it does not provide physicians with the same level of dynamic anatomical information as other imaging modalities.

Magnetic resonance imaging (MRI) is a medical imaging modality that does not expose patients to ionizing radiation and images with superior soft tissue contrast. MRI visibility in polymers is a topic being explored in biomaterial research. The best strategy for imparting MRI visibility into materials while avoiding device heating during imaging is to generate positive contrast with a passive technique. The most common manifestation of this approach involves MR contrast agents, most often gadolinium-based contrast agents (GBCAs), incorporated into the device in some manner to utilize the T_1-shortening effects of these agents.[46-47] Younis et al. grafted a GBCA onto a poly(methyl methacrylate) based copolymer which was ultimately utilized as a coating for a polypropylene mesh.[48] Other approaches for MR visibility in medical devices include incorporating other paramagnetic components; for example, Brocker et al. investigated the use of iron oxide woven into a polypropylene mesh material to achieve MRI visibility in devices.[49]

In general, these MRI contrast agents rely on paramagnetic effects to shorten T_1 relaxation times, decreasing T_1 saturation effects and leading to increased signal intensity when imaging using T_1-weighted sequences.[50] Gadolinium is commonly used in this way to generate MRI contrast because it enhances the proton relaxation of surrounding water and its paramagnetism is preserved when complexed with or conjugated to other molecules.[50-51] Weems et al. previously incorporated the monomer

diethylenetriaminepentaacetic (DTPA) acid gadolinium (III) dihydrogen salt hydrate also known as gadopentetic acid (GPA) into thermoset SMP foams based on trimethyl hexamethylene diisocyanate (TMHDI).[36] The carboxylic acid groups on this monomer allow for incorporation into the polymer backbone. This approach also utilized the same structure of gadolinium chelate in the commercially available GBCA Magnevist, which provides a reference for acceptable, nontoxic levels of gadolinium.

This paper will explore a SMP material with both X-ray and MR visibility that could be modified for multiple applications. A few groups have previously successfully modified polymers containing dual-modality contrast including Goodfriend et al. who synthesized a bioresorbable polyester named poly(gadodiamide fumaric acid) that is X-ray visible in its liquid coating form and MRI-visible in nanoparticle form.[52] Weems et al. also physically incorporated iron oxide nanoparticles for enhanced SMP visibility on both X-ray and MR imaging modalities.[36]

The proposed material platform could be used in many applications requiring guided delivery and follow-up monitoring. For example, X-ray fluoroscopy could be used in device delivery, but MRI could be used for post-procedural monitoring which would reduce the lifetime exposure to ionizing radiation and allow physicians to see soft tissue features. Combining the approaches established by Nash (ATIPA) and Weems (GPA) will create a new porous SMP with X-ray and MR visibility imparted by chemical modifications.

The material used in this work is based on Nash et al., which is an amorphous thermoset SMP where the glass transition temperature (T_g) is controlled by tuning the

material crosslink density.[8] The addition of GPA to this material system will increase T_g due to increased polymer network rigidity and crosslinking. Porosity is an important feature of these shape memory polymers and must be balanced with the correct amount of contrast monomers to ensure visibility in both compressed and expanded forms of the foam. Figure 1 shows the role of each monomer in the material system. Morphological, chemical, and thermomechanical characterizations were performed on multiple compositions. X-ray and MR imaging pilot studies were performed to verify visibility. Furthermore, extractions under simulated use conditions and indirect cytocompatibility studies were conducted to assess toxicity.

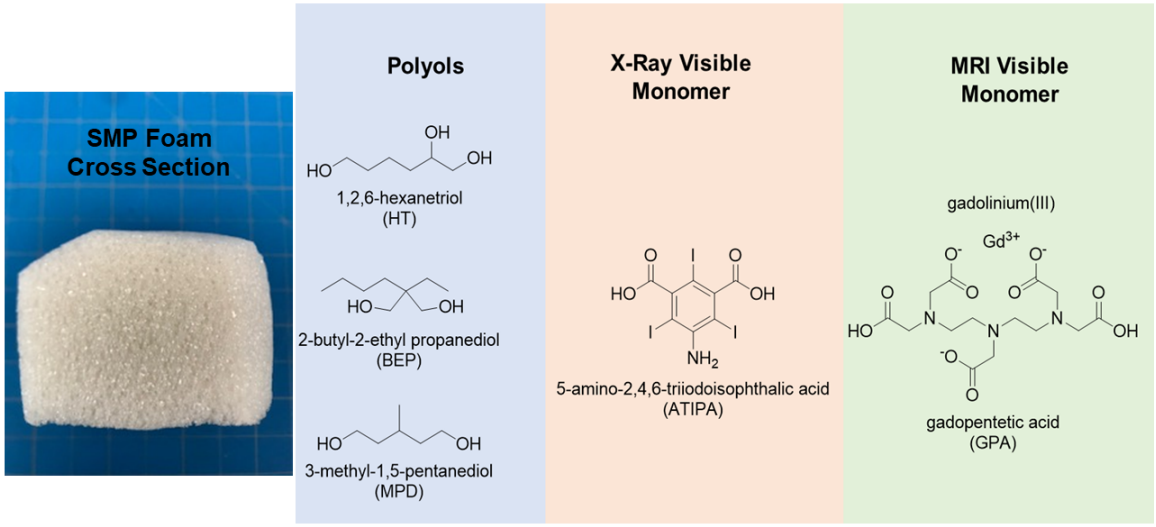

Figure II-1. Hydroxyl or carboxylic acid containing monomers and their role in synthesis of a porous SMP foam with dual contrast on X-ray and MRI modalities.

Results

The SMP foam compositions synthesized for the studies were named according to the convention delineated in Table 1. The compositional names arise from the amounts of ATIPA (X-ray visible monomer) and GPA (MR visible monomer) in each composition. These are reported as mol% of functionalities reactive with isocyanates (OH, COOH, NH_2). The isocyanate used in this work is hexamethylene diisocyanate (HDI).

Table II-1. Hydroxyl components of shape memory polymer compositions synthesized for use in all studies.

Composition	ATIPA (eq%)	GPA (eq%)	MPD (eq%)	BEP (eq%)	HT (eq%)
20 AT 0 GPA	20	0	40	20	20
20 AT 20 GPA	20	20	20	20	20
20 AT 10 GPA	20	10	23.3	23.3	23.3
20 AT 5 GPA	20	5	25	25	25
20 AT 2.5 GPA	20	2.5	25.8	25.8	25.8
20 AT 1 GPA	20	1	26.3	26.3	26.3
20 AT 0.05 GPA	20	0.05	26.7	26.7	26.7
20 AT 0.025 GPA	20	0.025	26.7	26.7	26.7
20 AT 0.01 GPA	20	0.01	26.7	26.7	26.7
20 AT 0.001 GPA	20	0.001	26.7	26.7	26.7

2.1. Physical Characterization

Physical characterization included density and pore size measurements. Table 2 contains the SMP foam densities and pore sizes for all compositions made. Pores were measured in the axial and transverse directions.

Table II-2. Physical and thermomechanical properties of SMP foams. Measurements are reported as mean ± standard deviation for the indicated sample size in top row.

Composition	Density (g/cm^3)	Pore Sizes (μm)	Dry T_g (°C)	Wet T_g (°C)	Gel Fraction (%)
	n=3	***n=30***	***n=3***	***n=3***	***n=3***
20 AT 0 GPA	0.076 ± 0.007	Axial 1447 ± 344 Trans 1523 ± 329	47.5 ± 0.9	32.1 ± 1.6	97.2± 0.3
20 AT 20 GPA	0.123 ± 0.007	Axial 702 ± 108 Trans 711 ± 118	66.8 ± 1.0	39.2 ± 1.1	98.8 ± 0.3
20 AT 10 GPA	0.039 ± 0.004	Axial 1853 ± 505 Trans 1493 ± 311	66.9 ± 0.3	37.1± 0.9	97.5 ± 0.1
20 AT 1 GPA	0.093 ± 0.003	Axial 920 ± 199 Trans 744 ± 122	64.0 ± 0.9	36.0 ± 1.0	98.0 ± 0.1
20 AT 0.01 GPA	0.128 ± 0.004	Axial 1408 ± 93 Trans 798 ± 69	59.8 ± 0.5	36.4 ± 0.7	98.6 ± 0.3
20 AT 0.001 GPA	0.114 ± 0.010	Axial 1211 ± 364 Trans 1051 ± 229	54.9 ± 1.1	37.8 ± 1.8	98.3 ± 0.4

The SEM images of the foam (Figure II-2) show the effect of the cell opener as well as the thick struts in the ATIPA GPA foams. Pore size and morphology varied in compositions due to pre-polymer viscosity and amount of GPA. Foams with larger pores have elongated pores in the axial (foaming) direction. Thick struts were visible in both the 20 AT 0.01 GPA and 20 AT 0.001 GPA compositions.

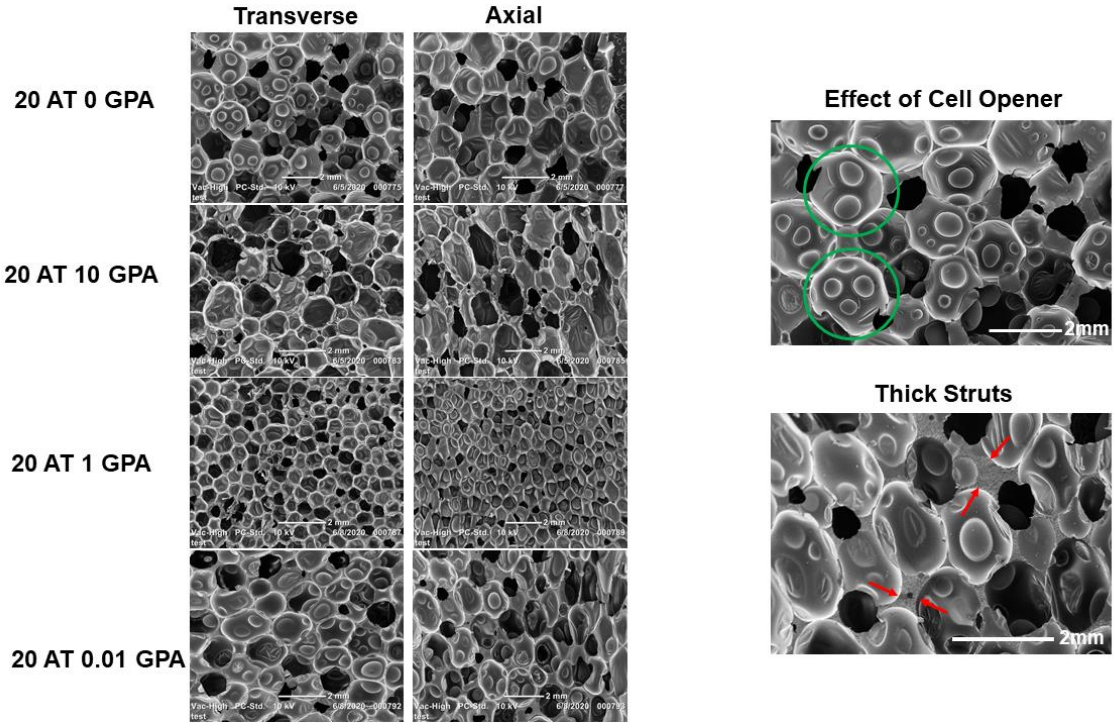

Figure II-2. Left - SEM Images of selected foam compositions highlighting pore size and morphology (scale bar 2 mm for all images). Right – Zoomed in SEM images highlighting unique morphological features. The green circle denotes the thinning of pore membrane due to the addition of cell opener in the 20 AT 0 GPA composition. The red arrows denote thick struts in composition 20 AT 0.01 GPA.

Figure 3 shows the ATR-FTIR spectroscopy for selected compositions. A strong urethane C=O peak is present at 1685 cm^{-1} for all compositions, so spectra were normalized to this peak. Compositions exhibit a urea C=O shoulder at 1650 cm^{-1} from the primary amine on ATIPA's reaction with isocyanate. The 20 AT 10 GPA composition has the strongest amide II peak at 1510 cm^{-1} due to higher carboxylic acid content in the synthesis from the GPA monomer.

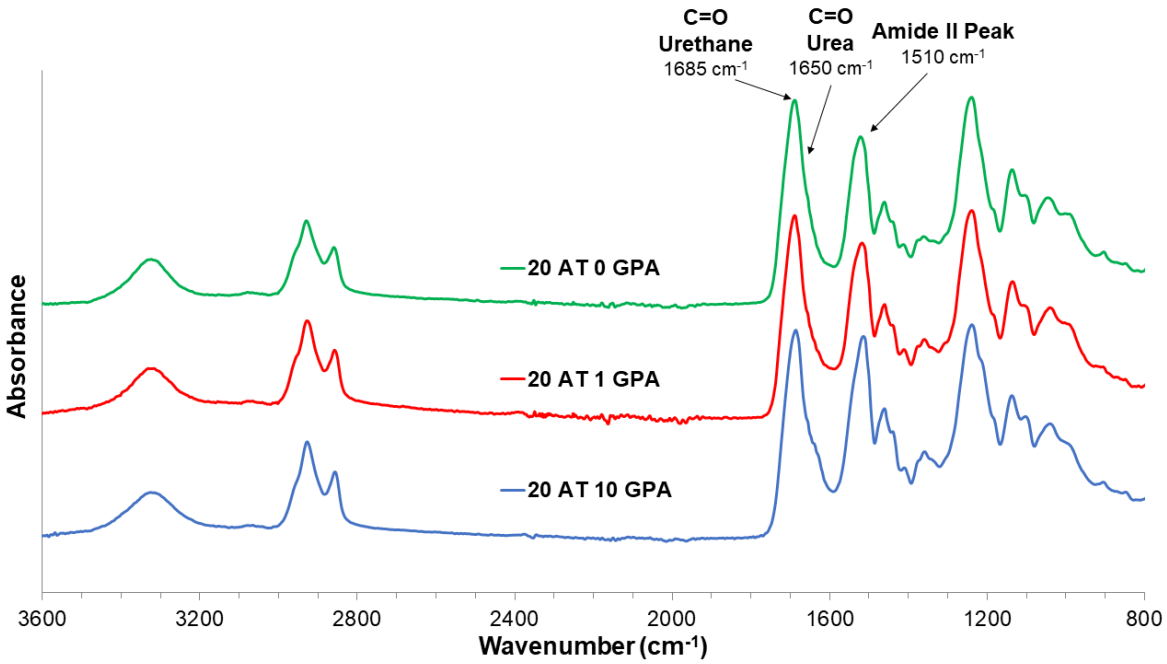

Figure II-3. ATR-FTIR spectroscopy results for a selection of compositions with peaks of interest identified (C=O Urethane 1685 cm^{-1}, C=O Urea 1650 cm^{-1}, Amide II 1510 cm^{-1}).

2.2. Thermomechanical Characterization

Glass transition temperatures (Table 2) increased with increasing GPA content. However, all compositions also demonstrated water plasticized transition temperatures (wet T_g's) close to body temperature. Figure 4 summarizes the unconstrained expansion behavior of the foams in a 37°C water bath. The 20 AT 10 GPA foam had the most rapid expansion, reaching 100% expansion at ~10 minutes. The 20 AT 0 GPA foam did not reach 100% expansion but also reached its terminal diameter quickly (~15 minutes). The 20 AT 0.01 GPA and 20 AT 0.001 GPA foams expanded the slowest and did not reach 100% expansion at 60 minutes. The expansion behavior of the foams seems to be related to both foam density and GPA content increasing hydrophilicity of the foam.

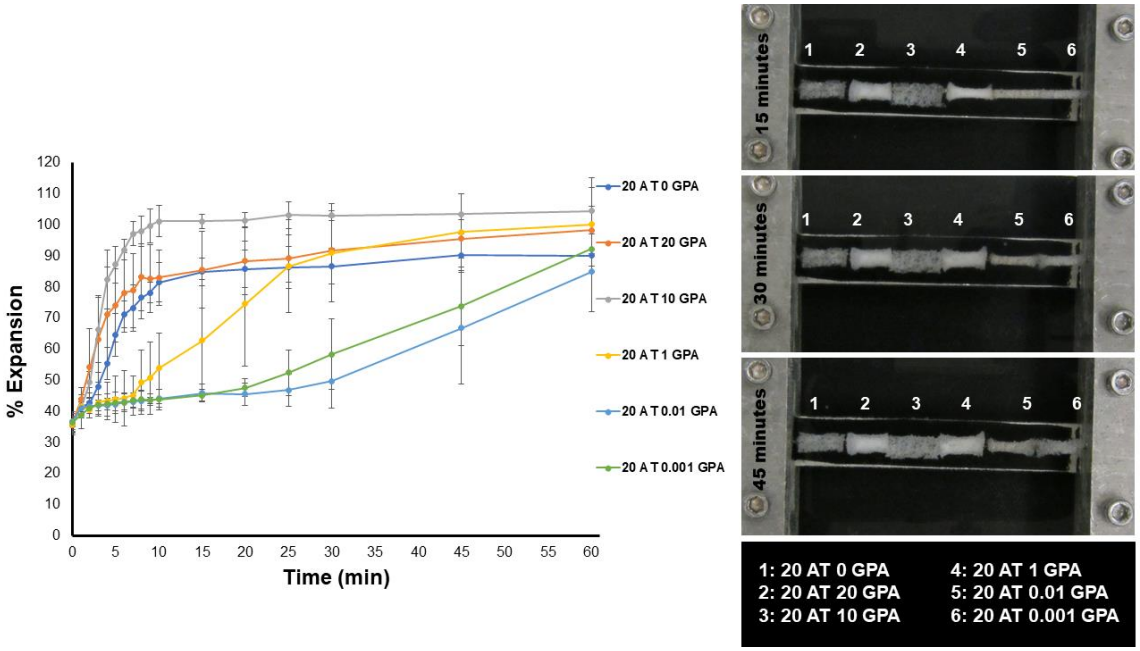

Figure II-4. Left - Unconstrained expansions of 6 mm diameter foam punches upon exposure to a 37°C water bath. Images were analyzed every minute for the first 10 minutes and at 5 minute intervals until 30 minutes, then at 15 minute intervals for the remaining time points. Right - Images from the water bath at the 15, 30, and 45 minute time points to show expansion of foams over time.

Tensile tests were performed on rectangular foam samples (n=3) affixed to wooden blocks. The ultimate tensile strength (UTS) was calculated from the peak stress on a stress-strain curve (Table 3). UTS and stiffness increases correlate to increasing SMP foam density, except in the case of the 20 AT 20 GPA formulation. This is likely due to increased loading of GPA.

Table II-3. Ultimate tensile strength (UTS) for compositions with varied GPA content**.**

Composition	Ultimate Tensile Strength (kPa)
20 AT 0 GPA	356.5 ± 36.3
20 AT 20 GPA	455.2 ± 92.2
20 AT 10 GPA	203.7 ± 41.1
20 AT 1 GPA	751.8 ± 126.8
20 AT 0.01 GPA	927.4 ± 101.0
20 AT 0.001 GPA	1061.1 ± 71.8

2.6. Magnetic Resonance Imaging

The T_1-weighted MR images were taken in both coronal and transverse planes. Low GPA concentration foams (Figure 5, A) did not enhance foam visibility in the coronal view relative to the positive oil control and negative DI water control. However, the 20 AT 10 GPA foam (#5 on Figure 5, B) showed a marked brightening effect around the foam and the vial in the coronal view. This intensity exceeds that of the fiduciary control (oil capsule) and the other foams in the same image. There is a slight brightening effect of the 20 AT 1 GPA (#1 on Figure 5, C) foam in the transverse view. 20 AT 20 GPA composition is excluded from MR images because we observed darkening due to high concentrations of gadolinium.

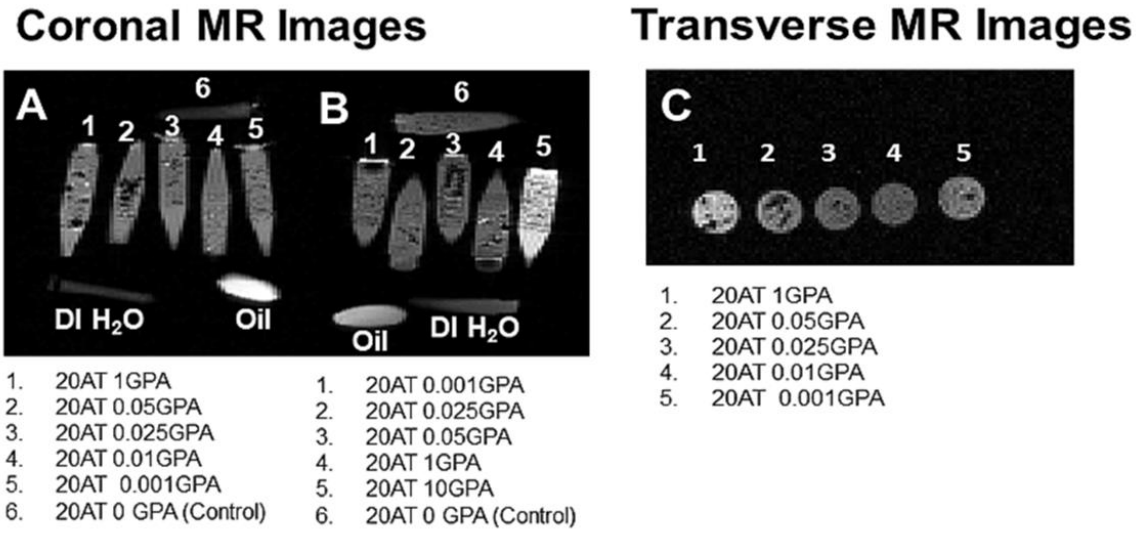

Figure II-5. MR images using T_1-weighted parameters (TE=30 msec, TR=500 msec) are shown: (a,b) Coronal MR images of compositions as labelled with oil and water controls; (c) Transverse MR images of compositions as labelled.

2.7. X-Ray Imaging

The X-ray images were performed on multiple foams with varying densities. The images were taken both directly and through a ½" aluminum plate to mimic attenuation from bone (e.g. skull).[53] The X-ray images obtained (Figure 6) were analyzed by measuring the pixel intensity 60 points on the sample of interest (Figure 7). This was performed after background removal processing step in ImageJ. The ATIPA-GPA foam X-ray pixel intensity values were compared to those for the platinum coil (Pt Coil) of the IMPEDE device (Shape Memory Medical Inc, Santa Clara, CA), which was analyzed as a control for the opacity of metallic device components.

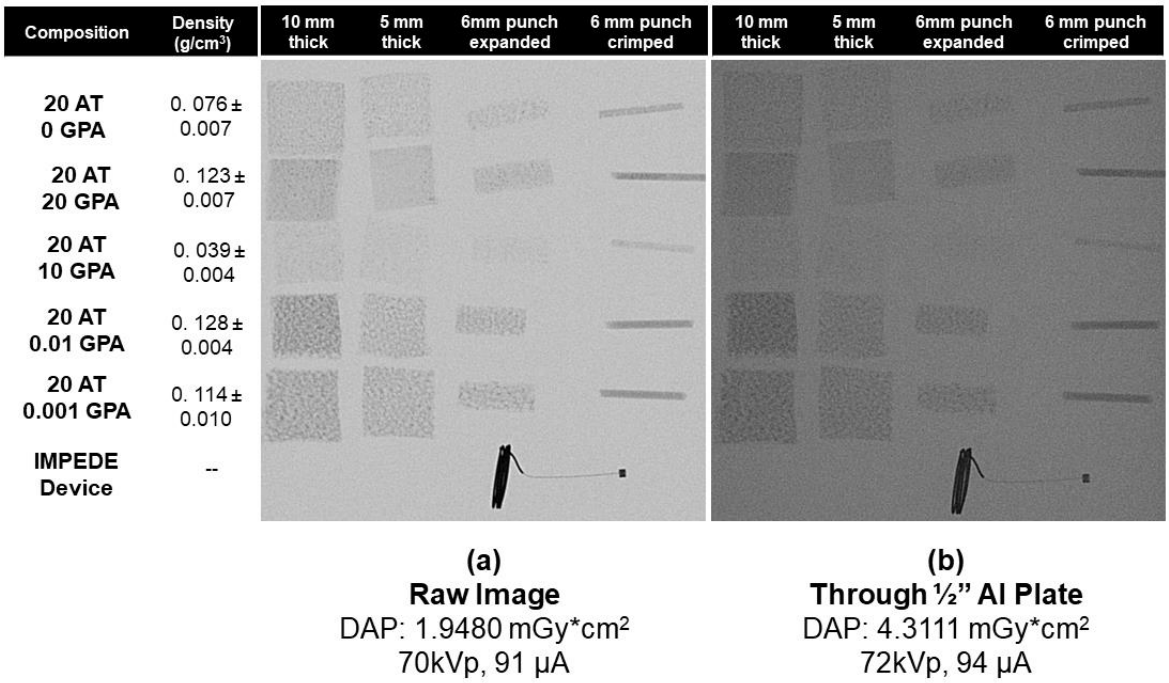

Figure II-6. Selected SMP foams with 20 mol% ATIPA and varying amounts of GPA imaged on OrthoScan C-arm. Right image (b) was performed through a ½" Al plate to simulate imaging through bone. Foam samples in columns are labeled with thickness for cubes and crimp state of 6 mm diameter cylindrical biopsy punch samples.

Figure 7 shows the relative X-ray densities of the 6 mm foam samples in crimped and expanded forms. The images taken with a ½" aluminum plate on top all have lower X-ray densities than their raw image counterparts, which is expected due to X-ray attenuation. Foam density was the largest factor in X-ray opacity since all compositions contained the same amount of ATIPA monomer (20 mol%). The 20 AT 20 GPA, 20 AT 0.01 GPA, and 20 AT 0.001 GPA compositions are the highest density materials and show the greatest X-ray density in both the baseline and attenuated images. Porous morphology of the 20 AT 0.01 GPA and 20 AT 0.001 GPA foams is visible in the X-ray images due to thicker struts.

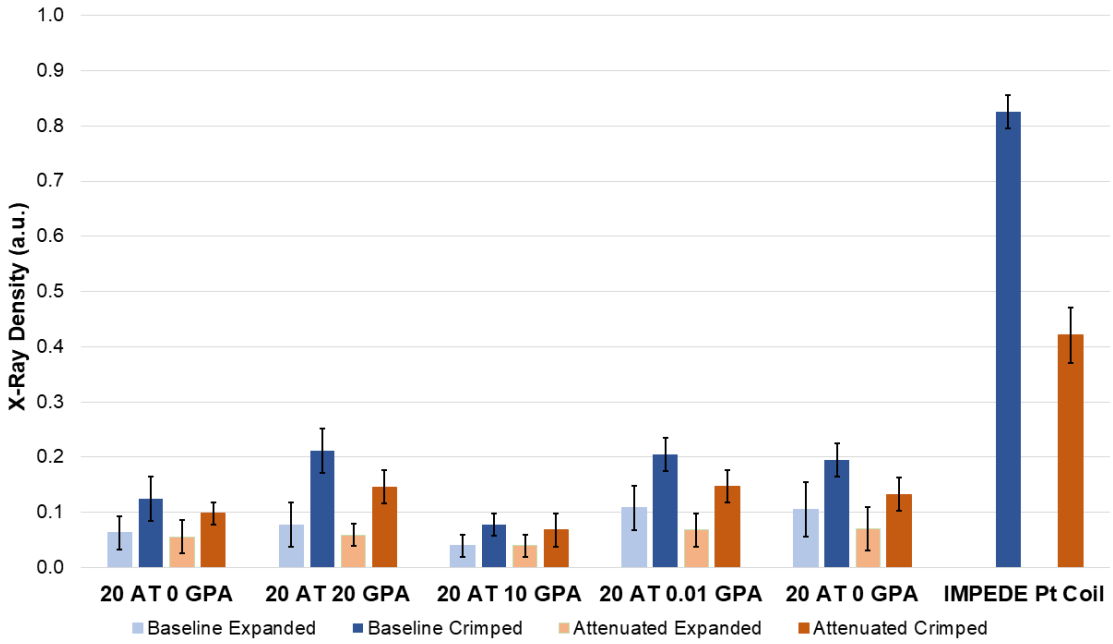

Figure II-7. The 6 mm cylindrical foam punches of multiple compositions in expanded and crimped form for each of the X-ray images were analyzed to determine their relative opacity: (Blue) Baseline X-ray image; (Orange) Attenuated X-ray image taken through ½" aluminum plate.

2.8. Mass Spectroscopy of Extractables

Extractions were performed in DI water and 50% ethanol extraction vehicles to identify the amount of extractable and leachable gadolinium under simulated use conditions. The highest reported extraction concentration of 7510 ng/mL was reported for the 20AT 20 GPA composition extracted in 50% ethanol, equivalent to a total extracted weight of 75.1 mg for the sample. This is approximately 8 times more gadolinium than the equivalent extraction in DI water.

Table II-4. ICP-MS results for the ATIPA-GPA foam samples in different extraction vehicles. Results are displayed as Gd concentration ± uncertainty.[1]

Composition	DI Water Extract Gd Concentration (ng/mL)	50% Ethanol Extract Gd Concentration (ng/mL)
20 AT 20 GPA	938 ± 47	7510 ± 380
20 AT 10 GPA	259 ± 13	2160 ± 110
20 AT 1 GPA	116 ± 6	419 ± 21
20 AT 0.01 GPA	2.4 ± 0.1	38 ± 2
20 AT 0.001 GPA	<0.1*	0.30 ± 0.02

[1] Uncertainties provided at the 1 s (67% confidence level)
*Quantitation limit

2.9. Indirect Cytocompatibility

Media extracts were exposed to 3T3 cells in order to determine the compositions' cytocompatibility and results are displayed in Figure 8. Cell viability was determined using a resazurin assay and calculated from Equation 3. While the composition with the highest GPA content (20 AT 20 GPA) did have the lowest cell viability, all compositions were above the IC30 threshold indicated by the red line on Figure 9.

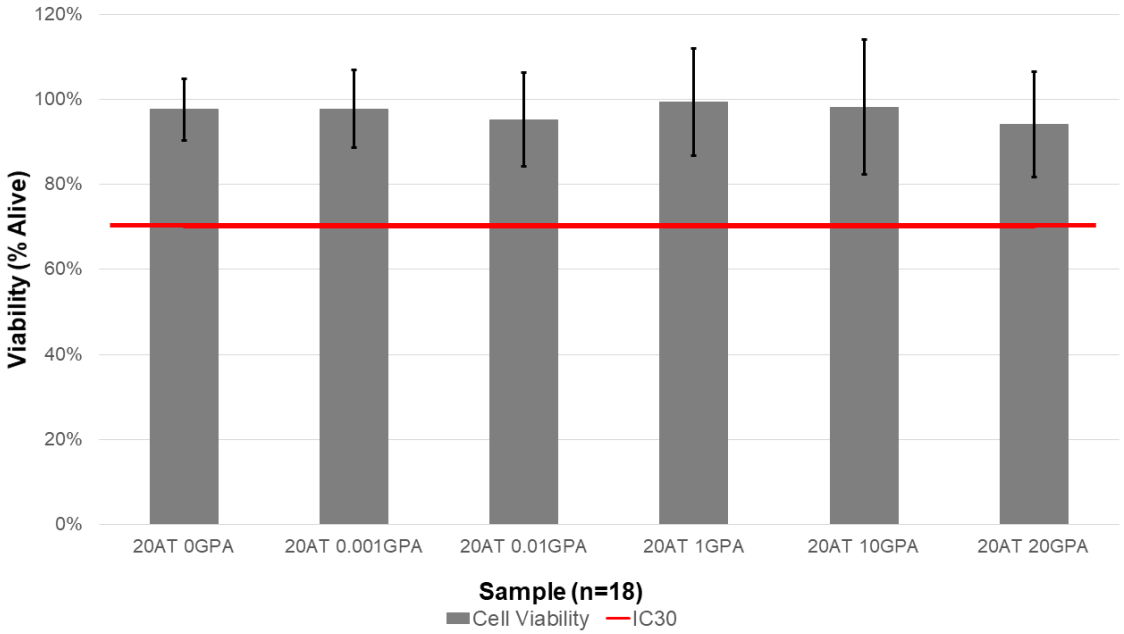

Figure II-8. Cell viability was calculated from RFU in resazurin assay performed upon 3T3 cell exposure to media extracts with compositions of SMP foams. Extractions and cytocompatibility assays (n=6 wells for each assay) were repeated in triplicate for a total sample size of 18. Red line indicates IC30 or threshold where 70% of cells are alive. All compositions were above the IC30 threshold.

Discussion

In general, as GPA content decreased, the density of the polymers increased. This is due to the GPA monomer's carboxylic acid groups, which acted as an additional blowing agent due to the generation of carbon dioxide upon reacting with isocyanates. The exception to this trend was the 20 AT 20 GPA composition with a higher density. This level of GPA in the 20 AT 20 GPA composition increased the reactive mixture's viscosity, which decreased the average pore size and increased ultimate material density, despite increased carboxylic acid chemical blowing.

Glass transition temperatures (Table 2) increased with increasing GPA content. This trend was also observed in Weems et al.[36] and is due to restricted chain mobility in the polymeric structure with increasing rigid GPA monomer incorporation. However, all compositions demonstrated water plasticized transition temperatures close to body temperature. The materials' high dry T_g's are beneficial in terms of medical device shipping and storage conditions to maintain secondary geometries without premature actuation.

The unconstrained expansion behavior of the foams in a 37°C water bath (Figure 4) was more affected by material density and pore size than composition T_g. The lowest density 20 AT 10 GPA foam was the quickest to expand. This is due to higher density materials contributing a more significant physical diffusion barrier to moisture plasticization. Moisture plasticization depresses the transition temperatures due to disruption of hydrogen bonding between adjacent urethane and urea linkages, resulting in increased segmental mobility within the polymer network. All compositions had moisture plasticized transitions close to body temperature, therefore linking expansion rate to plasticization rate.

The pilot MR imaging studies provided a range of acceptable concentrations of gadolinium. Gadolinium causes shortening of both T_1 and T_2. When using T_1-weighted imaging sequences, the T_1 shortening manifests as the clinically desired image brightening, while T_2 shortening will result in image darkening. Depending on the concentration of gadolinium used, one of these effects will be dominant. The 20 AT 20 GPA composition had too high of a concentration of gadolinium and T_2 effects

dominated, so it was excluded from further study. While brightening was seen for the 20 AT 10 GPA and 20 AT 1 GPA compositions, the pilot MR images are somewhat limited since all materials were imaged in vials containing DI water. Although DI water is not entirely representative of T_1 and T_2 tissue MR properties, general trends of increased brightening for GBCA incorporated compositions should still be clinically relevant for T_1-weighted imaging sequences. In general, visibility of any foam is expected to be dependent on the surrounding tissue properties as well as the exact imaging parameters used. Future imaging studies should be conducted in animal tissues using a variety of imaging parameters to account for tissue variations in MR and X-ray imaging properties.

While reaction conditions were kept constant between compositions, the differences in viscosity of monomer solution and amount of the GPA monomer resulted in different material density and pore sizes. Since material density played a large role in material performance (expansion, tensile strength, and X-ray visibility), it will likely be tuned for specific performance outcomes depending on the chosen application. For example, larger pore and lower density foams will expand faster, but have lower mechanical strength and require a higher loading of contrast agents for visibility, whereas higher density foams will expand slower, but have superior mechanical strength and visibility. Ideal material density can be tailored in each composition by changing the amount of physical blowing agent and reactive mixture viscosity.

The extractions of the 20 AT 20 GPA composition using a 50% ethanol extraction vehicle in simulated use conditions had the highest amount of extracted gadolinium, however it was well below the maximum doses administered for adult and

pediatric populations. Magnevist is prepared at a concentration of 469 mg/mL and administered at a maximum dose of 0.6 mL/kg for adult patients and 0.4 mL/kg for pediatric patients. Using these dosing guidelines, almost 19 devices with a similar footprint (6 mm diameter, 25 mm length cylinder) as the extracted foam sample could be delivered to a 10 kg pediatric patient. In adult patients of 50 kg, approximately 187 devices could be delivered while being in the dosing safety threshold (CDC currently reports an average weight of women and men in the US of ~77 kg and 89 kg respectively).

Indirect cytocompatibility study results complement the extraction ICP-MS data. The 20 AT 20 GPA composition had the lowest average cell viability (94.1 ± 12.3%). However, all compositions were above the IC30 threshold. Gadolinium is toxic because a free Gd^{3+} ion can interfere with normal biological processes due to its similarity to the Ca^{2+} ion.[54] Chelated versions of gadolinium are used to prevent this, but future *in vivo* studies should carefully monitor accumulation of Gd^{3+} in tissue as well as renal function.

The approaches for imparting X-ray and MRI visibility to SMP foams through chemical modification described herein could be translated to many material systems. Additionally, SMP foam properties could be tuned for specific device requirements. These foams could be incorporated into current embolic device designs to reduce or eliminate metallic components used for visualization. The foam itself being visible provides more information about the expansion and volume-filling properties of the devices. An example of a new application amenable to the developed material system is a biopsy sealing device. The benefit of the X-ray and MRI visibility for this application

would be that the device could be imaged during delivery and the polymer plug could act as a fiducial to mark the tract where the biopsy was taken from.

Materials and Methods

4.1. Materials

All chemicals were used as purchased unless otherwise indicated. 3-methyl-1,5-pentanediol, 2-butyl-2-ethyl propanediol, 1,2,6-hexanetriol, 5-amino-2,4,6-triidoisosphthalic acid (95%), and gadopentetic acid (97%) were all purchased from Sigma Aldrich. Hexamethylene diisocyanate was purchased from TCI. The cell opener Tegostab B8523 and surfactant DC1990 were provided by Evonik. Tetrahydrofuran was from EMD Millipore and was stored over molecular sieves. Isopropanol was purchased from VWR. Enovate was purchased from Honeywell.

4.2. SMP Foam Synthesis

All foam compositions used in the study are listed in Table 1. Foams were synthesized using a classic hydroxyl (OH) and isocyanate (NCO) polyurethane reaction scheme. The hydroxyl components used were 3-methyl-1,5-pentanediol (MPD), 2-butyl-2-ethyl propanediol (BEP), and 1,2,6-hexanetriol (HT). The isocyanate component was hexamethylene diisocyanate (HDI). The X-ray visible monomer used was 5-amino-2,4,6-triiodosphthalic acid (ATIPA). The MRI visible monomer was diethylenetriaminepentaacetic acid gadolinium (III) dihydrogen salt hydrate also known

as gadopentetic acid (GPA). All monomers were used as received and premixes were prepared in a glovebox.

The foaming procedure was adapted from Nash et al. to accommodate addition of gadolinium.[8] The hydroxyl components (0.6 molar eq.) of the OH premixes (MPD, BEP, HT, ATIPA) were measured out into a 150 mL Flacktek mixing cup two days before foaming. They were mixed in a Flacktek high speed mixer (Model DAC 150 FVZ-K, Flacktek Inc, Landrum, SC) for 30 seconds at 3540 rpm and placed in an oven at 50°C. After 1 hour, the cup was mixed again for 30 seconds and remained in the 50°C oven overnight.

Similarly, the hydroxyl components (0.4 molar eq.) of the NCO premixes were added to a separate Flacktek mixing cup two days prior to foaming. They were mixed in a Flacktek high speed mixer for 30 seconds at 3540 rpm and placed in an oven at 50°C. After 1 hour, the cup was mixed again for 30 seconds and remained in the 50°C oven overnight. The following day, the contents were mixed another 30 seconds before adding the diisocyanate equivalents (1.02 molar eq.). The mixture was mixed in a Flacktek high speed mixer for 5 minutes at 3540 rpm and placed on a shaker plate at room temperature overnight or until the mixture's viscosity increased to a honey-like consistency.

The surfactant DC1990 (4 wt%) and the cell opener Tegostab B 8523 (0.025 wt%) were added to the NCO premix prior to foaming and mixed for 30 seconds. GPA was added to the OH premix and mixed for 1 minute immediately before foaming. The OH premix was added to the NCO premix and mixed for 30 seconds. A physical blowing agent, Enovate, was added to that mixture and mixed for 15 seconds. The cup

was moved to an oven at 90°C and allowed to cure for 20 minutes. The foam was allowed to cool in a fume hood and the skin was removed with a razor blade before an overnight post-cure in a 50°C oven.

Foam samples were placed in a jar and submerged in DI water and sonicated for three 30 minute cycles to rinse before adding isopropyl alcohol (IPA) in a 20:1 IPA:foam volume ratio. The jars were subjected to three 30 minute intervals in a sonication bath, switching out IPA between intervals. They were dried overnight at 100°C in a vacuum oven and stored with desiccant before characterization took place unless otherwise noted.

4.3. Physical Characterization

4.3.1. Density

Cubes (~1 cm^3) from each foam block were used for density measurements. The dimensions of the block were measured (n=3) with calipers and volume was calculated. Mass of the blocks was measured on a balance (n=3). Density was calculated using averaged mass and volumes for the samples.

4.3.2. Pore Morphology

Foam slices were cut in the axial and transverse directions in the middle of the foam, mounted on carbon tape affixed to an imaging stub, dried, and sputter coated. Slices were imaged using a JEOL JCM-5000 Neoscope scanning electron microscope (JEOL USA Inc., Peabody, MA). 30 pores were measured per slice direction using ImageJ software.

4.3.3. Fourier Transform Infrared Spectroscopy (FTIR)

Foam samples were cut and compressed to be measured using a Bruker Spectrometer (Bruker, Billerica, WA). Spectra were obtained via a germanium attenuated total reflectance (ATR) probe. Thirty-two background scans were performed prior to each sample measurement. Samples were measured using 64 scans and the resulting spectra were corrected for atmospheric compensation using Bruker OPUS software and exported to Excel where they were normalized to the urethane peak.

4.4. Gel Fractions

Gel fraction was performed on cleaned and dried foams to determine the extent of crosslinking. The initial cleaning step removes excess surfactant and catalysts. Original dry weight was measured using a balance (Mettler Toledo, Columbus, OH). Foam blocks were incubated in THF for 3 days at 50°C. Foams were dried at 50°C under vacuum for 2 days and measured to get the final weight. Gel fraction was calculated using the equation:

$$\frac{m_1}{m_0} \times 100\% = G_{f.} \quad (1)$$

4.5. Thermomechanical Characterization

4.5.1. Differential Scanning Calorimeter (DSC)

Differential scanning calorimetry measurements were used to determine the glass transition temperature (T_g) of wet and dry samples. Measurement were obtained using a

TA Q200 Differential Scanning Calorimeter (TA Instruments, New Castle, DE). Hermetically sealed aluminum Tzero (Switzerland) pans with a hole poked in the top were used for all samples and goal foam sample weight was 5-10 mg. The cycle used for dry samples (Dry T_g) was first equilibrated at -40°C for 5 min, heated to 120°C (40°C/min) and cooled to -40°C. It was then reheated again at 10°C/min to 120°C. The second heating curve was analyzed using TA Universal Analysis software to determine dry T_g. Wet T_g foam samples were incubated in a 50°C water bath for 30 minutes and pressed between Kimwipes to remove moisture prior to running. The cycle for wet samples was equilibrated at -40°C for 5 minutes, with a single heating cycle that ramps to 100°C at 10°C/min. The wet T_g was determined from the inflection point on the heating curve using TA Universal Analysis software.

4.5.2. Unconstrained Expansions

After cleaning and drying, 6 mm cylindrical biopsy punches of foams (n=3) were threaded over a wire and initial images were taken. The punches were radially crimped using Machine Solutions SC250 radial crimper heated to 100°C. The crimped foams were allowed to relax at room temperature in a desiccated container for 24 hours before studying their expansion behavior. Images of crimped foams were taken to determine initial crimped diameter. A water bath was heated to 37°C and pictures were taken every minute until the 10 minute time point, then images were taken every five minutes until 30 minutes. All images were analyzed by measuring five points on each foam punch at

every time point using ImageJ. Results were reported as percent expansion with standard deviation.

4.5.3. Tensile Testing

Rectangular foam samples were cut to approximately 25 mm x 15 mm x 3 mm and epoxied to wooden blocks at the short end. Epoxy was allowed to cure overnight and samples were stored under vacuum in a bell jar for at least 24 hours prior to tensile testing to ensure ambient moisture did not affect mechanical properties. A MTS Insight 30 Universal Tensile Tester (MTS Systems Corp, Eden Prairie, MN) with a 50 N load cell was used in tensile testing. Clamps were tightened on the wooden blocks at either end of the sample and machine was zeroed. The protocol used was a strain to failure at 5 mm/min constant strain rate.

4.6. Magnetic Resonance Imaging (MRI)

Pilot magnetic resonance imaging (MRI) validation studies of the SMP foams were performed at the Magnetic Resonance Systems Lab at Texas A&M University. Cylindrical foam samples (6 mm diameter) were placed in DI water in microcentrifuge tubes and a fish oil tablet was used as a positive control for images. High resolution multi-slice T_1-weighted images (TR 500msec, TE 30 msec) were acquired on a 4.7T Varian Inova scanner using a standard spin-echo pulse sequence. Transverse images were taken with a 30mm x 60mm field-of-view and 64 x 128 matrix size for 469 μm resolution in both x (left-right) and y (anterior-posterior) dimensions with a slice

thickness of 1 mm. For coronal images, a 120 mm x 80 mm field-of-view and 256 x 128 matrix size were used for 469 µm resolution in the z (head-foot) dimension and 625 µm resolution in the x dimension with a slice thickness of 1 mm. All other parameters were kept constant throughout all acquisitions. The raw data acquired from the scanner was imported to Matlab® for reconstruction and display of all images.

4.7. X-Ray Imaging

Foam samples were cut into blocks (~10 mm x 10 mm) of 10 mm and 5 mm thicknesses and cylinders of 6 mm diameter. All samples were arranged according to composition and imaged using OrthoScan C-arm system (Mobile DI Model 1000-0005). There were 6 mm diameter cylindrical prototype devices made as well in crimped and expanded forms. IMPEDE device (Shape Memory Medical, Santa Clara, CA) containing a Pt coil and marker band was used as a positive control. Samples were also imaged through a ½" aluminum plate which served as a bone analog with respect to X-ray attenuation.[8] Images were converted to 8-bit grayscale, processed to remove background, and analyzed using ImageJ to determine X-ray density. Sixty measurements were taken using the multi-point selector yielded values between 0 (black) and 255 (white). X-ray density was calculated from using the equation:

$$X - Ray\ Density = \frac{255 - (Image\ J\ Pixel\ Intensity\ Value)}{255} \quad (2)$$

such that a density of 1 would correlate to an entirely black image.

4.8. Mass Spectroscopy of Extractables

The extraction conditions chosen were simulated use, batch extraction with agitation. Cylindrical (6 mm diameter x 25 mm length) SMP foam samples were incubated in 10 mL of extraction solution at 37°C in an incubation shaker at 90 rpm. DI water was used as the polar extraction solution and a 50/50 water/ethanol solvent mixture was used as the non-polar extraction solution. After 72 hours, samples were removed and 1% nitric acid was added to solutions to ensure metallic particle stability before samples were analyzed using a Perkin Elmer NexION 300D inductively coupled mass spectroscopy (ICP-MS) instrument in the Elemental Analysis Laboratory at Texas A&M University.

4.9. Indirect Cytocompatibility

Using sterile biopsy punches in an aseptic environment, foams were cut into 8 cm diameter discs with 2 mm thickness. The surface area of the discs was calculated based on the pore size of each foam composition as previously performed by Weems et al.[42] Foams were submerged in complete cell culture media for extraction at a ratio of 3 cm^2 foam per 1 mL of media for 72 hours at 37°C in a rotating incubator. An additional tube with media only was included as a cytocompatible control. Complete cell culture media was made from Dulbecco's Modified Eagle Medium (DMEM, MilliporeSigma, St. Louis, MO) and supplemented with 10% newborn calf serum (NCS, MilliporeSigma, St. Louis, MO), 1% penicillin-streptomycin (P/S, VWR, Radnor, PA) solution, and 0.1% fungizone (VWR, Radnor, PA).

Balb/3T3 cells, clone A31 (3T3s, ATCC, Manassas, Virginia) were thawed and passed at least once prior to plating for the cytocompatibility assay. All incubation periods were done in a humidified incubator at 37°C with 5% CO_2. Complete cell culture medium used for 3T3 culture and the assays was the same as described above for the extraction. 3T3s were harvested with trypsin and seeded in 96 well plates at 7,500 cells per well. After a 24-hour incubation, cell morphology and distribution were assessed, and images were acquired of each well using a Biotek Cytation5 Imaging Reader (Biotek, Winooski, VT). The media was then removed and replaced with media from the foam extractions or control. The cells were incubated with these treatments for 48 hours, then cell morphology and distribution were assessed and additional images were acquired of each well using the Cytation5. Finally, cell viability was measured indirectly using a resazurin assay to assess relative metabolic activity. Cells were incubated with 5% resazurin in complete media for 3 hours, then the fluorescence was measured using an excitation wavelength of 560 nm and an emission wavelength of 590 nm on a Tecan Infinite M200 Pro Plate Reader (Tecan, Morrisville, NC). Cell viability was calculated using the following equation:

$$\text{Cell Viability (X)} = \frac{\text{RFU}_{\frac{560}{590}}(\text{X}) - \text{RFU}_{\frac{560}{590}}(\text{blanks})}{\text{RFU}_{\frac{560}{590}}(\text{Untreated Control}) - \text{RFU}_{\frac{560}{590}}(\text{blanks})} \quad (3)$$

where X is any treatment group and RFU is relative fluorescent units (i.e. fluorescence intensity). Extractions and cytocompatibility assays were repeated in triplicate.

CHAPTER III

RADIOPAQUE THERMOPLASTIC COMPOSITIONS

Introduction and Background

Previously Hearon et al. developed a highly tunable and processable thermoplastic polyurethane (TPU) material platform, and despite its many benefits, it is currently underutilized in our lab. Due to its unique architecture, this material has advanced processing capabilities as a thermoplastic and can be crosslinked into a thermoset SMP post-processing. Thermoset materials have superior shape fixity and recovery in shape memory, so this post-process crosslinking enables a system where the benefits of each material system are realized. Synthesis and characterization of tunable TPU scaffolds using this previously developed system chemically modified to be X-ray visible will enhance their potential use in biomedical applications.

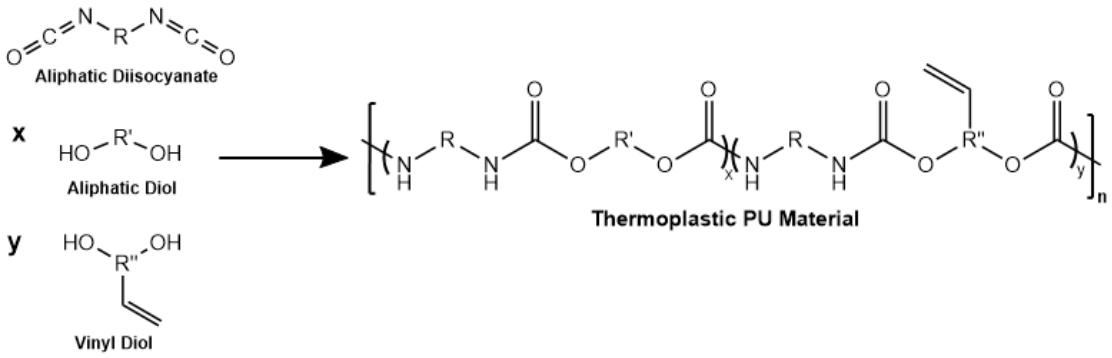

Figure III-1. General reaction schematic for TPU developed by Hearon et al. The structure is highly tunable for different applications and desired polymer properties.

Through monomer selection, TPU chemistry was tuned to achieve X-ray visibility alongside desired polymer behavior. TPU compositions that were synthesized were assessed to ensure they meet practical processability considerations and are crosslinkable. The ultimate success criterion for this project is adequate X-ray visualization.

Methods

TPU Synthesis

TPU synthetic protocol was adapted from that published by Hearon et al, with a focus on improving the safety and enhanced control over the resulting polymer properties.[14-16] Reaction temperatures were decreased below solvent boiling point and a nitrogen purge was added during the reaction. A triiodobenzene motif was added to the system through the replacement of allyl alcohol (AA) with triiodophenol (TIP) as shown in Figure II-10. The triiodobenzene motif was previously examined in thermoset SMPs, but this is the first translation of this approach to the TPU material.

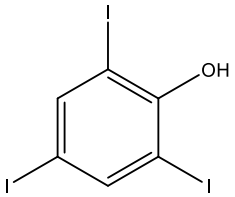

Figure III-2. Triiodophenol (TIP) monomer used as end-capping agent that will impart X-ray visibility to TPU system. This will replace allyl alcohol (AA) in the previous TPU system, which does mean you are losing C=C functionality at the end of the polymer chains.

Originally, 1-5% TIP compositions were piloted (Appendix B). Due to issues with injection molding the 5% TIP compositions and no major payoff in radiopacity, only 1% TIP and 2.5% TIP compositions were pursued further. The compositions used for studies are listed below in Table II-5.

Table III-1. Compositions of TPU used in studies with monomer (%mol) ratios varied.

Composition	TMPAE	DMPD	TIP
1% TIP 10% TMPAE	10	89	1
1% TIP 20% TMPAE	20	89	1
2.5% TIP 10% TMPAE	10	87.5	2.5
2.5% TIP 20% TMPAE	20	77.5	2.5
2.5% TIP 1,6 HD 10% TMPAE	10	87.5	2.5
2.5% TIP 1,6 HD 20% TMPAE	20	77.5	2.5

Gas Permeation Chromatography (GPC)

TPU samples were dissolved in THF at 1-2 mg/mL using a shaker plate overnight. GPC was performed by the Soft Matter Facility at Texas A&M University (College Station, TX) using a TOSOH GPC system equipped with autosampler and

quadruple-detection capabilities. Test conditions were at ambient temperature and the calibration standard used was polystyrene.

Differential Scanning Calorimetry

TPU samples were cut to ~10-15 mg mass and sealed in a Tzero hermetic pan using the Tzero press. A hole was poked in all lids to allow for venting of solvent during run. The DSC run that was used for all samples started by holding isothermal at -20°C for 2 minutes and then ramped 20°C/min up to 250°C. This is held isothermally for another 2 minutes before ramping down to -20°C at a rate of 20°C/min and holding isothermally 2 minutes. The final cycle that is analyzed is ramping back up to 250°C at 20°C/minute.

Injection Molding

Bulk TPU was pelletized by cutting the solvent cast films into small pieces and injection molded using an in-house pneumatically actuated injection mold machine (Figure III-3). Injection molding temperature was optimized according to DSC thermogram for the TPU compositions. Since the TPU is an amorphous thermoplastic, temperatures approximately 100 °C above T_g were used to mold to ensure flow of the polymer. The mold used for samples was an aluminum dogbone that was end-gated (Figure III-4). The dogbone was chosen for use in mechanical testing and X-ray imaging to gather preliminary information.

Figure III-3. Injection mold setup with pneumatically actuated barrel and temperature-controlled hopper.

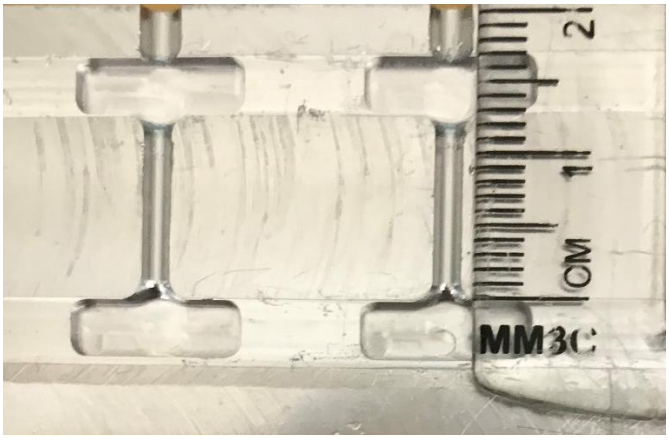

Figure III-4. Picture of mold used for this study. The dogbone shaped mold has a cylindrical gauge in the middle (gauge length is approximately 12 mm as measured on mold).

TPU Crosslinking

Each composition of TPU pellets was dissolved in THF to make a 50wt% solution. The method of crosslinking utilized was thiol-ene click reaction. The crosslinker chosen was the polythiol PETMP. BAPO was used as the UV-initiator and AIBN was used as the thermal initiator. Glass petri dishes for film casting were coated with RainX to prevent polymer adhesion. The FlackTek speedmixer and vortexer was used to combine all elements. For the BAPO crosslinking, mixture was poured into treated dish and UV irradiated for 15 minutes each side. Films were dried overnight before further characterization. For the AIBN crosslinking, mixture was poured into a treated dish and placed in an oven at 80°C for 24 hours.

Electron Beam (E-beam) Sterilization

Sterilization using electron beam irradiation at a target of 37 kGy was performed on bulk thermoplastic and injection molded dogbone samples by the National Center for Electron Beam Research (College Station, TX). Samples were placed in foil header bags (Beacon Converters, Saddle Brook, NJ) and separated based on composition in internal packages. The foil packages were purged with nitrogen gas prior to pulling vacuum to seal using the AVN packaging system (AmeriVacS, San Diego, CA). In most cases, multiple beam passes were required to achieve the 37kGy target level of irradiation. The minimum dose measured from a single run was 9.947 kGy and the max dose was 38.558 kGy. A dosimeter and alanine films arranged near the foil packages measured the actual irradiation dose.

Gel Fraction

Gel fraction was performed on bulk TPU, molded TPU, and crosslinked TPU. Two conditions were tested for crosslinking – use of a UV initiator (BAPO) and used of a thermal initiator (AIBN). For the bulk and molded TPU it was performed pre-and post-sterilization at 37 kGy. Samples were weighed prior to testing for initial weight. Gel fraction was calculated after incubating samples in THF in an oven at 50°C for 48 hours and drying under vacuum for 24 hrs after removing from solvent. Final weight was subtracted from initial weight and reported as a percentage of the initial weight using Equation 4 as described above:

$$\frac{m_1}{m_0} \times 100\% = G_{f.} \quad (4)$$

Thermomechanical Testing

Differential scanning calorimetry (DSC) was used to analyze the polymer compositions. TPU samples of ~10-15 mg mass were hermetically sealed in a Tzero aluminum pan. A hole was poked in the pan top to allow for venting of any remaining solvent during heating cycles. The heating cycle used was equilibrating at -40°C and ramping to 250°C, returning to -40°C and ramping back up to 250°C at a rate of 1 °C/min. The second heating cycle was analyzed because residual solvent was evaporated and material stress in the first heating cycle. TA Instruments software was used for analysis using the T_g selector tool.

X-Ray Imaging

Samples from each composition were injection molded using a simple dogbone mold. All samples were arranged according to composition and imaged using OrthoScan C-arm system (Mobile DI Model 1000-0005). Platinum/irradium (Pt/Ir) and platinum/tungsten (Pt/W) guidewires were used as positive controls, but otherwise the protocol was the same as previously described. Molded TPU samples were imaged to get a baseline image and also imaged through a ½" aluminum plate which served as an analog for X-ray attenuation from skull thickness bone.[53]

As described previously by Nash and Jang, images were analyzed using the grayscale shift method.[8, 55] As published previously, images were converted to 8-bit

grayscale and mean pixel measurements on the sample region (ends of dogbone) and surrounding background were taken in ImageJ using the rectangular selector. The shift was reported as the sample's mean pixel value minus the local background.

Mechanical Testing

Mechanical testing was performed on injection molded dogbone samples for various compositions. Samples were epoxied (Gorilla Glue) to wooden block ends and allowed to dry overnight in a vacuum chamber. Tensile testing was performed on an Instron 5965 with Bluehill software. The crosshead was lowered and the clamps were tightened to the wooden blocks at either end. The force and length was zeroed prior to running all tests and actual gauge length and width was entered into the specimen test protocol. The tests were performed at a 5 mm/min extension rate and run until sample break. Analysis and raw data were exported using Bluehill software.

For recovery analysis, the maximum extension (extension at break) was taken from Bluehill software. Pictures were taken at 1 minute, 15 minute, and 24 hour intervals next to a ruler for scale. Length was calculated for each sample using ImageJ software and used to calculate recovery.

Results and Discussion

Injection Mold

High density polyethylene (HDPE) was used as the negative control for imaging and was molded in the suggested temperature range of 180-280°C at 210°C. All other

compositions were molded approximately 100°C above their T_g since they are amorphous materials and the pelletizing process has not been optimized to help the melt uniformity.

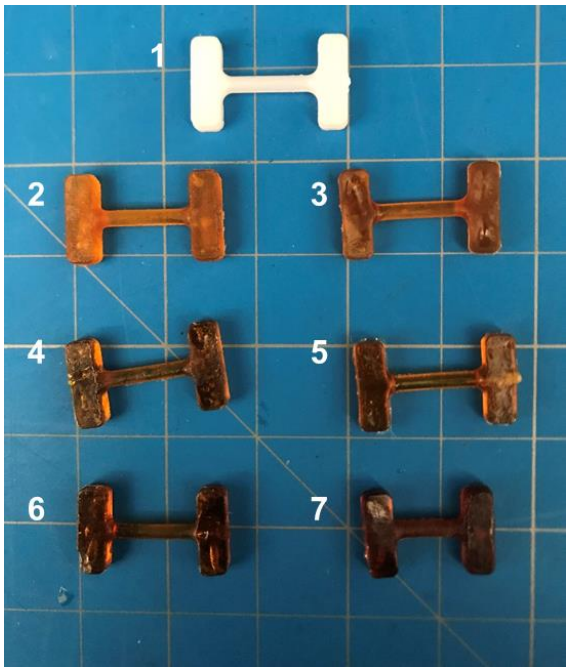

Figure III-5. Picture of injection molded dogbones of TPU compositions: 1) HDPE (control), 2) 1% TIP 10% TMPAE, 3) 1% TIP 20% TMPAE, 4) 2.5% TIP 10% TMPAE, 5) 1% TIP 10% TMPAE, 6) 2.5% TIP 10% TMPAE – 1,6 HD, 7) 2.5% TIP 20% TMPAE – 1,6 HD.

Composition 7 (2.5% TIP 20% TMPAE – 1,6 HD) shrunk after injection molding and continued to shrink over time (Appendix C). It is likely there were residual stresses in the polymer chains or the incorrect temperature was used for this material. This requires further investigation, which is discussed in Appendix C.

Injection molding still needs to be optimized, with much of this happening on the TPU process side. The pelletizing of the TPU in a more consistent manner will improve melt uniformity and prevent some of the bubble formation seen in molded plastic. There

is also likely residual solvent after the drying process, so this needs to be addressed to improve the molding.

Gel Fraction

Gel fraction was performed on bulk samples, molded samples, E-beam sterilized samples, and crosslinked samples to determine if any of the processes induced crosslinking through thermal initiation, electron beam irradiation at sterilization levels, or other means. A gel fraction of 0 indicates that there is no crosslinking present which is what we would expect in the bulk samples and molded samples. A gel fraction of 100 would indicate a 100% crosslinked network, which would be ideal for the crosslinked samples.

Table III-2. Gel fractions (%) reported for different TPU compositions in bulk samples with and without exposure to electron beam sterilization.

Composition	Bulk	Bulk E-Beam
2.5% TIP 10% TMPAE	0	0
2.5% TIP 20% TMPAE	0	0
2.5% TIP 1,6 HD 10% TMPAE	0	0
2.5% TIP 1,6 HD 20% TMPAE	0	0

Table III-3. Gel fractions (%) reported for different TPU compositions in injection molded TPU samples with and without exposure to electron beam sterilization. *Standard deviation not available because samples were combined and dried together due to low weights. <1 designates that it was below the detection limit, which is less than 1% of initial weights.*

Composition	Mold	Mold E-Beam
1% TIP 10% TMPAE	<1	3.4
1% TIP 20% TMPAE	1.5	<1
2.5% TIP 10% TMPAE	5.9	3.6
2.5% TIP 1,6 HD 10% TMPAE	2.7	<1

Table III-4. Gel fractions (%) reported for different TPU compositions post-crosslinking. Crosslinking was done using two initiators – BAPO and AIBN. **Standard deviation not available for AIBN samples because samples were dried together and unable to be separated, so initial sample weights were combined and total remaining weight was recorded.*

Composition	BAPO	AIBN*
2.5% TIP 10% TMPAE	84.9 ± 6.1	72.5
2.5% TIP 20% TMPAE	71.9 ± 8.5	33.2
2.5% TIP 1,6 HD 10% TMPAE	90.5 ± 1.5	63.1
2.5% TIP 1,6 HD 20% TMPAE	94.5 ± 4.9	62.2

The bulk thermoplastic dissolved completely for all compositions tested. There were low gel fractions for the molded and E-beam sterilized molded samples, indicating that the molding process may be inducing some thermal crosslinking. The highest reported gel fraction was 5.9% for the 2.5% TIP 10% TMPAE composition that was molded. In all compositions, the BAPO crosslinked materials had higher gel fractions relative to the AIBN. This means that the system is more effectively crosslinked with UV than thermal initiator under the conditions used. In each group, the 2.5% TIP 20% TMPAE crosslinked compositions had the lowest gel fractions.

Molecular Weight

I focused on compositions with the diol 2,2-dimethyl-1,3-propanediol (DMPD). Hearon et al. previously reported M_n and M_w of 17.0 and 41.4 kDa, respectively, for this polymer composition.[14] A longer diol, 1,6 hexanediol (HD) was incorporated into some compositions as well. Polymer compositions were dissolved in THF at 1-2 mg/mL and analyzed using gas permeation chromatography (GPC) with a THF column and a polystyrene control.

Table III-5. Molecular weight and PDI of compositions of X-ray visible TPU.

Composition	M_n (kDa)	M_w (kDa)	PDI
1% TIP 10% TMPAE	16.9	72.1	4.3
1% TIP 20% TMPAE	16.5	74.4	4.5
2.5% TIP 10% TMPAE	15.8	52.5	3.3
2.5% TIP 1,6 HD 10% TMPAE	9.5	25.9	2.7

2.5% TIP compositions with 20% TMPAE were not able to be run through the GPC column and therefore are not included in Table III-5. The Soft Matter facility scientist who ran these samples reported that they were "impure," so it is likely that the synthesis needs further optimization or the samples were not fully dissolved.

Thermomechanical Testing

Differential scanning calorimetry (DSC) was used to analyze the polymer compositions. TPU samples of ~10-15 mg mass were hermetically sealed in a Tzero aluminum pan. A hole was poked in the pan top to allow for venting during heating

cycles. The heating cycle used was equilibrating at -40°C and ramping to 250°C, returning to -40°C and ramping back up to 250°C at a rate of 10 °C/min. The second heating cycle was analyzed because residual solvent was evaporated and material stress in the first heating cycle.

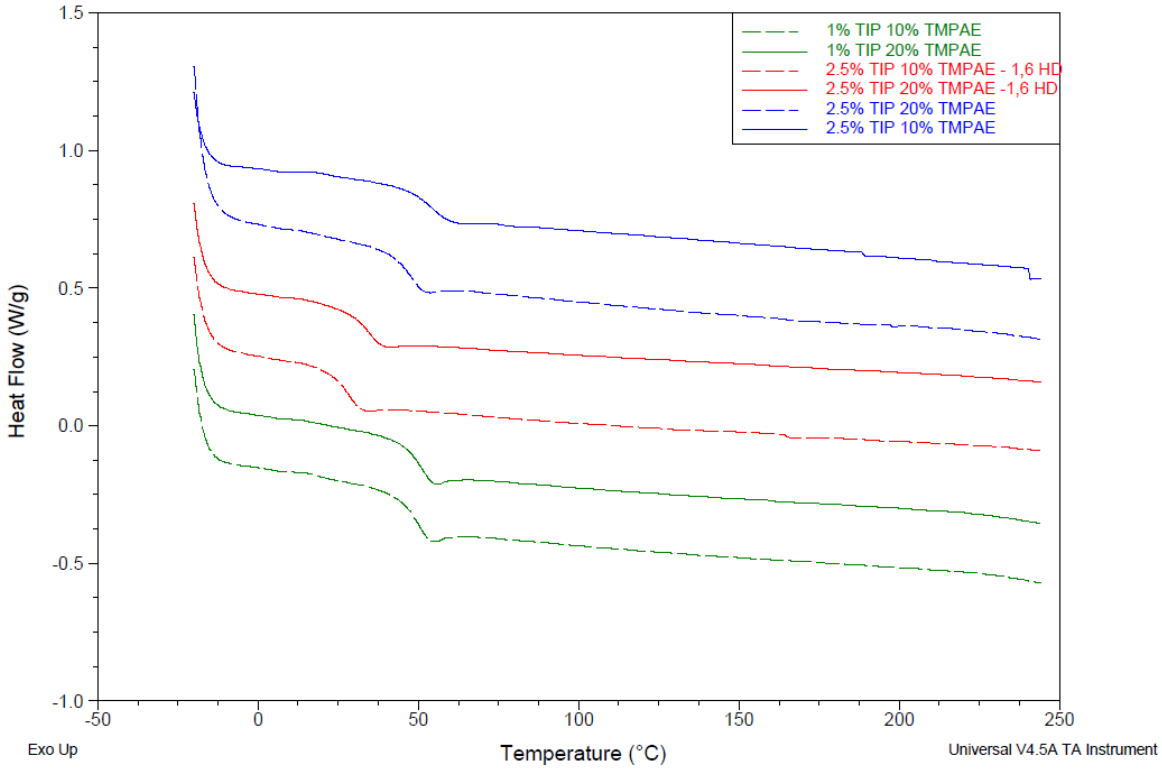

Figure III-6. DSC thermograms of various compositions of X-ray visible TPU as labeled. The addition of 1-6 HD to the compositions lowered the T_g due to increased chain mobility.

All of the compositions containing 2.5% TIP were lower in molecular weight which correlates to a lower T_g. The 2.5% TIP 10% TMPAE 1-6 HD and 2.5% TIP 20% TMPAE 1-6 HD compositions have the lowest T_gs of all the compositions. This is due to the longer diol (hexanediol vs. pentanediol) allowing more movement of the chains.

Table III-6. Glass transition values for X-ray visible TPU compositions.

Composition	T_g (°C)
1% TIP 10% TMPAE	50.3 ± 0.5
1% TIP 20% TMPAE	51.3 ± 0.05
2.5% TIP 10% TMPAE	53.8 ±0.4
2.5% TIP 20% TMPAE	46.9 ± 2.2
2.5% TIP 10% TMPAE, 1-6 HD	28.2 ± 0.2
2.5% TIP 20% TMPAE, 1-6 HD	34.8 ± 0.06

X-Ray Imaging

Baseline and attenuated (1/2" Al plate) X-ray images were acquired using the OrthoScan C-Arm. Baseline image parameters were DAP 1.8410 mGy•cm^2, 63 kVp, 79 µA and the attenuated image parameters were DAP 3.0844mGy•cm^2, 65 kVp, 82 µA. Qualitatively, the 2.5% TIP compositions were the most radiodense samples in both imaging conditions, which is expected due to increased amount of triiodobenzene motifs.

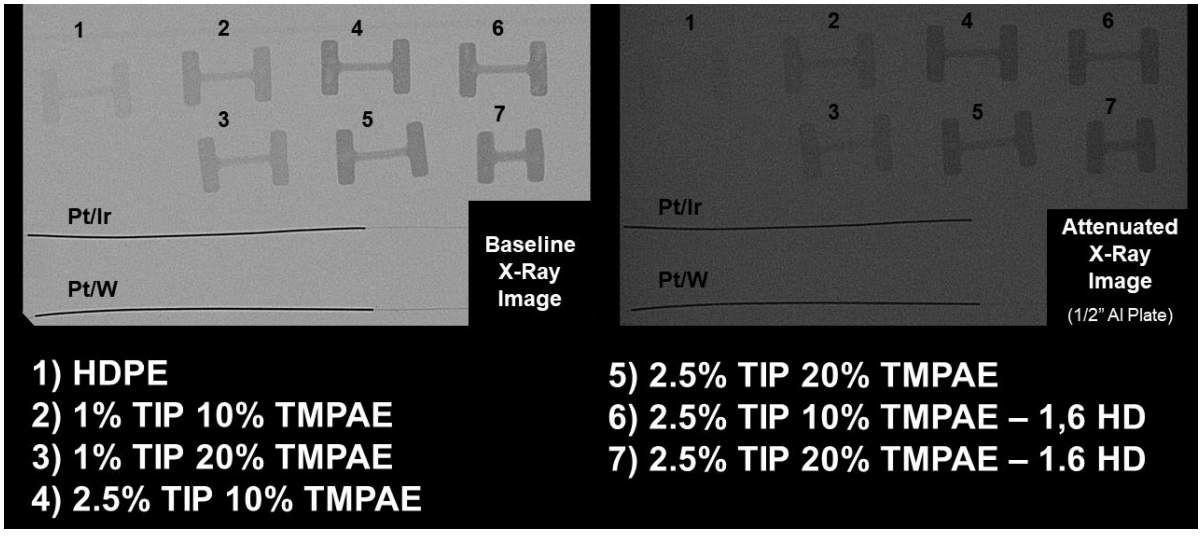

Figure III-7. Baseline and attenuated X-ray images of injection-molded TPU samples taken with the OrthoScan C-arm. High density polyethylene (HDPE) was used as a negative control for these images. 90/10 Pt/Ir and 92/8 Pt/W bare platinum coils (both of

0.008” OD) were used as positive controls. Attenuated images were taken through a ½” aluminum plate to simulate imaging through bone**.**

Images of the injection molded dog bones were analyzed using the grayscale shift method. Specimens were analyzed relative to their surrounding background value to account for image variations locally. Table III-7 outlines the mean grayscale shift values measured for molded samples and controls. There is an increased grayscale shift as the mol% of TIP increases in the samples. Relative to previous work by Nash and Jang, all these values for molded TPU are much higher, but the samples are not low density, porous materials. Previously a grayscale shift value of ~6 in attenuated images was considered adequate visibility and all compositions are at or above that threshold.

Table III-7. Grayscale shift values for X-ray visible TPU compositions, HDPE (negative control), Pt/Ir and Pt/W guidewires (positive controls).

	Specimen	Baseline	Attenuated
1	**HDPE**	6	3
2	**1% TIP 10% TMPAE**	17	7
3	**1% TIP 20% TMPAE**	17	6
4	**2.5% TIP 10% TMPAE**	29	11
5	**2.5% TIP 20% TMPAE**	29	11
6	**2.5% TIP 1,6 HD 10% TMPAE**	31	12
7	**2.5% TIP 1,6 HD 20% TMPAE**	33	12
Pt/Ir	**Platinum/Irradium Guidewire**	131	40
Pt/W	**Platinum/Tungsten Guidewire**	132	40

Electron Beam (E-beam) Sterilization

E-beam was piloted as the sterilization method for these materials due to the previous use in SMP thermoset foam embolic devices.[56] The materials were analyzed by gel fraction to see if the irradiation induced any crosslinking and DSC to see if there was any change in the thermomechanical behavior. Figure III-8 shows thermograms for the

chosen compositions. Figure III-9 and Figure III-10 show direct comparisons of the 1% TIP compositions to their E-beam irradiated samples. There was no major difference in the thermomechanical behavior and lack of crosslinking on bulk TPU was confirmed by gel fractions and FTIR.

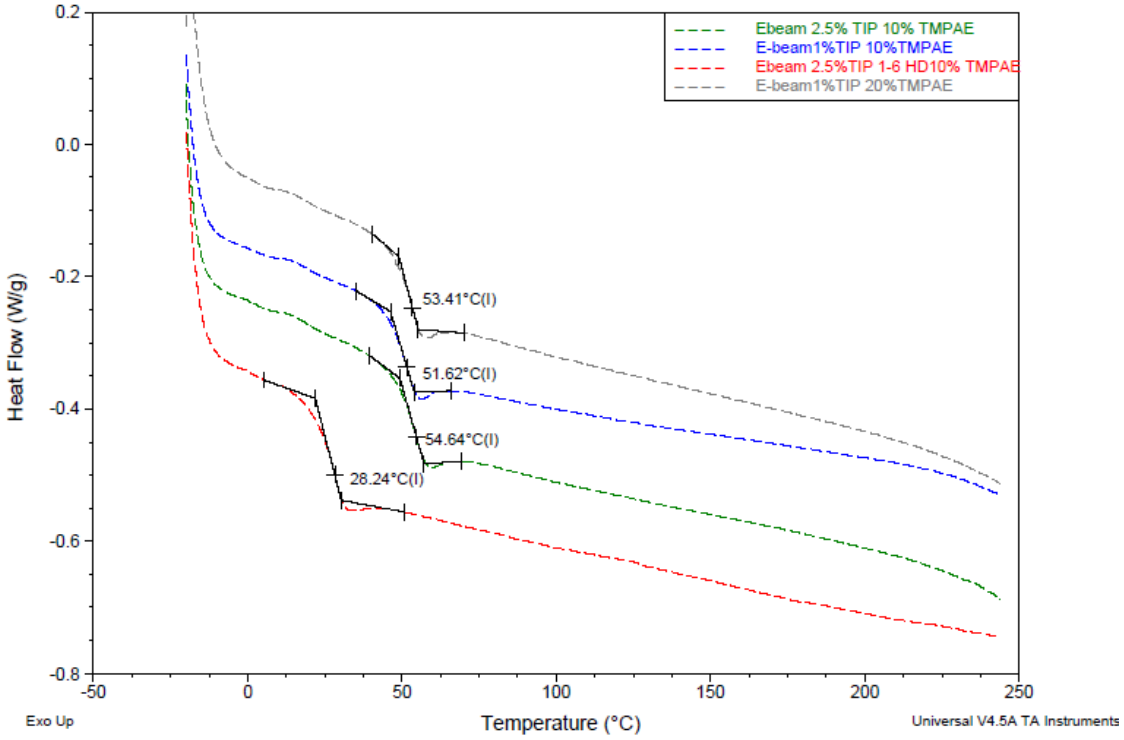

Figure III-8. E-beam was run on 1% TIP, 20% TMPAE (gray), 1% TIP, 10% TMPAE (green), 2.5% TIP, 10% TMPAE (red), 2.5% TIP, 1-6 HD, 10% TMPAE (blue) at an irradiation dosage of 37 kGy and samples were run on DSC to see if there was any change in thermomechanical behavior.

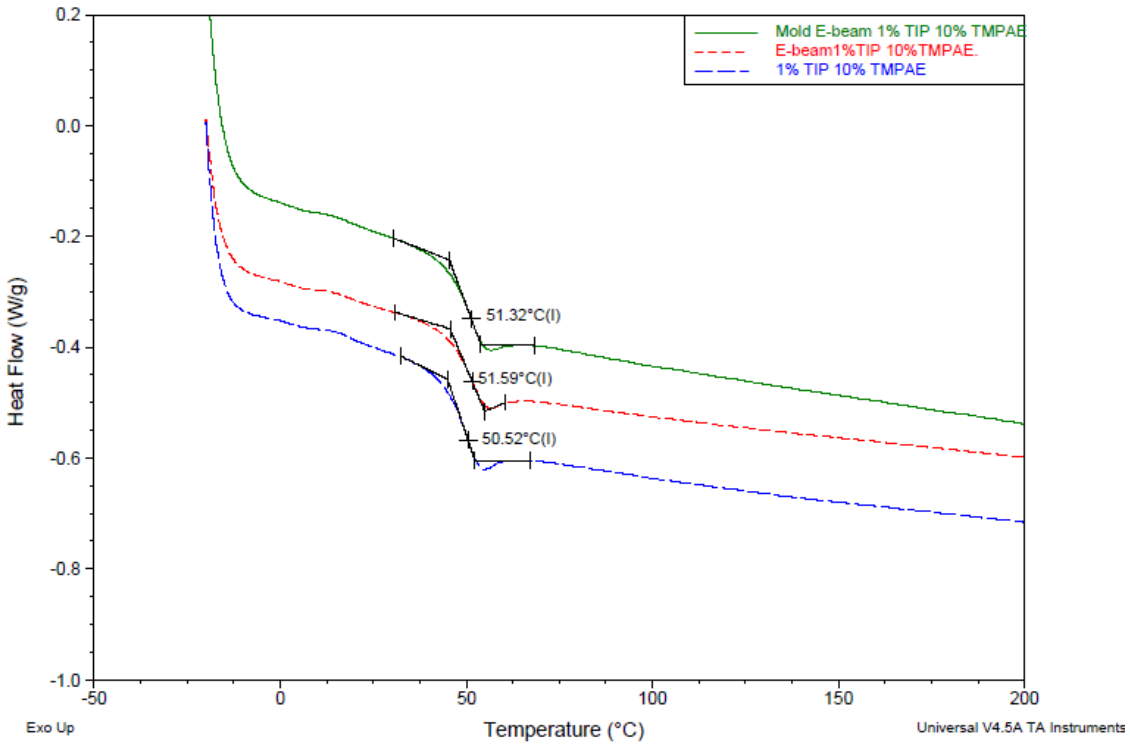

Figure III-9. Direct comparison of 1% TIP 10% TMPAE. Blue is non-sterile bulk sample, green is a molded sample that was subsequently sterilized, and red is a bulk sample that was E-beam sterilization. The values were manually offset, but do not exhbit major differences.

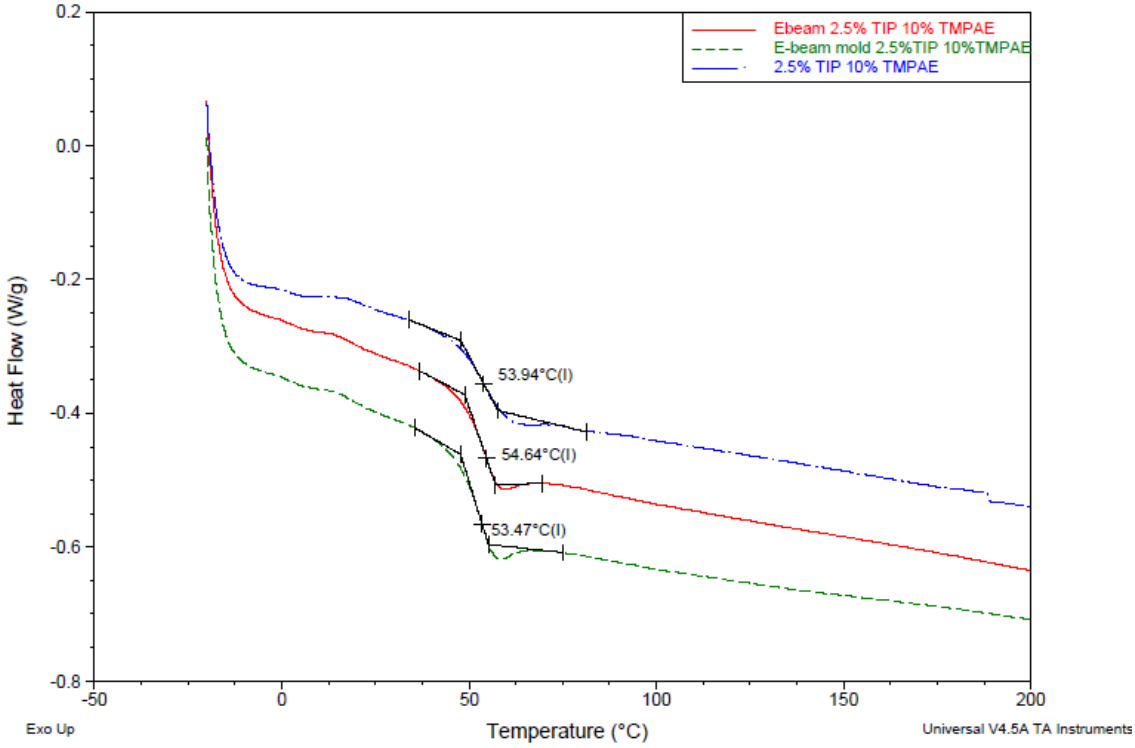

Figure III-10. Direct comparison of 2.5% TIP 10% TMPAE composition. Blue is non-sterile bulk sample, green is a molded sample that was subsequently sterilized, and red is a bulk sample that was E-beam sterilization. The values were manually offset, but do not exhbit major differences.

Tensile Testing

An Instron 5965 (Instron, Norwood, MA) universal testing machine with a 500 N load cell was used to perform tensile tests on dogbone samples. Extension rate for the tests was 5 mm/min. Bluehill software was used for analysis and export of raw data. Figure III-11 shows the stress/strain curve comparisons by composition for base and E-beam specimens.

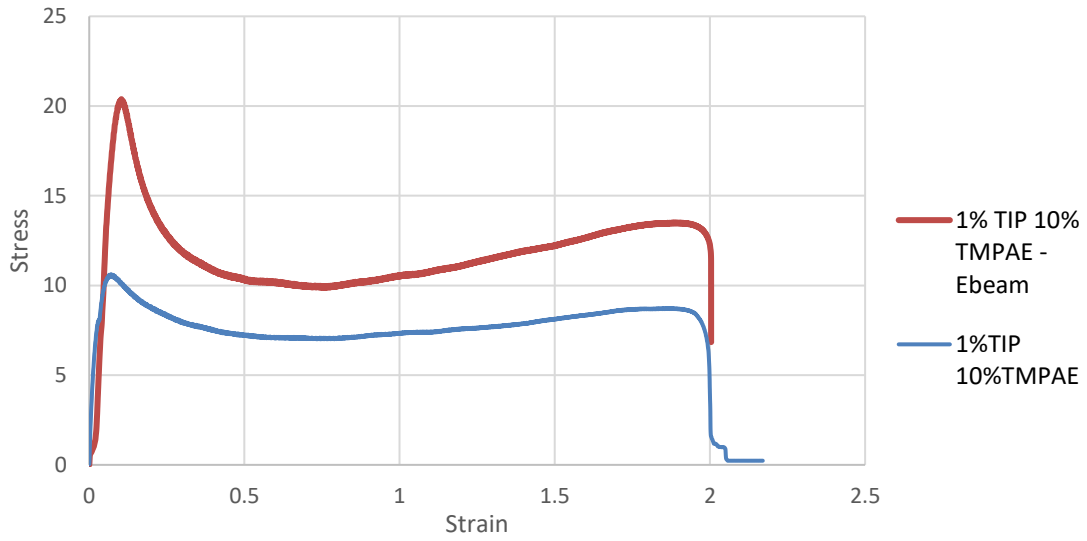

1% TIP 10% TMPAE

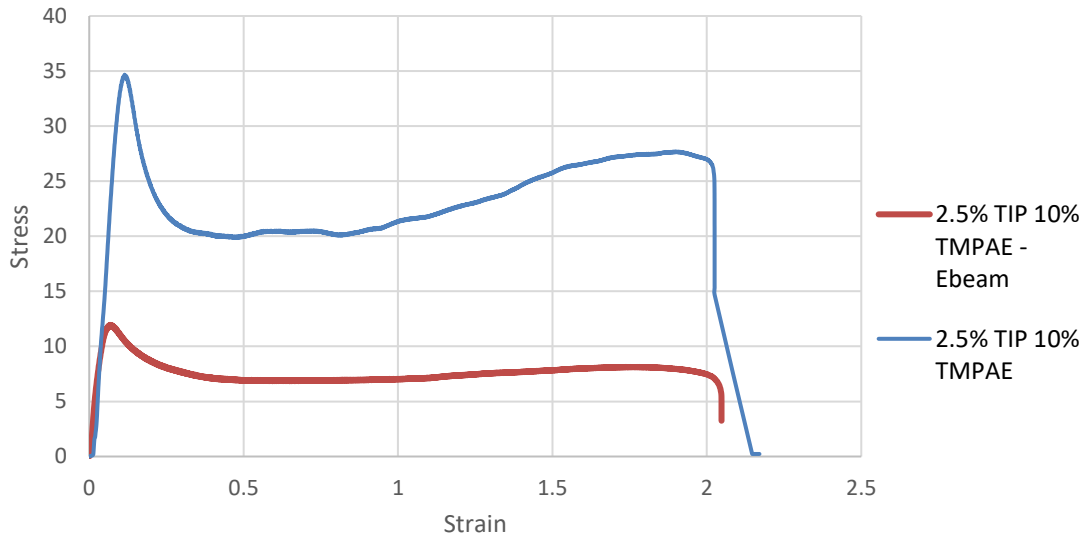

2.5% TIP 10% TMPAE

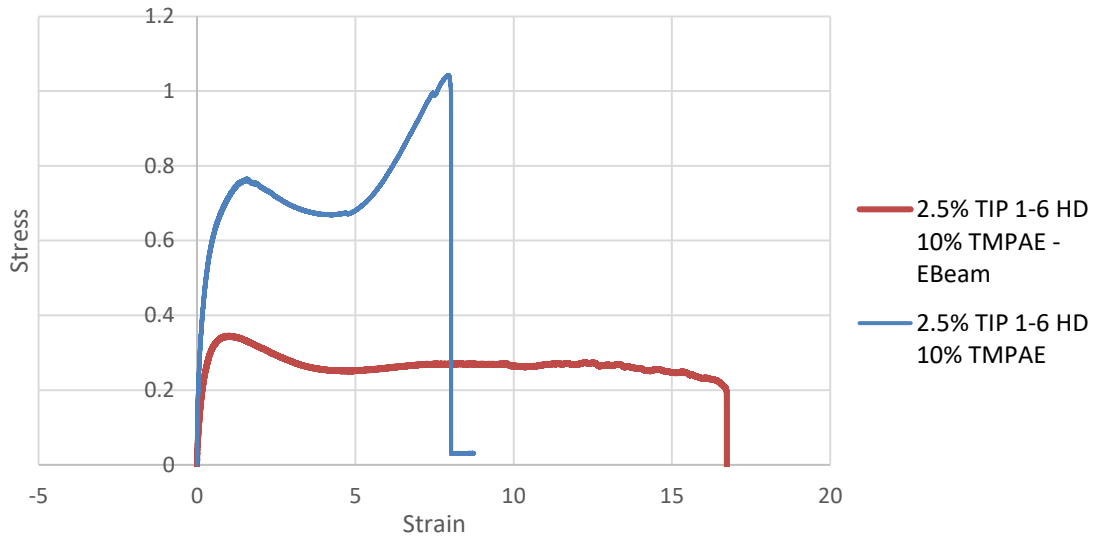

2.5% TIP, 1-6 HD, 10% TMPAE

Figure III-11. Representative Nominal Stress-Strain curves of tensile testing for respective compositions. All compositions are plotted together with the E-beam sterilized versions of the composition. Strain rate was 5mm/min for all experiments.

The highest elongation of samples occurred in the 2.5% TIP 1-6 HD, 10% TMPAE compositions. This is due to the longer diol increasing the viscoelasticity of the material. The 1% TIP 10% TMPAE compositions were very similar in non-sterile and sterilized specimens. It is the only one where the E-beam sterilized version has a higher strength, although the difference is marginal.

Table III-8. Modulus and load at tensile strength of molded compositions exported from Bluehill software. Reported as average calculated from n=3 samples for each composition.

	Modulus (MPa)		**Peak Load (N)**	
	Non-Sterile	*E-beam*	*Non-Sterile*	*E-beam*
1% TIP 10% TMPAE	537.7 ± 189.5	387 ± 93.1	61.9 ± 12.8	81.3 ± 24.5
2.5% TIP 10% TMPAE	388.6 ± 97.4	363.3 ± 188.9	94.0 ± 26.7	48.6 ± 51.5
2.5% TIP 1-6 HD 10% TMPAE	1.1 ± 0.6	1.2 ± 0.5	4.4 ± 2.4	1.6 ± 0.1

Recovery Rate

The recovery after tensile testing was taken by comparing the extension at break and then 1 min, 15 min, and 24 hrs after test. They were allowed to passively recover at ambient room temperature and photographs were taken at time points as shown in Figure III-12 and later analyzed using ImageJ. Table III-9 contains the raw data of the average gauge lengths measured for samples (n=3). In Table III-10, deformation and recovery is reported. Deformation was reported as a percent according to the equation:

$$\left(\frac{l_{ext} - l_0}{l_0}\right) \times 100\%$$

where l_{ext} is the length at extension and l_0 is original gauge length. Similarly, for the recovery of the materials100% recovery would be returning to the original gauge length following this equation:

$$\left(1 - \frac{l_{rec} - l_0}{l_{ext} - l_0}\right) \times 100\%$$

where l_{ext} is the length at extension, l_0 is the orginal length, and l_{rec} is the length it recovered to.

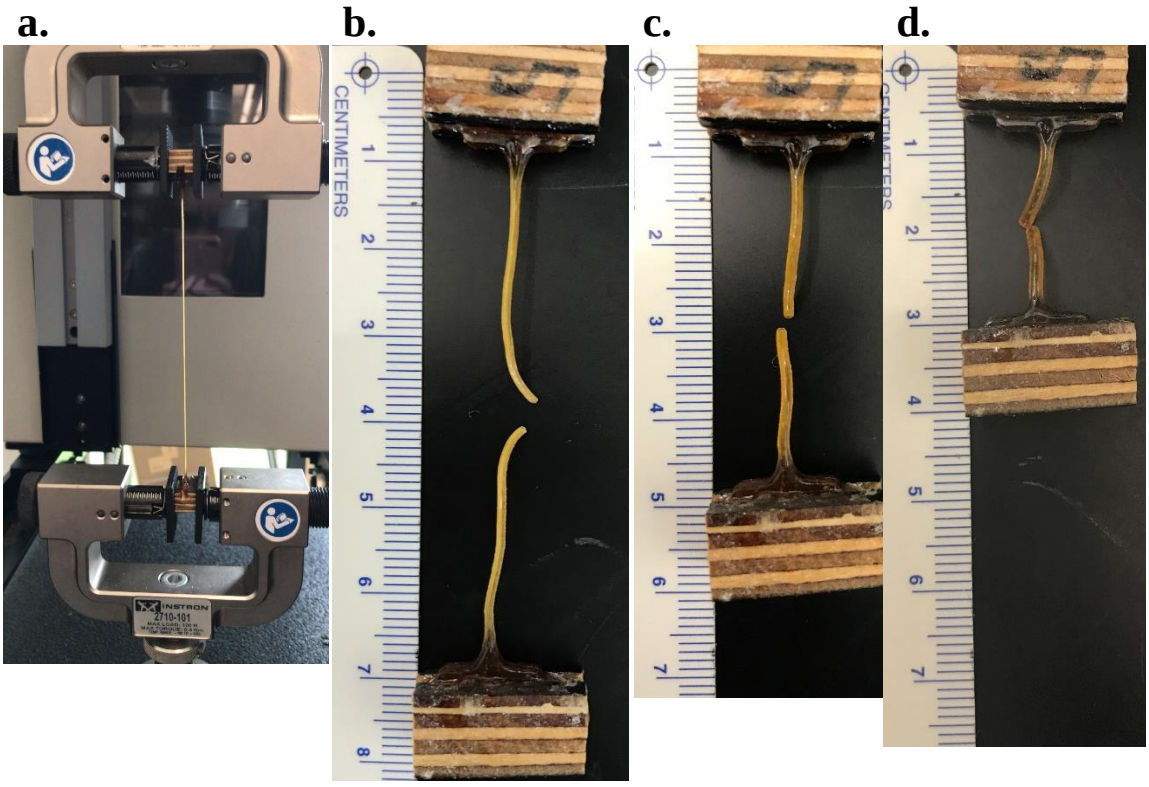

Figure III-12. Passive recovery of polymer test specimens will be monitored: a. max extension (length in testing before break), b. 1 minute after testing, c. 15 minutes after testing, and d. 24 hours after testing.

.

Table III-9. Average gauge length (reported in mm) over time after tensile testing. Extension is the extension prior to break. Original mold gauge length is 12 mm.

	Extension	**1 min**	**15 min**	**24 hrs**
1% TIP 10% TMPAE	28.1 ± 4.8	22.7 ± 3.0	17.2 ± 2.6	12.0 ± 1.4
1% TIP 10% TMPAE E-beam	30.8 ± 6.0	25.2 ± 3.1	22.0 ± 1.6	14.3 ± 1.8
2.5% TIP 10% TMPAE	28.2 ± 4.7	24.0 ± 2.9	19.2 ± 3.3	14.5 ± 0.8
2.5% TIP 10% TMPAE E-beam	32.8 ± 1.3	26.9 ± 3.7	20.7 ± 3.4	14.0 ± 2.0
2.5% TIP 10% TMPAE 1-6 HD	112.9 ± 27.0	67.3 ± 13.9	35.5 ± 6.8	26.9 ± 10.4
2.5% TIP 10% TMPAE 1-6 HD E-beam	202.7 ± 95.8	100.7 ± 45.6	57.5 ± 28.6	36.1 ± 16.6

Table III-10. Percent recovery at 24 hours after tensile testing. Passive recovery at room temperature was monitored over 24 hours in both molded and E-beam sterilized samples. Recovery is percent of length relative to original gauge length of molded dogbone.

	% Deformation		**% Recovery**	
	Non-Sterile	*E-beam*	*Non-Sterile*	*E-beam*
1% TIP 10% TMPAE	134.3%	156.8%	99.9%	87.5%
2.5% TIP 10% TMPAE	135.2%	173.6%	84.3%	90.3%
2.5% TIP 1-6 HD 10% TMPAE	840.7%	1589.6%	85.2%	87.4%

Viscoelastic polymers have had their behavior modeled by the Kelvin-Voigt model which has a damp and a spring in parallel, indicating the viscous (damp) and elastic (spring) duality of the material behavior. The material's response to deformation is dependent on the load as well as the strain rate. For each composition and strain rate, the system may need to be modeled differently. In pilot experiments, the strain rate was 5 mm/min, but some of the tests took more than half an hour for a single specimen so it may be better to increase strain rate moving forward for practicality and to see how this

affects material response. Additionally, the recovery behavior was only observed at room temperature and in future studies should be performed at different temperatures.

Conclusion

Pilot studies of the X-ray visible TPU have shown its potential utility as a biomaterial. The primary criterion for success was adequate radiopacity of the TPU. The mean grayscale shift values of the samples imaged was within the previously established threshold for visibility in an attenuated image. The second criterion for success was injection moldability. All samples were able to be molded, but the compositions with 10% TMPAE were more straightforward to mold. The other factors investigated in these pilot studies were the crosslinking, E-beam sterilization, and mechanical behavior. Crosslinking for this material system was more effective with a UV initiator compared to the thermal initiator used. Electron beam sterilization and molding induced very minimal crosslinking, as shown by the gel fractions of these samples. Finally, the mechanical behavior of these materials is viscoelastic, which is desirable in medical devices due to its similarity to tissue. This material may be useful as a suture or another application requiring viscoelasticity and radiopacity.

CHAPTER IV

DRUG DELIVERY FROM SHAPE MEMORY POLYMERS TO REDUCE LOCAL CANCER RECURRENCE

Background

Motivation

Solid tumors like those in breast cancer are often treated by surgical resection. However, if the margins of the surgical resection are not sufficient to get all of the cancerous cells, patients can experience recurrence. This tumor recurrence may necessitate a second surgical procedure and if site is not monitored and regrowth goes undetected, the recurrence may lead to metastasis. The proposed drug-eluting SMP foam would enable controlled release of chemotherapy drugs locally while aiding in healing the cavity left after tumor resection.

Approach

We synthesized a porous shape memory foam that was coated with polyvinyl alcohol (PVA) and chemotherapeutic agent. Acriflavine was used in initial testing to prove concept of small molecule delivery using a SMP foam matrix. Doxorubicin, an anthracycline antibiotic that induces apoptosis, was chosen as the chemotherapeutic agent of choice because of its broad use in solid organ tumors, specifically breast cancer. It also has a slew of negative side effects, most notably cardiotoxicity, that could be reduced by targeted, local delivery of the agent. Polyvinyl alcohol (PVA) was incorporated to aid in tuning the release profile of the drug from the SMP foam matrix.

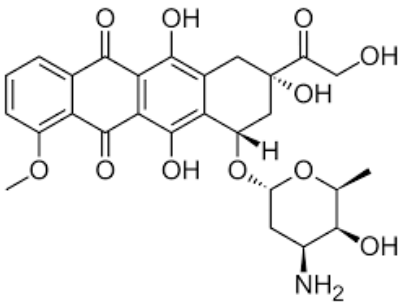

Figure IV-1. Structure of doxorubicin. It is hydrophobic in this state, but becomes water soluble when an HCl group is added (doxorubicin hydrochloride).

Proof of Concept Studies

Methods

SMP Foam Synthesis

SMP foams of two compositions were fabricated to pilot for the drug delivery application. The first composition is TH60 (TMHDI based SMP) and the second is HH80 (HDI based SMP) with the hydroxyl and isocyanate compositions in Table IV-1. All compositions were made from a two-sided polyurethane synthetic protocol originally developed by Singhal et al and later optimized for occlusion applications (synthetic protocol previously described in Chapter II).[4, 12] Side A contained all isocyanate components that were fabricated in a pre-polymer mixture and Side B contained the remaining hydroxyl components, water, catalyst, and surfactants. The sides were combined and a physical blowing agent was added to aid in the gas-blown porous polymerization. Prior to use or characterization of foams, they were allowed to cold cure at room temperature overnight.

All foams in the non-pilot studies were TH60 composition, which was chosen due to its increased hydrophobicity and smaller pore size. Hydrophobicity of the polymer matrix is desired due to the use of doxorubicin. The smaller pore sizes are advantageous in small diameter devices because there are more pores along the width to provide integrity.

Table IV-1. Compositions of PU SMP foams used in this study. Hydroxyl monomers were varied according to the percentages listed. Either HDI or TMHDI were used in 100mol% and are indicated by the first letter of the composition name (H=HDI and T=TMHDI). The second letter (H) of the composition name followed by a number indicates the amount of HPED.

Composition	**Hydroxyl Monomers (mol%)**		**Isocyanate Monomers (mol%)**	
	%HPED	***%TEA***	***%HDI***	***%TMHDI***
TH60	60	40	0	100
HH80	80	20	100	0

Drug and PVA Coating

Polyvinyl alcohol (PVA) was dissolved in water at 80°C. Drug solution 0.017 mg/mL acriflavine was dissolved in 0, 1, 2, 3, and 10% PVA in mass/volume. Acriflavine was used as a model small-molecule analog in these preliminary experiments to reduce cost before concept was proven. The acriflavine stock was 1 mg/mL in DMSO. DMSO has previously been used to depress the T_g of SMP foams as well as swell molecules into them.[57] Doxorubicin hydrochloride (Fisher Bioreagents, Thermo Fisher Scientific) was similarly used to create drug solutions for studies past the pilot. SMP foams of the composition TH60 (n=3) were incubated with the drug/PVA solutions

overnight on a rotator at room temperature. Foams were removed from the respective solutions and subsequently dried in a vacuum chamber for 1 week.

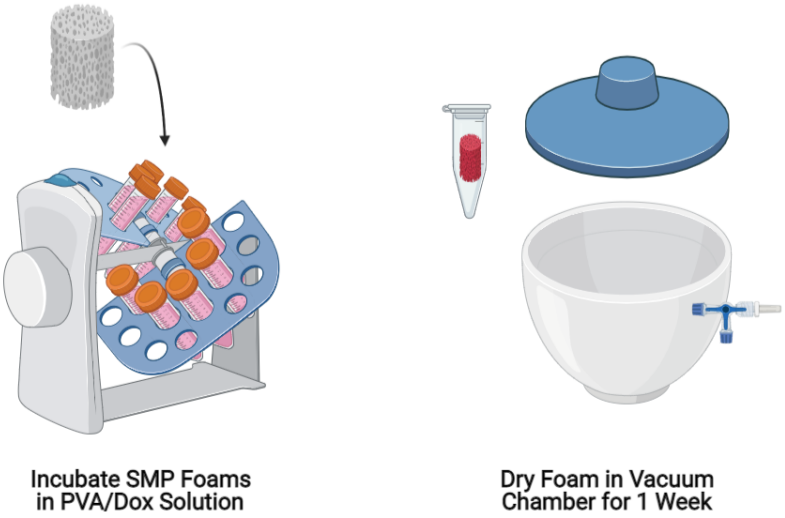

Figure IV-2. Schematic of SMP foam drug coating process. Foams are placed in tubes containing a drug/PVA mixture and incubated for 24 hours. The drug-coated foams are then dried under vacuum for 1 week. *(Created with BioRender.com)*

Preliminary Release Study

Once drug-coated foams were dried, the foam matrices were incubated in 0.4 mL PBS at 37°C for release. The supernatants were removed at various timepoints and the fluorescence was measured at 416/514 nm (Ex/Em) using the plate reader and compared to a calibration curve. The experiment was conducted over 7 days and both non-cumulative and cumulative release was reported.

Temperature-Dependent Viability

Dox solution was prepared at a concentration of 0.08 μM in DMEM HG from an original stock solution of 1 mg/mL in DMSO. 1 mL of the diluted Dox solution was exposed to various temperatures (37, 50, 65, 75 °C) in an oven for 15 minutes and allowed to cool to room temperature in order to model the temperature exposure in crimping SMP foams.

Preliminary Results and Discussion

Preliminary Release Study

Non-cumulative drug release profile shows burst release in the case of the acriflavine 0% PVA between 1 and 2 days. The compositions with higher amounts of PVA show more sustained release over the testing period. Cumulative release profiles show an increase in drug relative to the 0% PVA content. Interestingly, 2% PVA showed the highest cumulative release.

a.

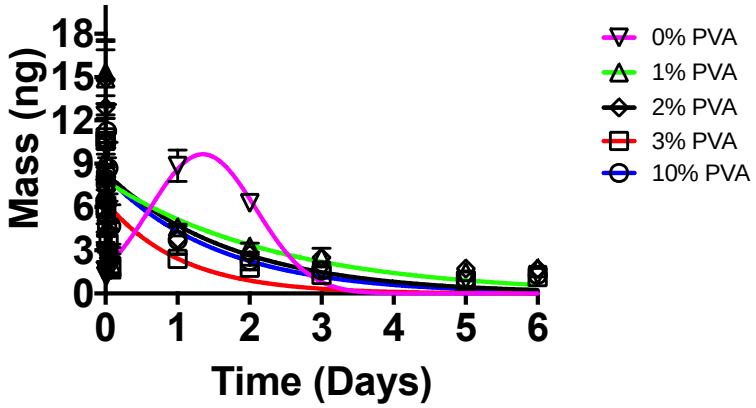

b.

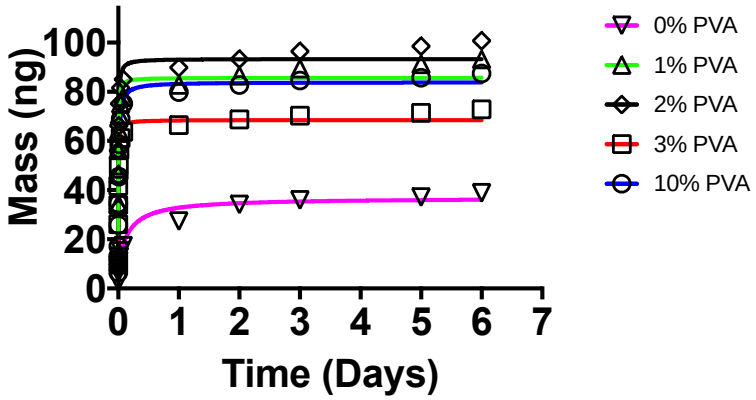

Figure IV-3. a) Non-cumulative and b) cumulative release curves indicate that acriflavine release from TH60 shape memory foams increased with increasing PVA concentration. *Data courtesy of Shreedevi Arun Kumar*

Drying Time Comparison

Confirmation of the drying procedure and the drying time was done using DSC. The dry T_g's of 10% PVA containing SMPs were compared for 1 week and 1 month drying time. This study was performed to ensure that the foams are adequately dry from a drying in a vacuum chamber and another approach like lyophilization is not required.

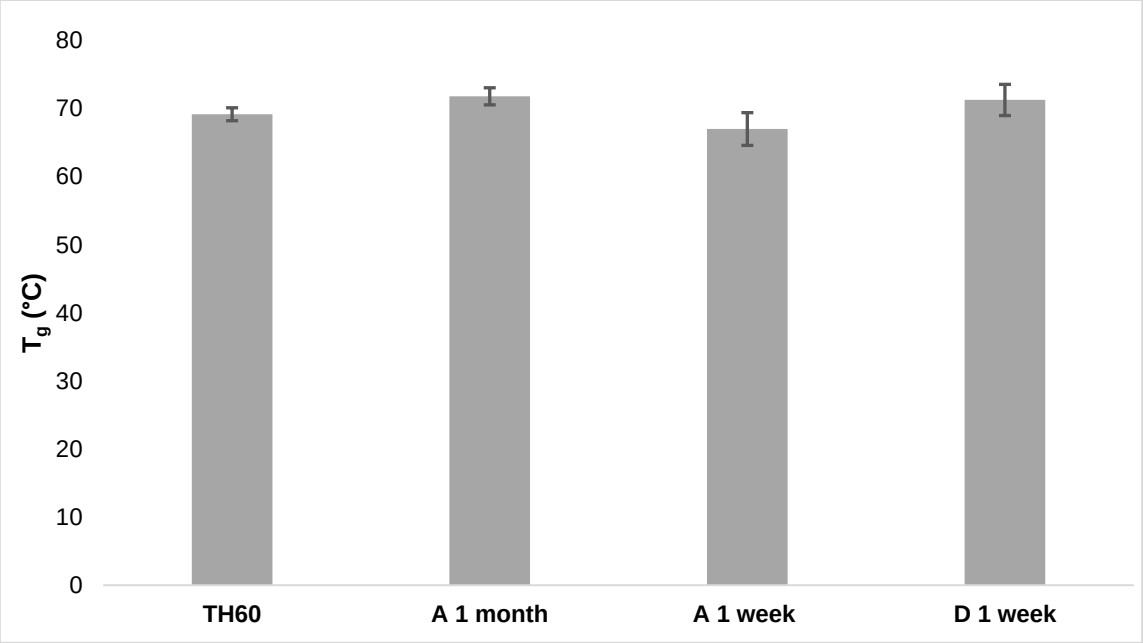

Figure IV-4. Average T_g (n=3) for various drying times compared to TH60 foams. Error bars represent standard deviation. A=acriflavine, D=doxorubicin.

All of the drug-containing compositions used in this study were with 3% PVA and respective drug. TH60 foams with no drug and 3% PVA were used as the control. Acriflavine was used to test the two timepoints because it is a less expensive drug than doxorubicin. It was confirmed that the 1-week drying time was acceptable for doxorubicin as well (Figure IV-4).

Temperature-Dependent Viability

The foam must be heated in order to radially crimp into a secondary, compressed geometry. A variety of temperature conditions were tested to ensure that the equivalent exposure (15 min) to high temperatures does not decrease the drug efficacy. Foams were exposed to 37, 50, 65, 75, 85, and 100 °C conditions for 15 minutes and allowed to cool

to room temperature to simulate the crimping. The metabolic activity was measured via a MTS proliferation assay using the MCF-7 breast cancer cell line. Metabolic acitivity did not decrease relative to room temperature (25°C) until 100°C where only 10% metabolic activity is seen. Metabolic activity was also previously measured for a lower range of temperatures (25, 50, 60, 70°C) using the SKOV ovarian cancer cell line and that cell line was not as susceptible.

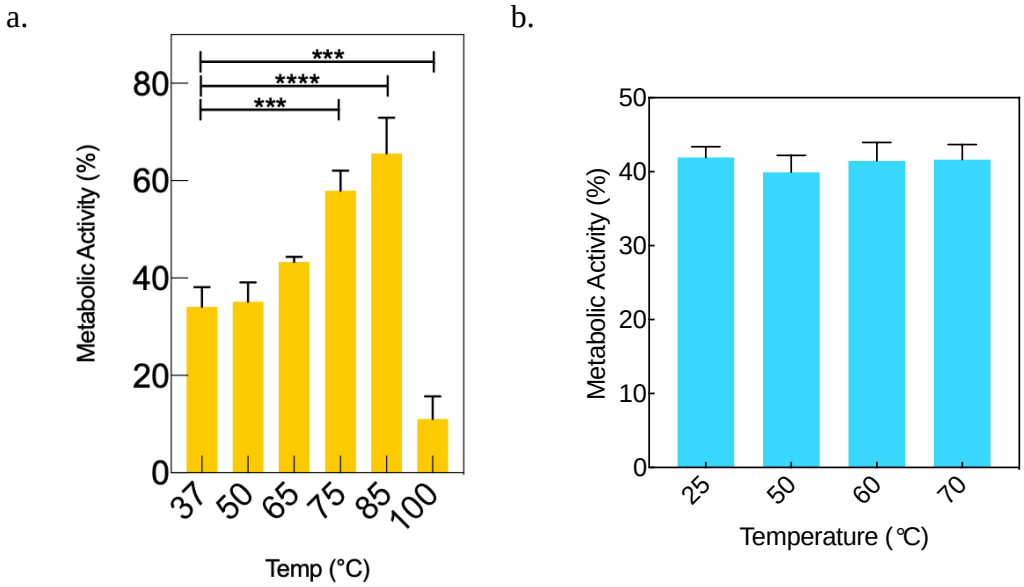

Figure IV-5. Temperature dependence on a) MCF-7 cell viability b) SKOV cell viability. Samples were incubated at indicated temperatures for 15 minutes to simulate exposure. *Data courtesy of Shreedevi Arun Kumar*

Drug Loaded *In Vitro* Characterization Studies

Thermomechanical Characterization

The thermomechanical characterization protocol is two steps. The first is running dynamic scanning calorimetry (DSC) to get the glass transition temperature of the foams. The next step is to crimp the foams axially over wires and allow them to passively expand in a water bath at body temperature. These expansions are monitored at predetermined time intervals. The protocol is represented in Figure IV-6 and more details on both steps are included below.

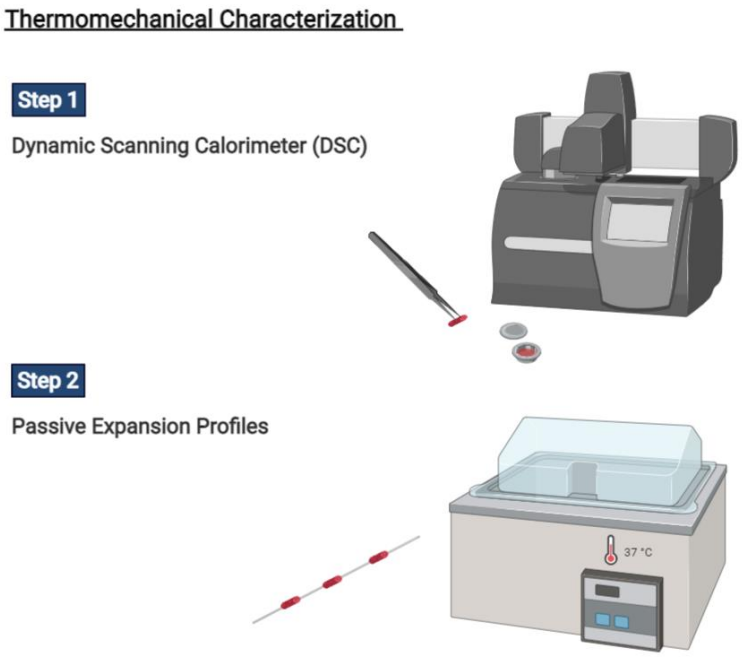

Figure IV-6. Outline of thermomechanical characterization protocol. Dynamic scanning calorimetry (DSC) is used to determine the glass transition temperatures of SMP foam-drug compositions. Passive expansion profiles are performed on crimped foams in a water bath at body temperature (37°C). *(Created using BioRender.com)*

Glass transition temperatures depended on PVA concentration coating. The 10% PD had the lowest dry T_g. The PVA is playing a role in depressing the T_g. This is possibly due to these samples being more difficult to dry and remaining solvent from the drug coating process.

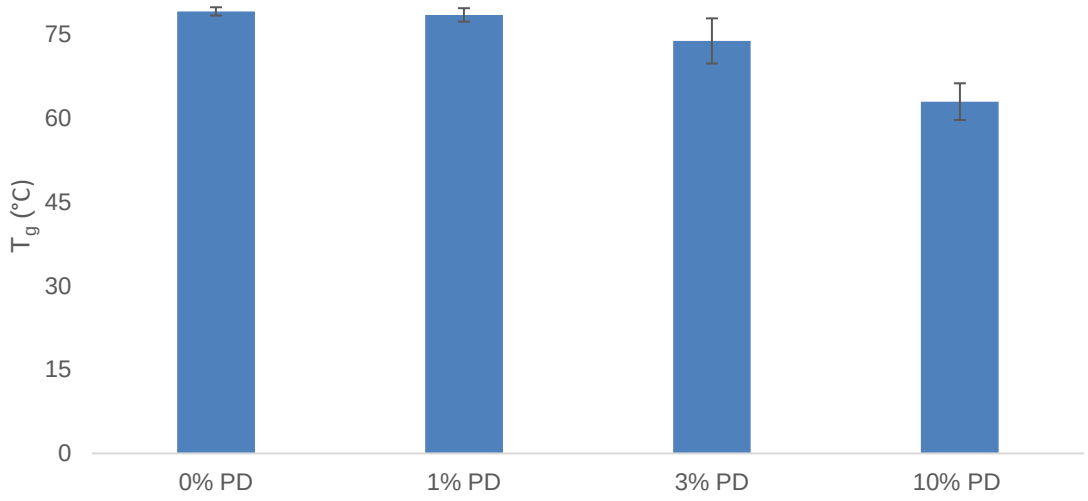

Figure IV-7. Average dry T_g of SMP foams containing various amounts of polyvinyl alcohol (PVA) and doxorubicin drug. With increasing PVA amount, T_g is depressed.

The next step for the drug-coated SMPs will be optimization of sterilization and characterization to determine if the E-beam process negatively affects the thermomechanical behavior of the foams or the efficacy or release profile of the drug.

Electron Beam Sterilization

Electron beam sterilization was performed on packaged foams. The foams were run through multiple beam passes to get a cumulative target dose of 37 kGy irradiation. Actual doses from a single run ranged from 9.947 to 38.558 kGy. The 37 kGy irradiation

was chosen as it is the higher end of irradiation dosage used on sterilizing SMP devices and starting at the higher end range before the sterilization procedure has been validated is a conservative approach.

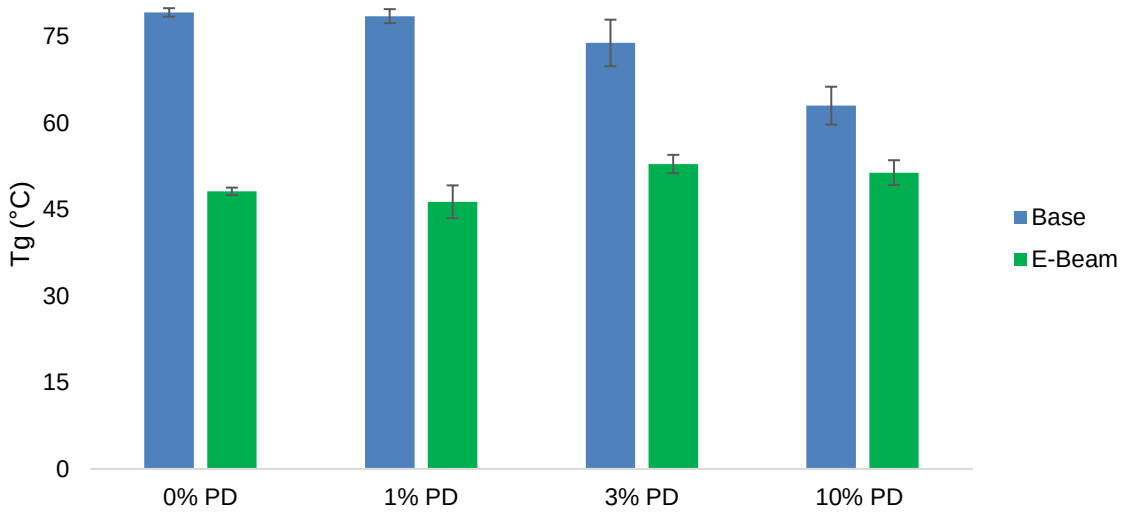

Figure IV-8. Changes to T_g of base foams after E-Beam sterilization at 37 kGy. DSC measurements (n=3) were compared for 0, 1, 3, 10% PD.

There was a decrease in T_g after E-beam sterilization that was seen in all compositions (0, 1, 3, 10% PD) such that all foams were in a much tighter range of ~46-53°C (Figure IV-8. **Changes to T_g of base foams after E-Beam sterilization at 37 kGy. DSC measurements (n=3) were compared for 0, 1, 3, 10% PD.** The decrease was the least in the case of the 10% composition. In order to decouple this T_g decrease from the foam, this was also compared for bare foams pre- and post-sterilization (Figure IV-9) which showed no decrease in T_g. Therefore, this change must be due to the Dox

since it was also seen in the 0% PD foams which do not contain PVA. Follow-up studies to determine whether this affected the action of Dox are needed.

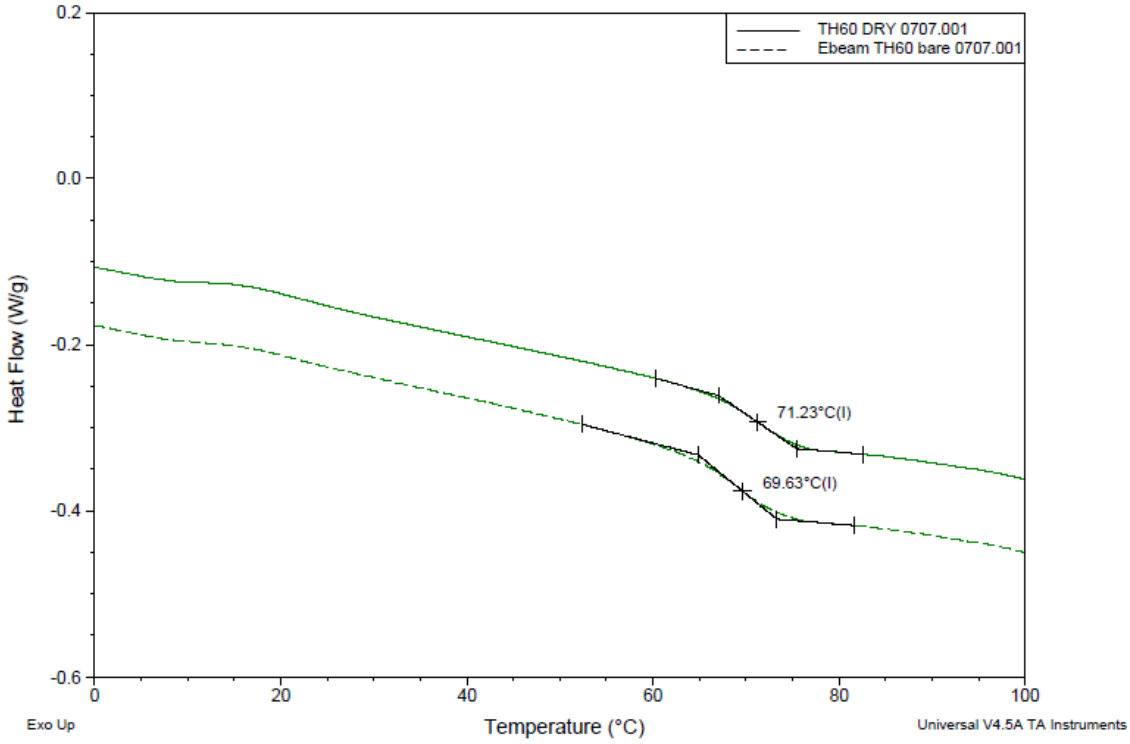

Figure IV-9. DSC thermogram comparing bare foam pre- and post-sterilization via E-beam irradiation at 37 kGy. This confirms that the depression of T_g after E-beam that is seen in the foams is not happening at the SMP foam level.

Passive Expansion Profiles

Expansion studies were conducted first to compare the TH60 bare foam, 3% PVA compositions with Doxorubicin and Acriflavine. The study was terminated at 30 minutes since that is too long for expansion, but both the Acriflavine and Dox foams had not reached 100% expansion at 30 minutes when the bare TH60 foams had reached 100% . Ideally, the foams would expand in 10 minutes or less for clinical translation.

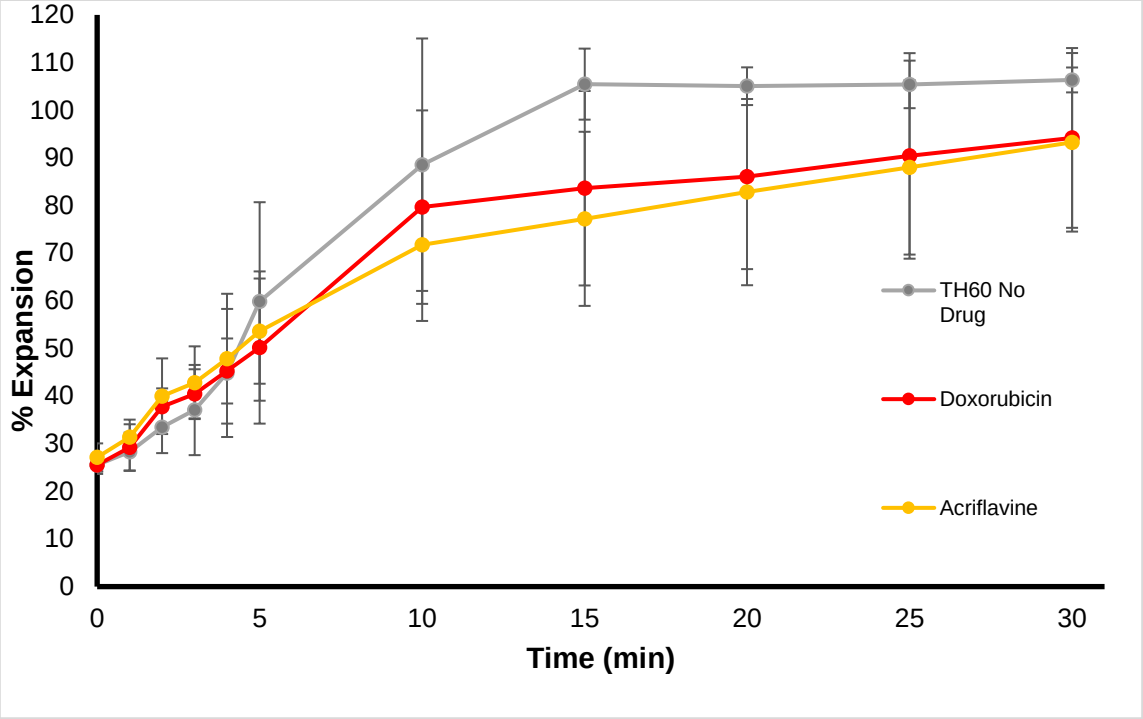

Figure IV-10. Passive expansion profiles of bare foams, Dox and Acriflavine loaded foams. The fastest expansion was seen in the bare foams, and the drug loaded foams did not reach 100% expansion within the 30 minute testing window.

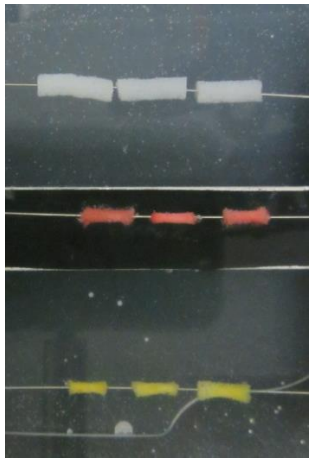

Figure IV-11. 15 minute time point image of passive expansions in water bath (37°C). White=bare TH60 foam, red=Doxorubicin, yellow=Acriflavine. The middle bar is 13 mm for scale.

A follow-up study was performed on the 4 compositions of PD foams that were characterized later in the study (0%, 1%, 3%, and 10% PD) and summarized in Figure IV-12. The quickest to expand were the 10% PD foams due to the increased PVA content which undergoes some swelling as well as the hydrophilicity which keeps water near these foams.

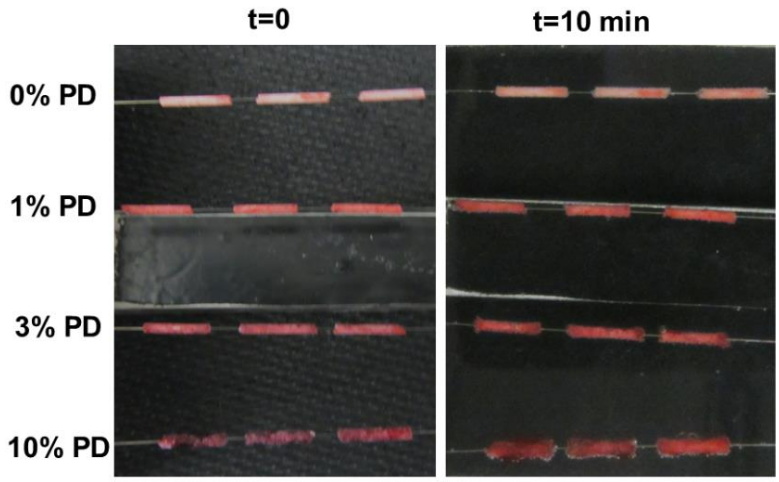

Figure IV-12. Timepoints of drug-loaded SMP expansion studies performed in 37°C waterbath. Increasing PD content increased the expansion rate of the SMP foams. This is likely due to the hydrophilic character of PVA as well as swelling seen in the PVA coating on top of the foam expansion. The middle bar on the image is 13 mm.

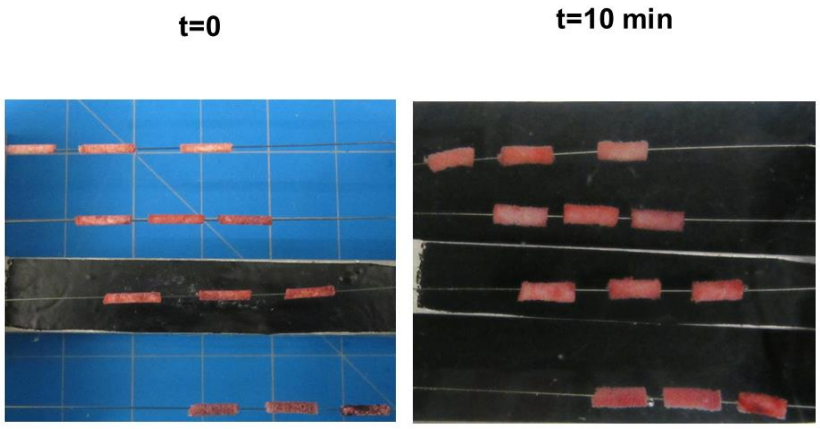

Figure IV-13. Timepoints of E-beam sterilized drug-loaded SMP expansion studies performed in 37°C waterbath. All compositions were fully expanded at 10 minutes. This decrease in expansion time relative to non-sterile compositions is due to the decrease in T_g. The middle bar on the image is 13 mm.

Table IV-2. Expansion (%) at 10 minutes for non-sterile and E-beam sterilized compositions. This study was performed in a 37°C water bath with foams (n=3) of initial diameter of 3mm.

	Non-Sterile	**E-Beam**
0% PD	47.0 ± 4.1%	104.1 ± 8.0%
1% PD	48.9 ± 4.7%	106.2 ± 5.3%
3% PD	59.9 ± 9.1%	106.5 ± 5.9%
10% PD	84.5 ± 9.7%	116.1 ± 13.9%

Imaging of Drug-Coated SMP Foams

Keyence images and SEM images were taken of cross sections of 3mm diameter SMP foam cylinders coated with various amounts of the PVA/drug mixture. The Keyence images (Figure IV-14) are a high-resolution color image that shows the distribution of coating along the cross-section of the foams. SEM images (Figure IV-15) show the surface of the 10% foam showing a thorough coating of the PVA/drug mixture.

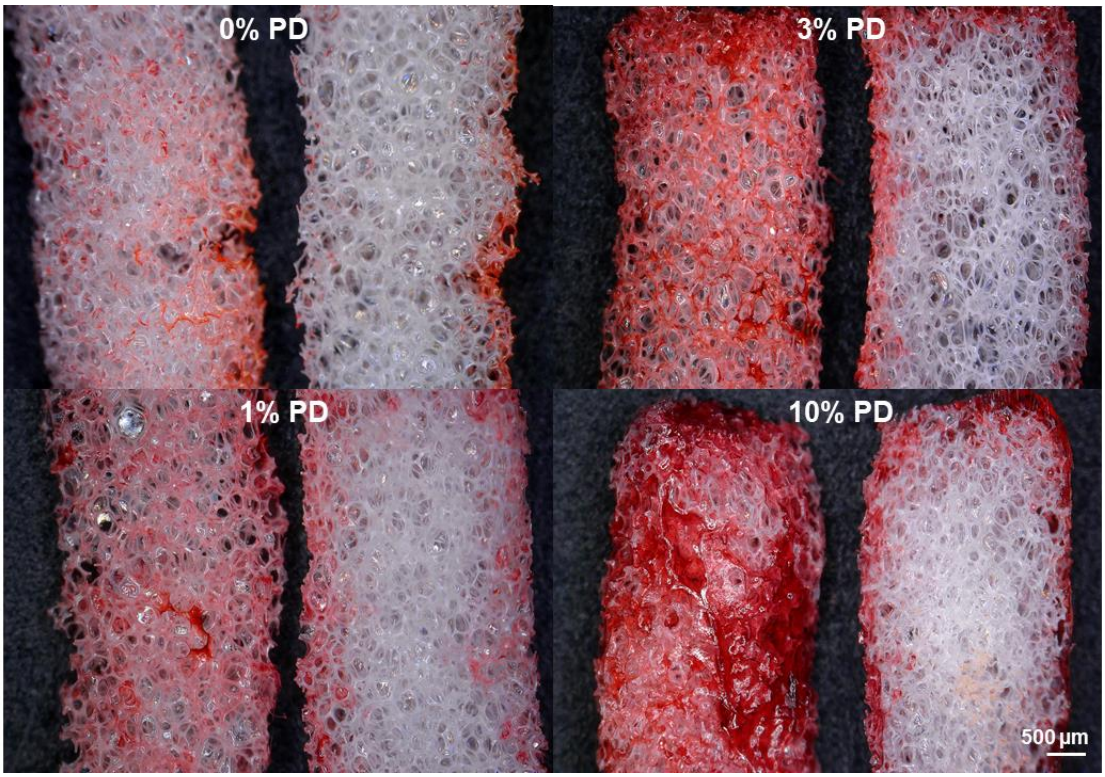

Figure IV-14. Keyence images of cross-sections of 3mm diameter foams with various amounts of PVA/Dox (PD). The doxorubicin is red in color and is visible on the SMP foam with 0% PVA. As the amount of PVA increases, the coating is thicker and more drug is attached to the foam.

	Outer	Inner
10% PD	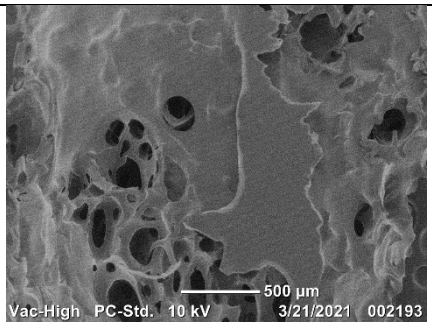	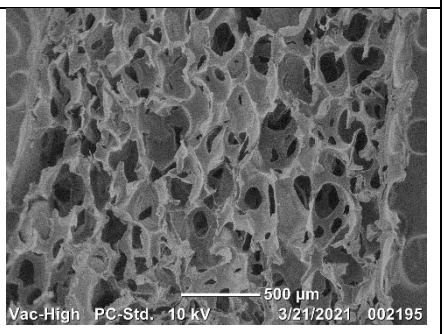
3% PD	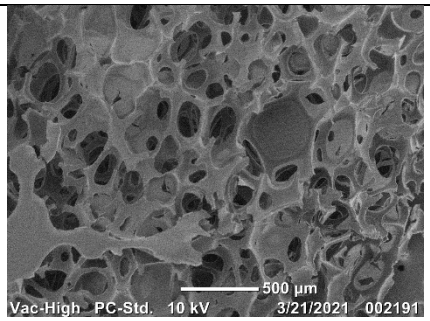	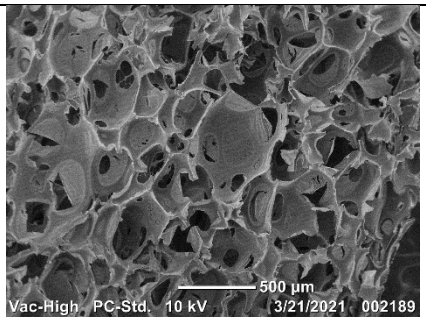
1% PD	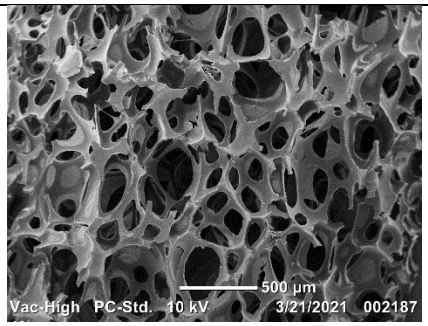	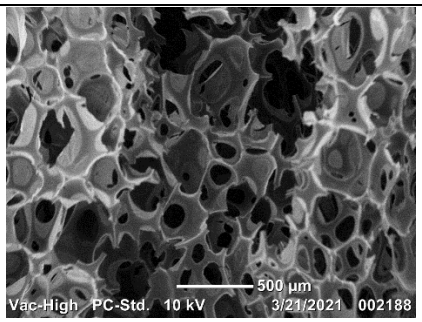

Figure IV-15. Scanning electron microscopy (SEM) images of cross-sections of the 10% PD, 3% PD, and 1% PD foams. The outer surface of the 10% PD composition is thoroughly coated with the PVA/drug mixture.

Crimping

Cylindrical foam punches (3mm diameter) were crimped radially after sitting in the barrel for 15 minutes at 65°C using a Machine Solutions SC250 stent crimper. The foams were cooled to room temperature while the barrel was closed. Foams were allowed to sit at room temperature in a dry environment for 48 hours before handling for experiments to prevent premature expansion.

For proof of concept of injection feasibility, crimped punches were inserted into needles of various gauge sizes. The 0% PD composition fit into an 18 G needle, while the 10% PD composition fit into a 16 ½ G needle. This is due to the thicker PVA coating on the 10% PD composition. Keyence images of each instance were taken (Figure IV-16) and diameters of crimped foams were recorded.

Figure IV-16. Keyence image of Dox-loaded SMP foams in needles for injection. The right-hand side shows a 0% PD foam that is loaded into an 18G needle. The left-hand side of this image shows the 10% PD foam that is loaded into a 16 1/2 G needle. In order for some procedures to be considered "non-invasive" it must be injected from a needle of 18 G (or higher gauge, smaller diameter). Our study design for the intended application in breast cancer does not necessitate injection, and this is just a proof of concept for future work where this may be desired.

Metabolic Activity of Compositions

The metabolic activity of the 0, 1, 3, 10% PD foams were determined from indirect exposure using an MTS assay at time points over a 2-week period. As previously described, MTS/PMS reagent is added to cell culture media and incubated with cells in a 96 well plate for 3 hours in culture conditions (37°C incubator with 5% CO_2). The plate is shaken and read at 490 nm. The metabolic activity is calculated relative to the control (MCF-7 cells with DMEM).

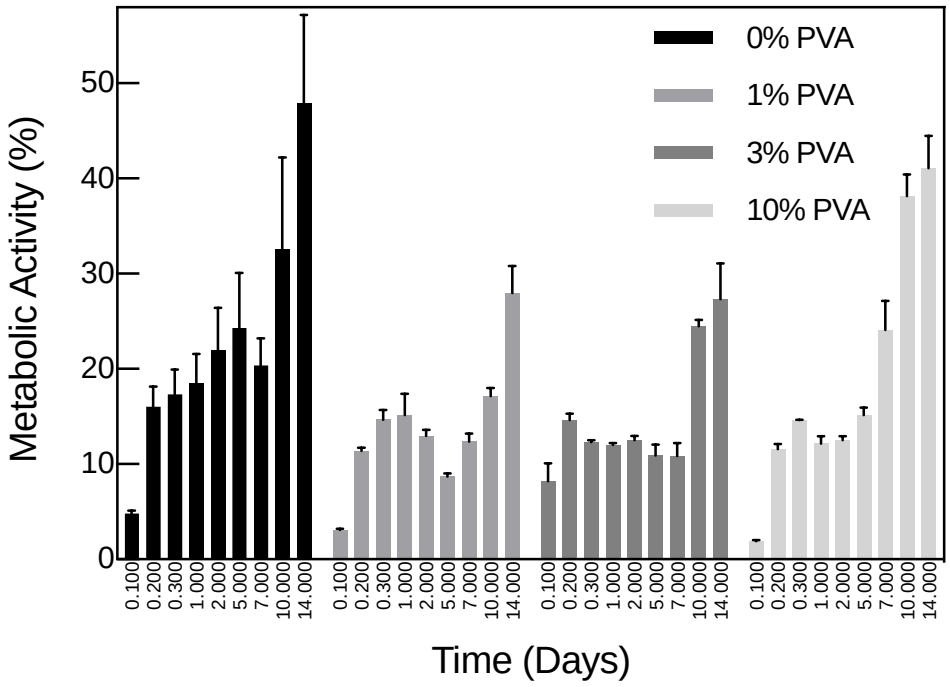

Figure IV-17. Metabolic activity of SKOV cell line over 14 days of exposure to drug-coated SMP compositions. The metabolic activity is inversely proportional to the efficacy of the drug-coated SMP devices. *Data courtesy of Shreedevi Arun Kumar*

Apoptosis Assay

A caspase activity assay (Caspase-Glo® 3/7 Promega, Madison, WI) was used to measure the cell's apoptotic activity after exposure to supernatants containing Dox. This is particularly important in the case of Dox, because the drug has demonstrated an apoptotic mechanism and it is important to characterize this effect in our device's efficacy and how long this activity lasts after implantation.

High apoptotic activity was observed in both 0% PD and 10% PD compositions at Day 0, but 10% PD was the only composition to maintain the apoptotic activity over 7

days (Figure IV-18). These results show that in the 10% PD composition, we were able to achieve sustained release and is a promising result for translation of this technology.

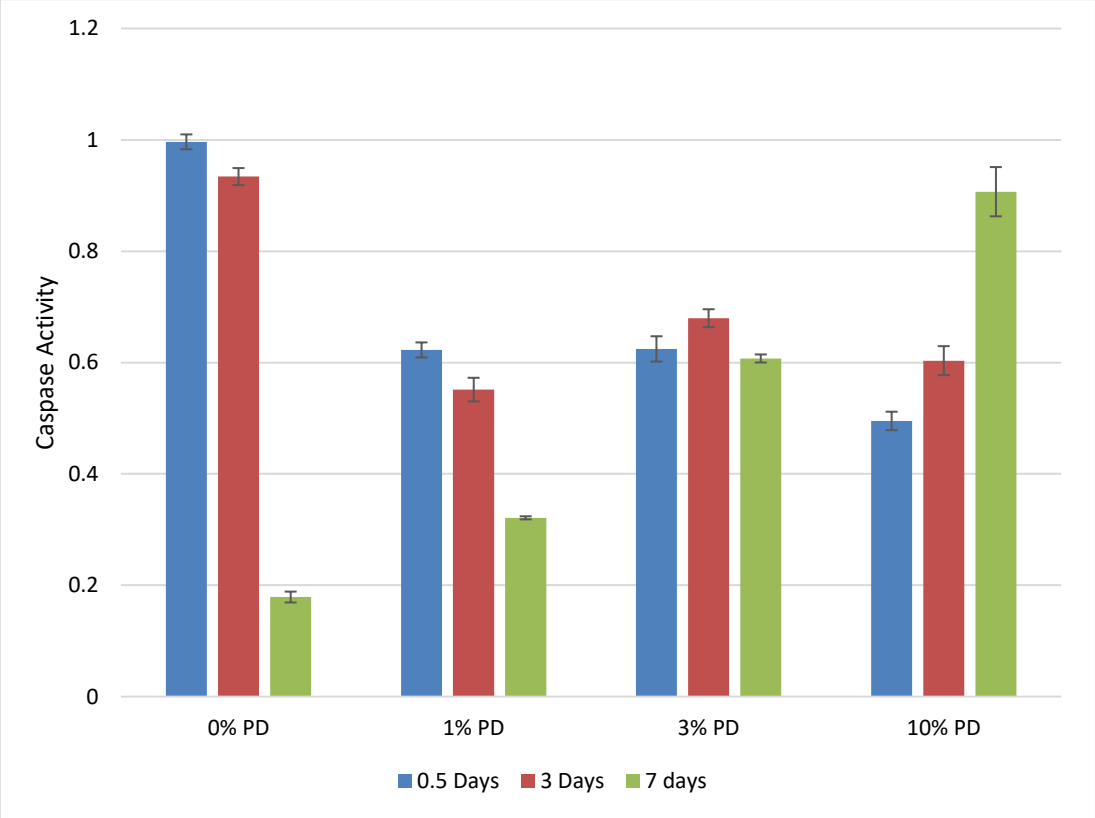

Figure IV-18. Results from caspase assay measuring the apoptotic activity of the drug-coated foam at designated time points (0.5 days, 3 days, and 7 days). The assay was conducted with samples of n=3 for each composition and timepoint. Doxorubicin works is an apoptotic molecule, so it is important to quantify how long the apoptotic activity lasts. Peak apoptotic activity was reached in the 10% PD composition at 7 days. *Data courtesy of Shreedevi Arun Kumar*

Drug Release Study

The release study was conducted over a period of 3 weeks (21 days). The supernatant from each timepoint was retained in a freezer (-80 °C) until the study was terminated so that all could be run at once. Frozen supernatant samples were thawed

prior to use in cellular studies or analysis. The mass of drug was calculated from a calibration curve for fluorescence as described above.

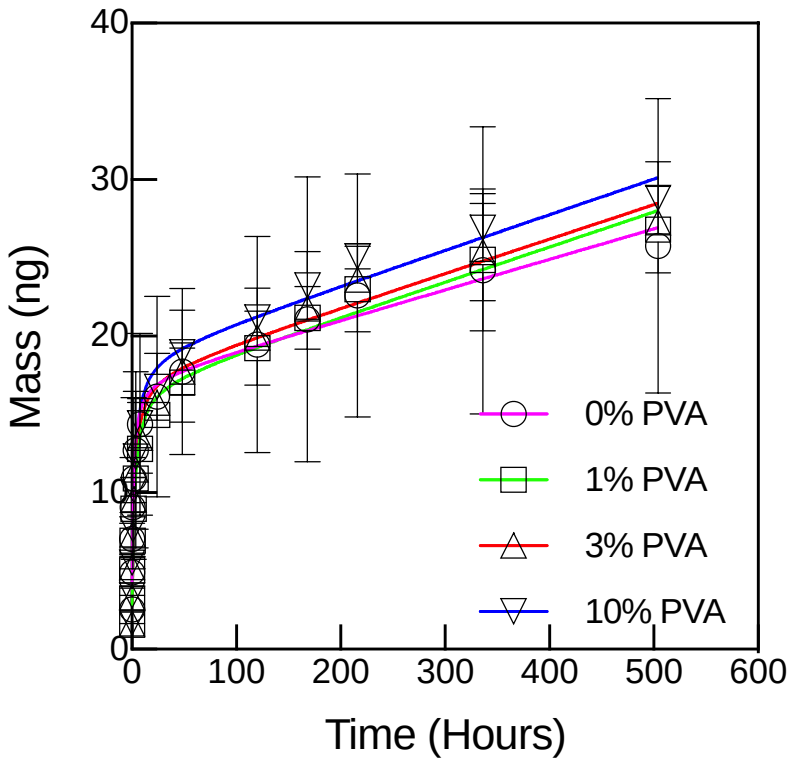

Figure IV-19. Cumulative drug delivery of doxorubicin from various SMP formulations over 504 hours (21 days). *Data courtesy of Shreedevi Arun Kumar*

Conclusions

Thermomechanical Characterization

The thermomechanical behavior of the foams was affected by the addition of the PVA/Dox mixture. The Dox increased the T_g as seen in the 0% PD samples. E-beam sterilization did depress the T_g for all compositions. There is a possibility that the foams were not fully dry prior to packaging or residual moisture was left in

packages, as it has been previously established that moisture affects E-beam sterilization. In future runs, desiccant packs in the foil pouch and more thorough drying should be employed.

Drug Delivery Feasibility

We showed that drug loading could be improved with increased PVA concentration. Delayed burst and sustained release of the drug were also achieved based on the PVA concentration used. We also established that the released chemotherapy can successfully induce inhibition of tumor cell growth in *in vitro* studies and that the apoptotic activity of Dox can last over 7 days. Currently, we are investigating the potential of this drug-loaded foam to prevent tumor recurrence in a breast cancer mouse model after tumor resection.

Electron Beam Sterilization

The E-beam sterilization of the drug-coated foam devices did alter the thermomechanical behavior of the materials. The T_gs of 0, 1, 3, and 10% PD compositions were depressed after E-beam. A 37 kGy irradiation dose was used, which is on the higher end of sterility assurance levels (25 kGy is accepted level). It was determined that it is likely Dox that is affected by the E-beam since there was no change seen in the bare foams and the 0% PD composition (which contains no PVA). Follow-up studies using an apoptotic assay will confirm whether this affected the action of Dox. There is a previous study that asserted that E-beam irradiation can actually increase the

pro-apoptotic activity of Dox, but the highest irradiation level tested was 25 kGy in these studies.[58] Caspase activity assays will be repeated on E-beam sterilized foams to confirm whether this was seen with our devices as well.

CHAPTER V

APPLICATION-DRIVEN MODIFICATIONS OF THERMOSET POLYURETHANE SHAPE MEMORY POLYMERS FOR MEDICAL DEVICES

Disclaimer

These sections highlight work that was done during my Ph.D. where I performed early-stage proof of concept work for projects intending to expand the potential utility of the SMP foam platform. Both of these projects resulted in co-authored publications and important modifications to the SMPs for different applications. Unless otherwise indicated none of the data or figures is from those publications and was simply preliminary work.

*Antimicrobial SMP work was published in *ChemPhysChem* in 2019.[59]

**Degradation-resistant work was published in *Polymers* in 2020.[60]

Introduction

Both of the modifications described in this chapter were developed with a specific application in mind. The first modification was the incorporation of a phenolic acid compound which is naturally antimicrobial. Natural antimicrobials also address the rising issue of antibiotic resistant bacteria. These modified SMP materials are proposed for use in hemostats or other wound treatment dressings due to their shape-filling behavior and rapid induction of clotting. The second modification was the incorporation of glycerol to replace triethanolamine to minimize the number of oxidatively-susceptive tertiary amine linkages. The material application that these glycerol foams are the

peripheral occlusion that may be necessitated by venous insufficiency. The application-specific modifications discussed in this chapter expand the SMP foam platform's utility to be used in wound-healing applications and longer residence devices.

Antimicrobial Shape Memory Polymers

Shape memory polymers have been proposed for use as hemostatic materials to improve wound healing. The advantages of SMP foams developed in our lab is that they have a tunable, open-pore structure, and demonstrate rapid volume recovery at body temperature. Additionally, they have exhibited exceptional biocompatibility and stable blood clotting in embolic applications.

Previous work by Landsman et al explored the use of a hydrogel-coated SMP foam doped with povidone for use as a hemostatic device for wound treatment.[20] Jang et al similarly explored a composite approach utilizing nanosilica plates and gelatin which aid in clotting, but did not incorporate any antimicrobial component. The approach used in this work is through direct incorporation of antimicrobial agents (specifically cinnamic acid) into the SMP foam chemistry. This is better than a composite material because there is not a risk of separation at the material interface that could complicate wound healing or destabilize, furthermore cinnamic acid is a naturally-occurring antimicrobial found in honey. The use of phenolic acids has been widely researched and is a good alternative to broad-spectrum antibiotics that are prophylactically used in military combat wound care.

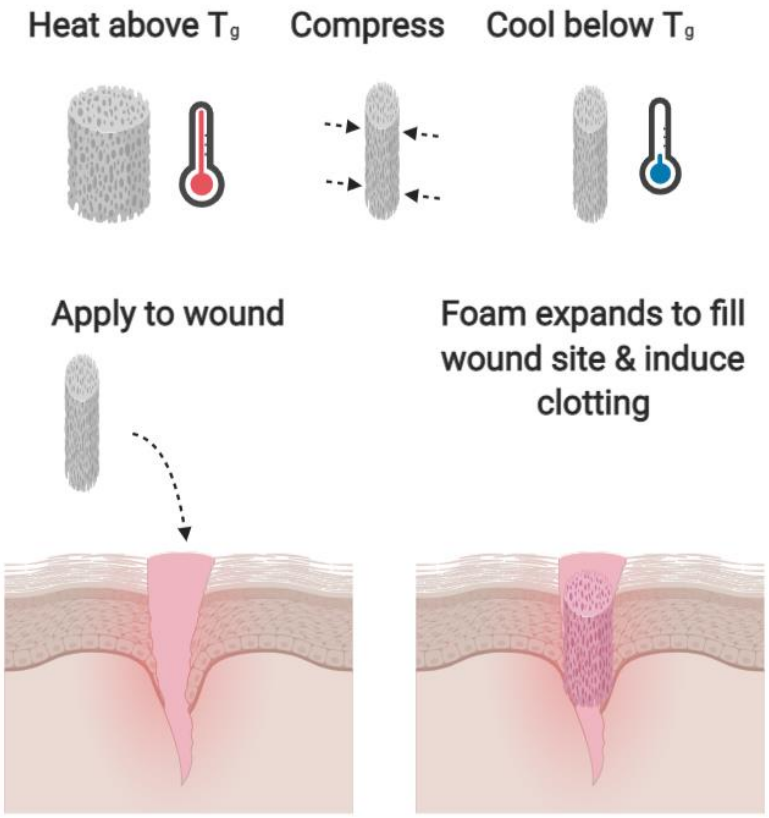

Figure V-1. Schematic showing rationale of SMP foams as a hemostatic device. A compressed foam SMP applied to a bleeding wound would passively expand at body temperature to fill the wound and induce rapid clotting. *(Created using BioRender.com*)

Important considerations for the design of this device are: 1) ensuring a similar pore morphology to control SMP foams can be synthesized, 2) thermomechanical behavior appropriate for deployed conditions, 3) antimicrobial efficacy, and 4) adequate volume expansion to fill irregular wound sites (Figure V-2).

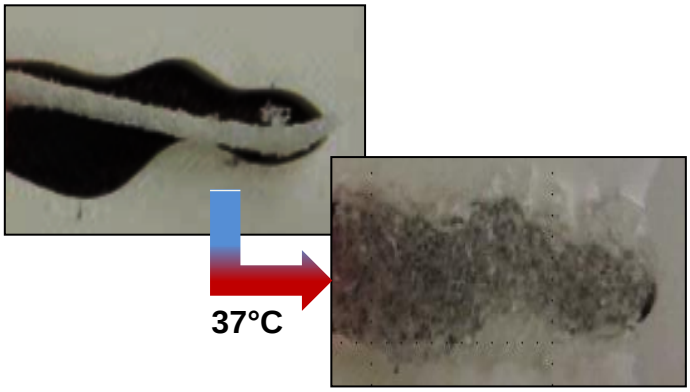

Figure V-2. Pictures showing that a compressed SMP foam could fill an irregular shape upon exposure to physiologic temperatures. This was performed with a compressed SMP foam in 37°C water.

Synthetic Strategy

Two approaches were pursued with the synthesis of antimicrobial shape memory polymer foams.[59] The first was direct incorporation of the antimicrobial agent cinnamic acid into the SMP premix and again prior to foaming. The second approach involved modification of one arm of HPED with the same antimicrobial monomer via Steglich esterification to yield an antimicrobial triol. The direct antimicrobial incorporation is referred to as AM whereas the modified antimicrobial is referred to as MAM throughout the section. Figure V-3 below outlines the two routes of incorporation.

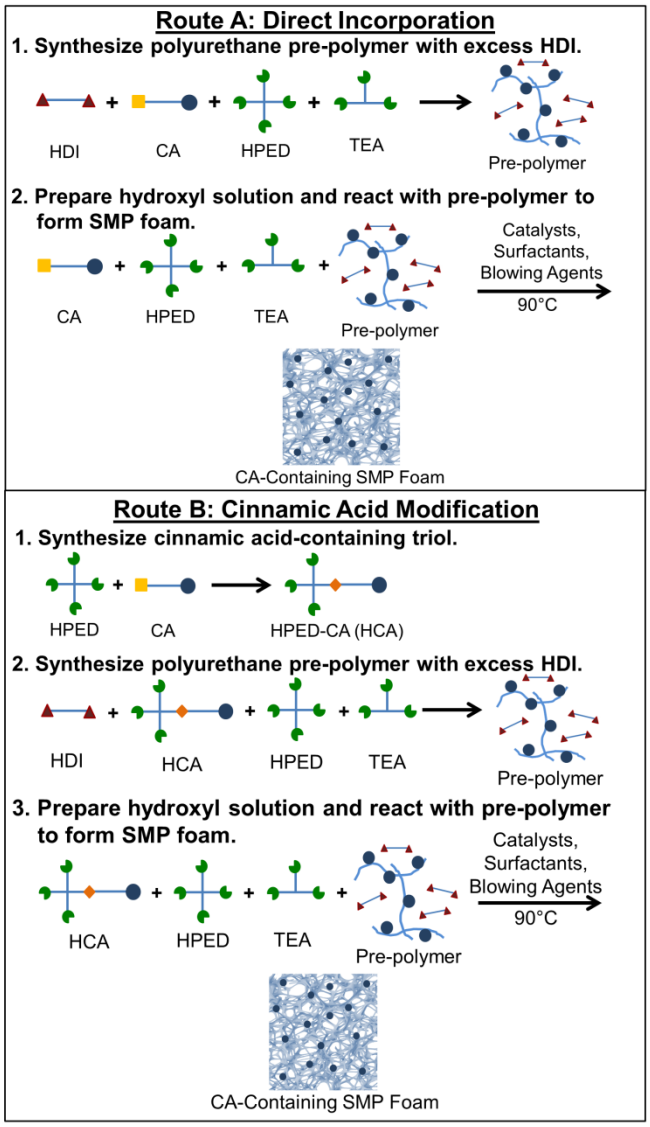

Figure V-3. Two routes for incorporation of antimicrobial agents into SMP foams. Route A or AM: Direct incorporation of the antimicrobial agent cinnamic acid (CA) into the SMP polyurethane pre-polymer as well as the hydroxyl side of the reaction prior to foaming. The reactive group of the CA was the carboxylic acid. Route B or MAM: In a Steglich esterification, the polyol HPED was modified with CA to form HCA. This yielded an antimicrobial triol, which was then incorporated into the SMP polyurethane pre-polymer and hydroxyl side of the reaction prior to foaming. In this case, both the 3 alcohol and the carboxylic acid groups are available for incorporation into polyurethane structure.
Figure from: M.B. Monroe, A.D. Easley, K. Grant, G.K. Fletcher, C. Boyer, D. Maitland Multifunctional Shape Memory Polymer Foams with Bio-inspired Antimicrobials. ChemPhysChem. 2018. 19, 1999. Copyright Wiley-VCH GmbH. Reproduced with permission.

Methods

Foam Synthesis

The SMP foaming procedure was a 3-step polyurethane reaction adapted from Singhal et al as previously described and modified as shown in Figure V-3 to explore both direct incorporation of antimicrobial agents and modified antimicrobial triols.[1] Step 1 was to make a prepolymer containing excess isocyanates, step 2 was to make a hydroxyl premix, and step 3 was to combine the NCO prepolymer with the OH premix. Pilot foams were made on an 8 gram scale (25% of typical synthesis) due to the scarcity of the custom MAM monomer in the pilot stage. The initial compositions made were 10% AM and MAM respectively (Table V-1). Foams were cured for 5 minutes at 50°C in an oven and removed and allowed to cool for 12 hours before any material preparation or characterization.

Table V-1 Antimicrobial SMP foam compositions with mol% of isocyanate and hydroxyl monomers.

SMP Foam Formulation	HDI	HPED	TEA	AM	MAM
Control	100	70	30	-	-
AM	100	70	20	10	-
MAM	100	70	20	-	10

Film Synthesis

Films were synthesized with the same monomer compositions, but with a 1:1 OH:NCO ratio and without the catalyst, surfactants, water, or Enovate that is added to foam synthesis. The polymer mixtures were poured into molds and put overnight in a vacuum chamber at 60 psi to eliminate bubbles before curing in an oven cycle. Films were cleaned and cut with a biopsy punch prior to using in experiments.

Pore Morphology

Foams were cut in the axial direction and colored with Sharpie to show the morphology of the foams and get preliminary pore size measurements. A Dinolite camera was used to take foam images and ImageJ was used to measure 30 pores in the longest direction on each image.

Thermomechanical Characterization

Differential scanning calorimetry (DSC) was used to analyze the glass transition temperatures in dry and wet conditions. Foam samples ranging from 5-9 mg were cut from various locations on the foam and hermetically sealed in a Tzero aluminum pan. Dry T_g cycle was ramped from -40°C to 120°C. Thermograms were analyzed using the TA Instruments software and T_g was determined using the T_g selector tool.

Passive Expansion Profiles

Foams were crimped radially using a stent crimper and allowed to sit for at least 24 hours prior to expansion study to allow for relaxation. To prepare the expansion study, water bath was heated to 37°C and camera was set up overlooking the location of the rig holding the crimped foams in the bath. Foams were submerged in the water bath and observed over 30 minutes of expansion. Final percent expansions at 30 minutes were reported.

Antimicrobial Activity of SMP Foams

Escherichia coli (*E. coli*) was chosen as a gram negative bacteria model for the studies. The E. coli was grown in a lysogeny broth (LB) at 37°C. The bacteria was plated onto LB-agar plates to grow in the presence of films of the same composition. Pictures were taken of each section of the plate and the colony forming unit (CFU) was calculated using the formula:

$$\text{CFU}=\frac{\#\ of\ colonies}{area\ of\ plate\ section}$$

Preliminary Results

Pore Morphology

SMP foams were optimized to have similar pore size and pore morphology as predicate device foams (Figure V-4, Table V-2). Observations of the foam images appear that the addition of both AM and MAM make the pores less elongated.

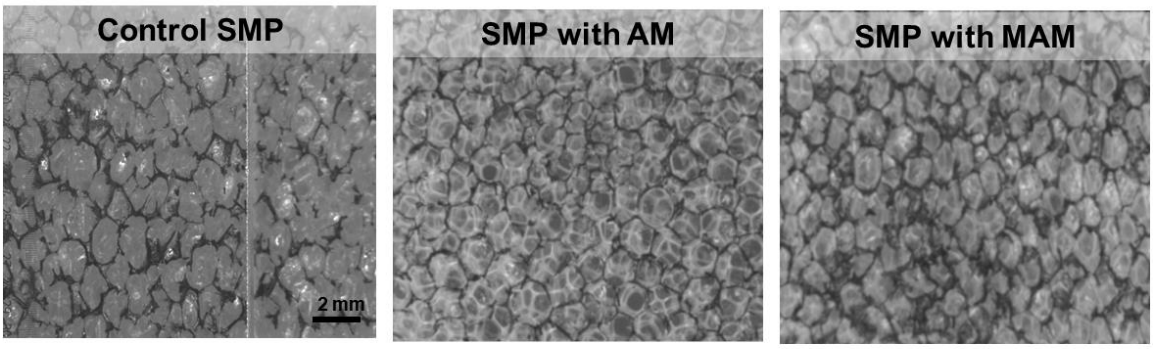

Figure V-4. Light microscope images of foams cut in the axial direction and colored with Sharpie to visualize the porous structure in the cross-section.

Table V-2. Pore size and density of preliminary antimicrobial SMP foam formulations. Both are reported with standard deviations for measurements (Pore Size n=10, Density n=3).

SMP Foam Formulation	Pore Size (μm)	Density (g/cm^3)
Control	960 ± 160	0.027 ± 0.002
AM	1100 ± 150	0.023 ± 0.001
MAM	1050 ± 150	0.018 ± 0.001

Thermomechanical Characterization

Both of the pilot antimicrobial SMP foams had similar dry T_g's to the control, but the AM and MAM foams had lower Wet T_g's. This is likely due to the increase in urea content through both methods of incorporation cinnamic acid.

Table V-3 A Sample Table in Chapter 4. Glass transition temperatures in wet and dry conditions for the antimicrobial SMP foam compositions.

SMP Foam Formulation	Dry T_g (°C)	Wet T_g (°C)
Control	67 ± 1	35 ± 2
AM	69 ± 1	26 ± 3
MAM	67 ± 1	23 ± 1

The SMP foams were crimped over a wire at 70°C. Pictures were taken before being placed in the water for the initial and exposed to 37°C water bath. Their expansions after 30 minutes of exposure was measured. We desired 100% volume recovery and 25 cm^3 volume expansion for this study. Both AM and MAM SMP compositions had acceptable volume expansion, but the AM composition only expanded to approximately 92%.

Table V-4. The expansion properties of antimicrobial SMP foam compositions at 30 minutes relative to the target volume recovery and volume expansion.

SMP Foam Formulation	Volume Recovery (%)	Volume Expansion (cm^3)
TARGET	100	25
AM	92.1 ± 0.2	27.1 ± 0.9
MAM	103.5 ± 0.2	25.3 ± 1.6

Antimicrobial Activity of SMPs

Escherichia coli (*E. coli*) was chosen as a gram negative bacteria model for the studies. The E. coli was grown in a lysogeny broth (LB) at 37°C. The bacteria was plated onto LB-agar plates to grow in the presence of films of the same composition. Pictures were taken of each section of the plate and the colony forming unit (CFU) was calculated using the formula:

$$\text{CFU}=\frac{\#\ of\ colonies}{area\ of\ plate\ section}$$

Figure V-5. AM and MAM films were placed in the agar plate with lysogeny broth and colonies were allowed to grow in the presence of the films. (*Made using BioRender.com*)

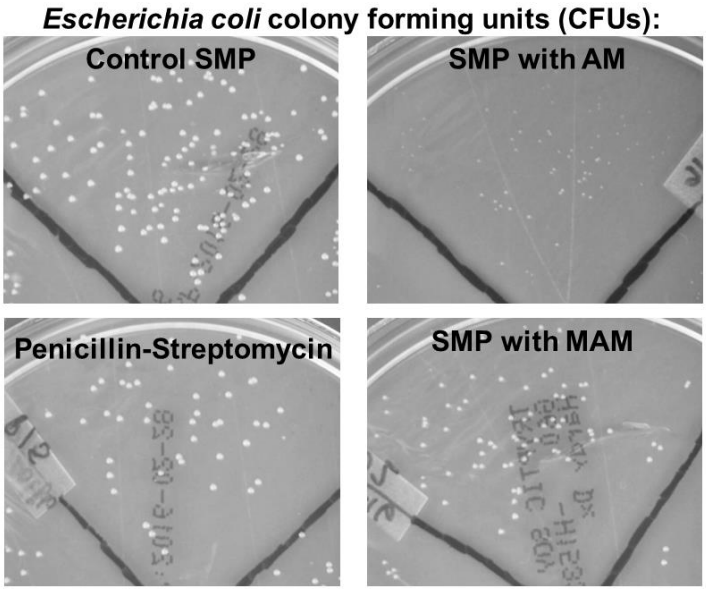

Figure V-6. Images of plate with *Eschericheria coli* colony forming units (CFUs). Each white dot is a colony. The density of the colonies and the area they cover are both indicators of microbial activity.

The AM and MAM SMP foams reduced CFU density and area as shown in Table V-5. They were compared to a penicillin-streptomycin (pen-strep) control as well as a control SMP foam. The AM and MAM SMP foams performed better than the control SMP. Relative to the pen-strep plate, the CFU densities were higher, but the AM and MAM foams decreased the CFU area.

Table V-5. Antimicrobial efficacy of SMP film compositions. CFU density and area both were calculated from pictures of the dish.

SMP Foam Formulation	CFU Density ($CFUs/cm^2$)	CFU Area (mm^2/CFU)
Penicillin-Streptomycin	3.9 ± 2.6	0.44 ± 0.14
Control SMP	10.5 ± 5.7	0.55 ± 0.17
AM	5.2 ± 1.1	0.31 ± 0.04
MAM	5.7 ± 0.8	0.20 ± 0.06

Discussion

The antimicrobial shape memory polymers show promise as wound-care device. The high dry T_g allows for use in hot climates, whereas the wet T_g below body temperature (37°C) allows for passive expansion upon exposure to a wound. The antimicrobial properties of the SMP foams were effective when exposed to *E. coli* and their efficacy was comparable to Pen strep. In future studies, a gram positive bacteria should be tested and perhaps a fungal species as well to more broadly test the efficacy of these foams.

Both the direct incorporation of the antimicrobial agent cinnamic acid and the modified version are viable approaches that need to be studied more. The content of the antimicrobial agents in the SMP foams could also be increased for future studies. It will be important to verify the exudate uptake properties of the bare foam, which is one potential drawback compared to the composite material.

Shape Memory Polymers with Improved Oxidative Stability

While the aliphatic PU thermoset foams show hydrolytic stability, they are still susceptible to oxidative degradation, which has been observed to result in mass loss *in vivo* after implantation. This mass loss can cause device failure and increases testing required for FDA approval. Previous work in our lab has focused on determining the degradation pathway and the resultant degradation products of our SMP polyurethane foams. The authors concluded that the tertiary amine on triethanolamine (TEA) was a site of chain scission due to oxidative degradation.

To address oxidative degradation concerns, glycerol, a triol without tertiary amine functionality was incorporated into our lab's SMP foam compositions. We were unable to synthesize foams where glycerol was 100% of the hydroxyl component due to miscibility issues encountered and therefore this approach does not eliminate all tertiary amines. Thus, foams will still be susceptible to oxidation, but are expect to slow in degradation due to the reduction in potential cleavage sites. The materials were characterized and *in vitro* degradation studies were used to determine if the changes made to foam chemistry were successful.

Methods

Foam Synthesis

Thermoset SMP foams were synthesized using a three-step gas foaming procedure adapted from Singhal et al.[1] Briefly, an isocyanate (NCO) pre-polymer was made by combining hydroxyl components outlined in Figure V-7 (N,N,N',N'-tetrakis(2-

hydroxypropyl)ethylenediamine (HPED), TEA, glycerol (G), or 3-methyl-1,5-pentanediol (PD)) and the aliphatic diisocyanate hexamethylene diisocyanate (HDI). In this approach, pentanediol was used as another hydroxyl monomer to improve glycerol's miscibility in the pre-polymer by acting as a chain extender. The pre-polymer mixtures contained an excess of isocyanates with varying ratios of HPED to TEA or glycerol and pentanediol.

Once the NCO pre-polymer mixture was cured in a 36-hour oven cycle, surfactants were added and it was mixed using a FlackTek speedmixer at 3540 rpm for 30 seconds. While the NCO mixture was cooling, the hydroxyl (OH) mixture was made using HPED, TEA, glycerol, PD, DI water, and catalysts. Once the NCO mixture was no longer warm to the touch (approximately 30 minutes), the OH mixture was added to it and mixed at 3540 rpm for 5 seconds. Enovate (2 mL) was added to the cup as a physical blowing agent and it was mixed for another 5 seconds before being poured into a container. The foams were allowed to cure for 2-5 minutes at 50°C and subsequently cooled for 24 hours in the fume hood before conditioning and cleaning was performed. The SMP foam compositions are summarized in Table V-6. The composition naming convention is such that the hydroxyl monomer components of H40T60 are comprised of 40 mol% HPED and 60 mol% TEA.

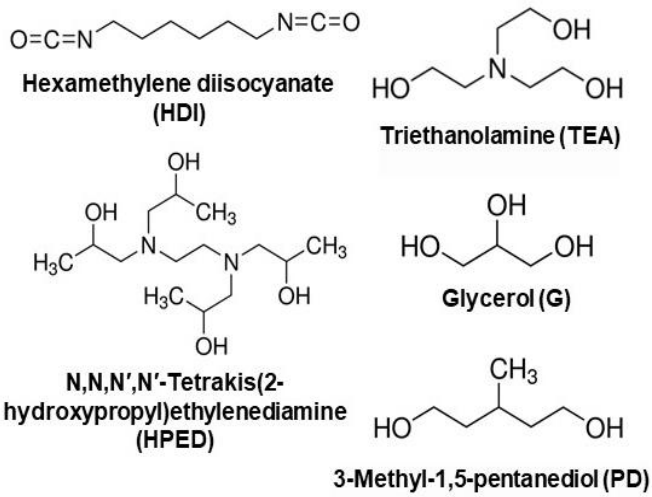

Figure V-7. Structures of monomers used in SMP foam synthesis. Hexamethylene diisocyanate (HDI) is the isocyanate monomer used for this work. Hydroxypropyl ethylenediamine (HPED) is a polyol with 4 hydroxyl groups. Both HDI and HPED were used in all compositions. Glycerol (G) is a triol that does not have the tertiary amine structure that is found in the triol triethanolamine (TEA) and replaced that monomer in the new generation of foams. 3-Methyl-1,5-pentanediol (PD) was used to improve the miscibility in compositions with higher amounts of glycerol.

Table V-6. Compositions of PU SMP foams used in this study. All compositions were made with 100% HDI for the NCO component. Hydroxyl monomers were varied according to the percentages listed.

Composition	**Hydroxyl Monomers (mol%)**			
	%HPED	***%TEA***	***%G***	***%PD***
H40T60	40	60	0	0
H60T40	60	40	0	0
H80T20	80	20	0	0
H40G30PD30	40	0	30	30
H60G40	60	0	40	0
H80G20	80	0	20	0

SMP Characterization

Foam morphology was assessed using scanning electron microscopy (SEM), pore size measurements, density, thermomechanical properties in wet and dry conditions, and passive expansion profiles in a 37°C water bath. The preservation of PU SMP chemistry was confirmed by attenuated total reflectance Fourier transform infrared (ATR-FTIR) spectroscopy where I verified the presence of carbonyl and amine peaks from urethane. Additionally, successful polymerization was verified by determining the gel fraction of foams to quantify the extent of crosslinking.

In Vitro Degradation Studies

The success criterion for this project is reduced *in vitro* degradation. To assess this goal, SMP foam blocks (~1 cm3) were weighed and placed in 20 mL vials containing accelerated oxidative (20% H2O2) or hydrolytic (0.1 M NaOH) degradative solutions in ovens at 37°C. Upon removal from solution, samples were washed in water, ethanol, and again in water to remove degradation media and placed in a 50°C oven under vacuum for 24 hrs. Dry weights were recorded and samples were placed back into fresh solutions. Accelerated oxidative samples were monitored for mass loss every 3 days and hydrolytic samples were measured every 7 days. In addition to measuring mass loss, the samples were also analyzed spectroscopically to determine any changes to the chemical structure as a result of degradation.

Preliminary Results

The changes to the PU chemistry affected the viscosity of the NCO pre-polymer, so tuning was required to achieve similar morphology. The preliminary physical and thermomechanical characterization results outlined in Table 2 demonstrate the ability to maintain an ultra-low-density pore morphology. The glycerol foams with the same amount of HPED were made with comparable pore sizes to the control foams with TEA, which have been optimized for device performance. The SMP foams containing glycerol had higher dry glass transition temperatures (T_g's) overall, but their wet T_g's were all below body temperature and fully expanded in less than 5 minutes in a 37°C water bath.

Table V-7. Physical properties of SMP foams. Measurements are reported as mean ± standard deviation for the indicated sample size.

Composition	Density (g/cm^3)	Gel Fraction (%)
	n=3	***n=5***
100HDI H40T60	0.0195 ± 0.0012	99.2 ± 1.2
100HDI H60T40	0.0194 ± 0.0001	98.7 ± 1.0
100HDI H80T20	0.0204 ± 0.0006	99.0 ± 0.6
100HDI H40G30PD30	0.0194 ± 0.0025	97.4 ± 1.9
100HDI H60G40	0.0157 ± 0.0019	93.1 ± 2.4
100HDI H80G20	0.0225 ± 0.0006	91.5 ± 3.5

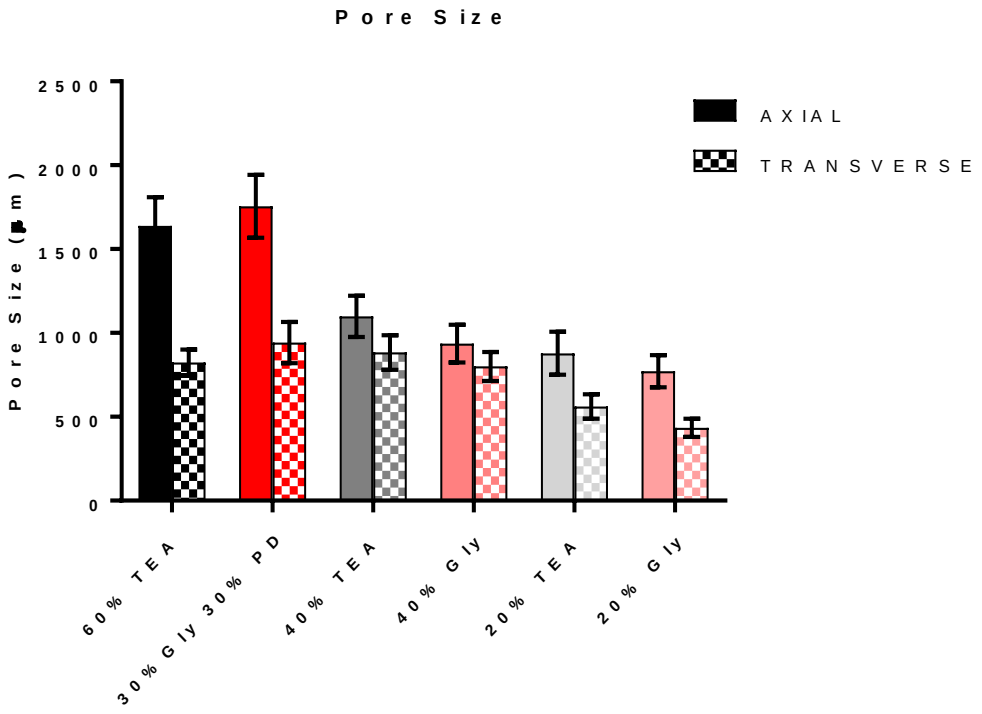

Figure V-8. Pore sizes of compositions in axial and transverse directions. The largest axial pore sizes were those with the least amount of HPED (highest amount of TEA or Gly/PD) Grey or black foams are Gen 1 foams with HPED and TEA. Red or pink are Gen 2 foams with Gly/PD.

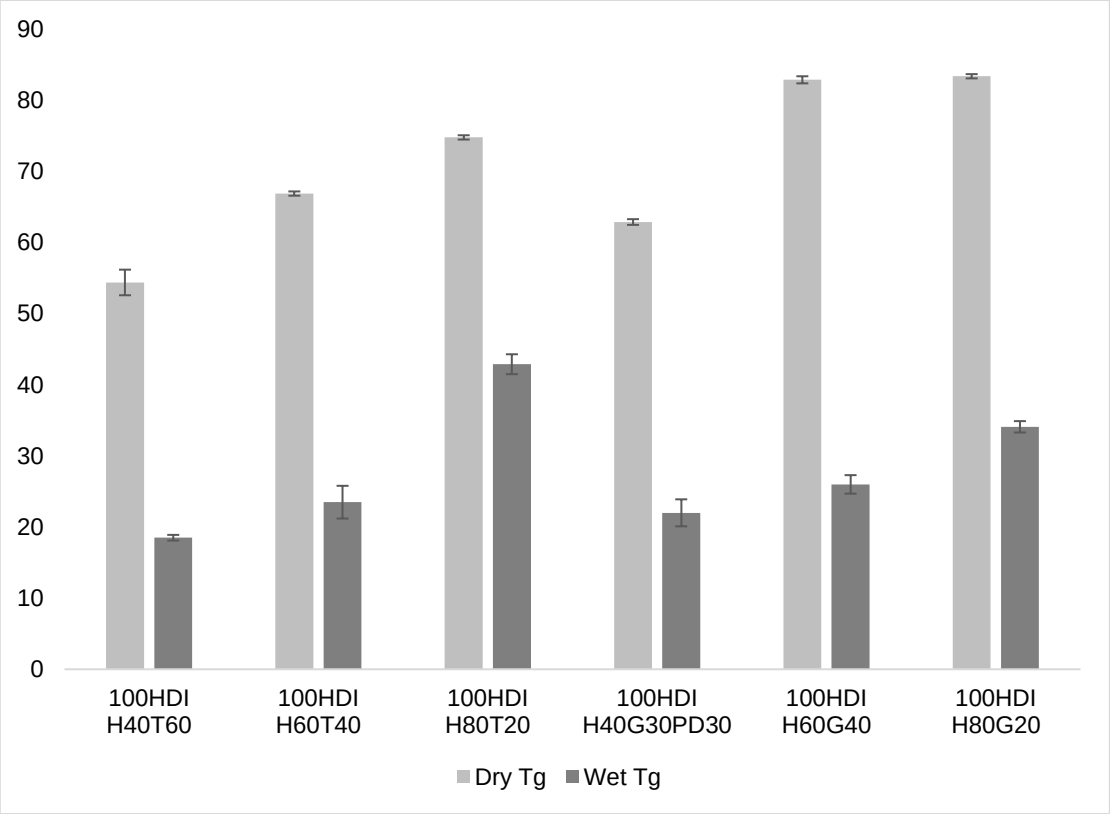

Figure V-9. Dry T_g and Wet T_g of the TEA and glycerol-based SMP foam compositions. In both compositions and both testing conditions, higher HPED content correlated with higher T_g's. Glycerol-based foams had higher dry T_g's than the TEA-based control foams. However, their wet T_g's were all below body temperature (37°C).

a.

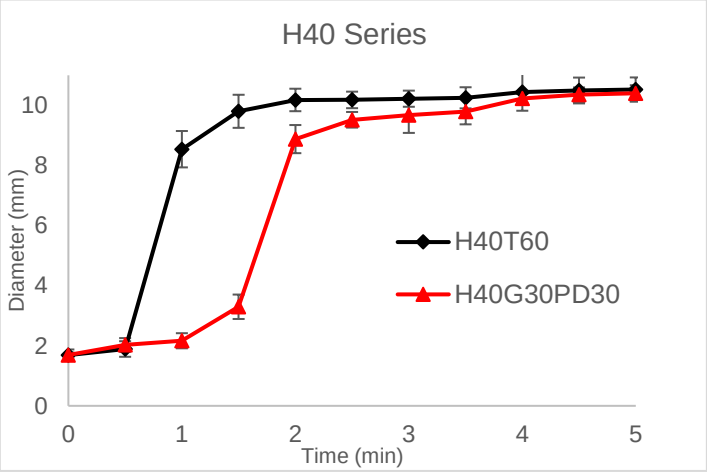
H40 Series
Diameter (mm)
Time (min)
H40T60
H40G30PD30
0
2
4
6
8
10
0
1
2
3
4
5

b.

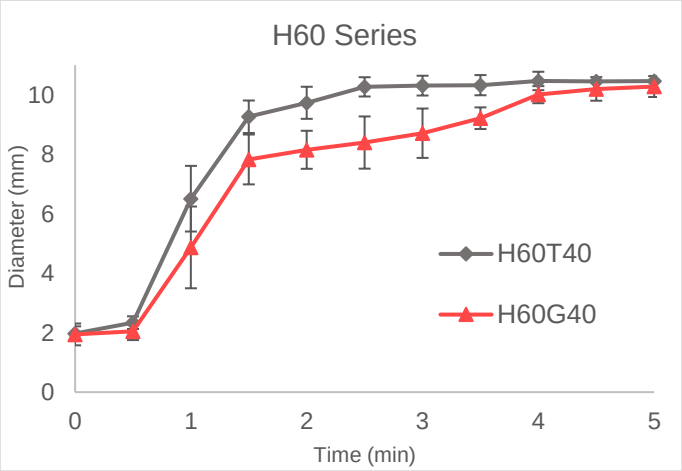
H60 Series
Diameter (mm)
Time (min)
H60T40
H60G40
0
2
4
6
8
10
0
1
2
3
4
5

c.

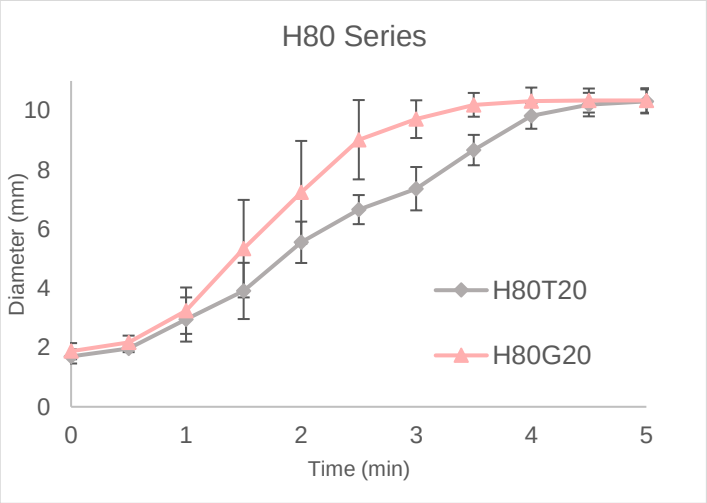

Figure V-10. Unconstrained expansion profiles in 37°C water bath of the following compositions: a. H40T60 and H40G30PD30 b. H60T40 and H60G40 c. H80T20 and H80G20

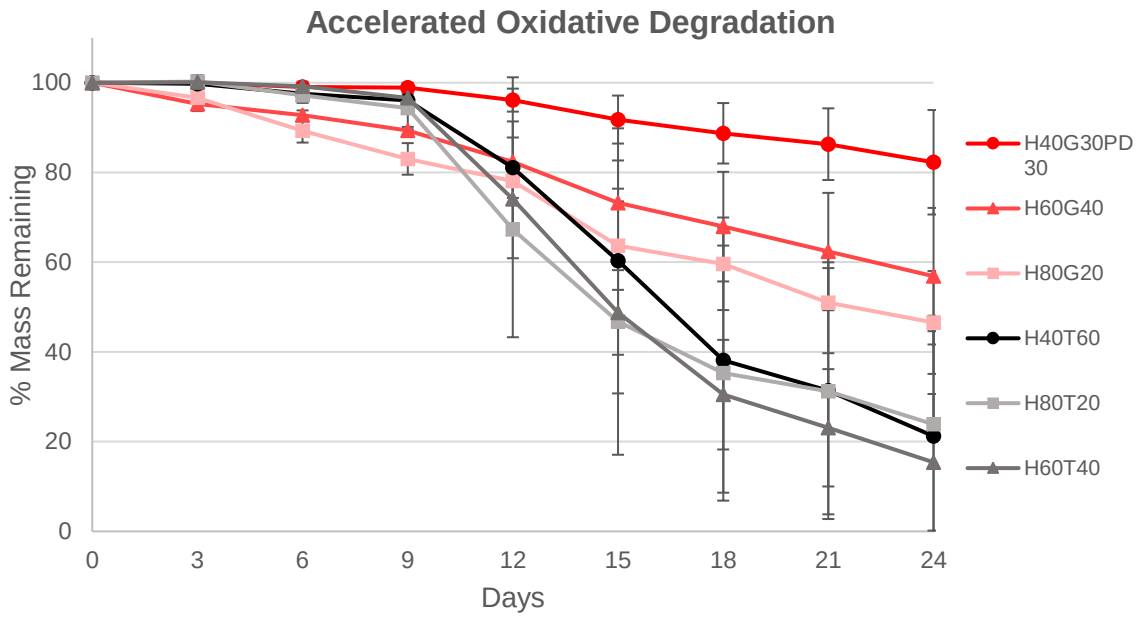

Figure V-11. Mass loss during first 24 days of accelerated oxidative in vitro degradation study. Mass was recorded every 3 days after washing and drying under vacuum at 50°C. The sample size for this study is 6 per composition and error bars are the standard deviation.

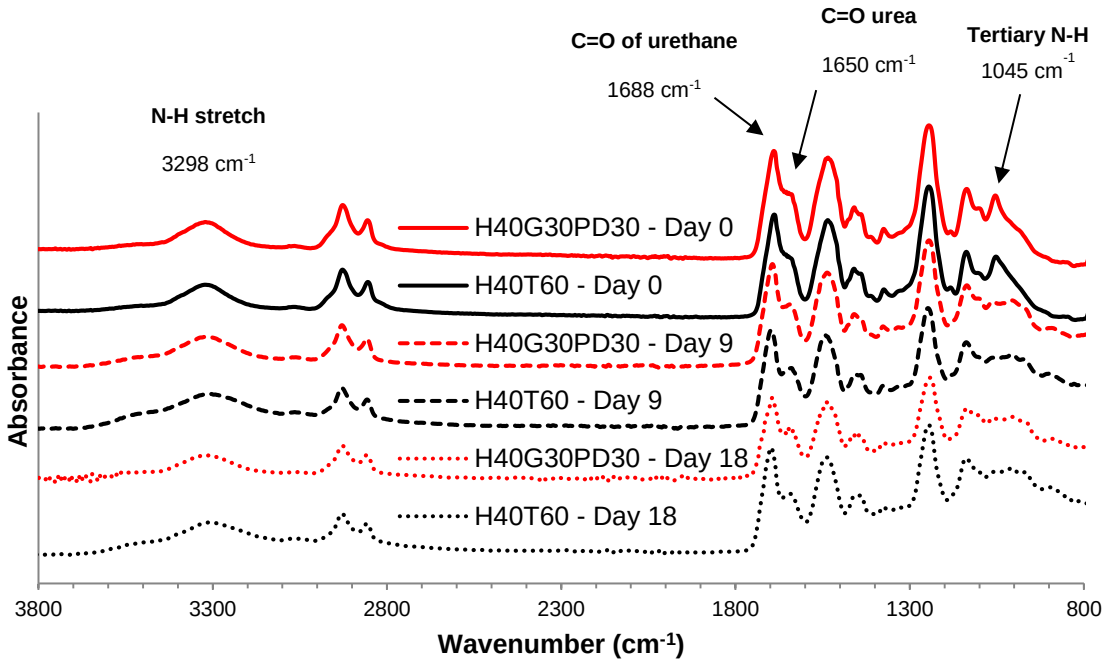

Figure V-12. ATR-FTIR spectra and SEM images at 0, 9, and 18 days in accelerated oxidative degradation solution (20% H_2O_2). Peaks of interest are labeled on Day 0 spectra.

Figure V-11 shows the chemical modification successfully extended the life of the proposed formulations relative to their compositional controls. Although mass loss was seen earlier (3-9 days) in the H60G40 and H80G20 formulations, this was likely due to the lower gel fractions of these materials due to issues with glycerol miscibility.

Changes to PU structure over 18 days of accelerated oxidative degradation were analyzed spectroscopically. Figure V-12 shows the progression for the H40 series. We observed a urethane C=O peak shift from 1688 cm-1 (Day 0) to 1698 cm-1 for H40T60 foams (Day 9 and 18) and 1693 cm-1 for H40G30PD30 foams (Day 9 and 18). Additionally, as degradation progressed, there was a loss of the Day 0 peak at 1048 cm^{-1} and reduction of the N-H stretch indicating the scission of the tertiary amine.

Discussion

The morphology of the foams was also able to be maintained after the incorporation of glycerol and hexanetriol. These materials were optimized for use in embolic devices and will require specific properties for other applications. The expansion profile of these foams was slowed relative to the controls due to increase in hydrophobicity. Finally, modification of the foam scaffolds with glycerol and hexanetriol was successful in reducing the oxidative degradation of the foams.

Future studies should be done on sterilized samples as well, since that could affect the degradation rate and this is not yet characterized for glycerol foams. Finally, the oxidatively biostable foams need to be tested *in vivo* to truly know the effect. All *in vitro* degradation tests are limited and the environment in different places in the body may produce different degradation rates due to factors like if it is in contact with blood flow, etc.

CHAPTER VI

CONCLUSIONS AND FUTURE DIRECTIONS

Conclusions

The conclusions for each project will be discussed individually for the materials and in the context of the larger goal of medical device translation.

Medical Imaging of Shape Memory Polymers[2]

Chapters II and III describe modifications made to both the thermoset and SMP systems to improve visibility on medical imaging modalities. The thermoset system was modified with ATIPA and GPA to be visible on both X-ray and MR imaging modalities. The goal of this work was to develop a thermoset shape memory polymer (SMP) foam with visibility under both X-ray and magnetic resonance imaging (MRI) modalities. A porous polymeric material with these properties is desirable in medical device development for applications requiring thermoresponsive tissue scaffolds with clinical imaging capabilities. Dual modality visibility was achieved by chemically incorporating monomers with X-ray visible iodine-motifs and MRI visible monomers with gadolinium content. Physical and thermomechanical characterization showed the effect of increased gadopentetic acid (GPA) on shape memory behavior. Multiple compositions showed

[2] Partially Reprinted with permission from "Chemical Modifications of Porous Shape Memory Polymers for Enhanced X-ray and MRI Visibility" by Fletcher, G.K.; Nash, L.D.; Graul, L.M.; Jang, L.K.; Herting, S.M.; Wilcox, M.D.; Touchet, T.J.; Sweatt, A.K.; McDougall, M.P.; Wright, S.M.; Maitland, D.J., 2020. Molecules, 25(20), 4660, Copyright retained by author [2020]. Published by MDPI.

brightening effects in pilot, T1-weighted MR imaging. There was a correlation between the polymeric density and X-ray visibility on expanded and compressed SMP foams. Additionally, extractions and indirect cytocompatibility studies were performed to address toxicity concerns of gadolinium-based contrast agents (GBCAs). This material platform has the potential to be used in a variety of medical devices.

A similar approach was translated to the TPU system wherein TIP (a monomer containing triiodobenzene motifs) was used as the end capping agent. The resulting compositions showed varied X-ray visibility based on the amount of TIP incorporated. The molded samples are higher density than all previous approaches with foams and therefore more similar in X-ray density to the guidewires that are used as positive controls. The grayscale shifts exceeded the previously reported threshold of 6 in all compositions. Additionally, the mechanical behavior of these materials is viscoelastic which is desired in biomedical applications.

Drug Delivery Shape Memory Polymer Devices

The SMP foams were coated with drug solutions containing PVA and characterized for their feasibility as a drug delivery device. The pilot studies were used to determine which foam composition was most appropriate for the drug delivery device and determine the crimping temperature to ensure it did not affect the efficacy of the drug. The thermomechanical behavior before and after E-beam sterilization was characterized. Images confirming the coating of the SMP foams with the different amounts of Dox/PVA solution. The current application we are pursuing for the drug

delivery devices is breast cancer recurrence. The pilot studies were performed on the SKOV cell line (ovarian cell line), but were repeated with the breast cancer cell line MCF-7 to be more relevant for the intended application.

Application-Specific Modifications of Shape Memory Polymers

The SMP materials' chemistry is tunable and, in this section, we explored two modifications for specific applications. The first application was hemostat devices for hemorrhagic wounds that are susceptible to infection. The antimicrobial foam is intended to promote rapid clotting, apply pressure to the wound as it expands, and prevent infection. The antimicrobial agent cinnamic acid was incorporated using two approaches into the SMP foam. The first approach was direct incorporation and the second approach was by creating a monomer modified with cinnamic acid. The antimicrobial SMP foams' morphology, thermomechanical behavior, and antimicrobial efficacy were all tested. Both the antimicrobial SMP foam approaches showed promise for use as an antimicrobial hemostat. The second application was to improve the biostability of the SMP foams by reducing the amount of oxidatively susceptible linkages that are present. Glycerol was the triol used to replace triethanolamine and foams were characterized to determine whether foam morphology and thermomechanical behavior were similar to the original foams. Then, the degradation behavior of the foams was compared and we saw an increase in biostability for the glycerol compositions.

Future Directions

Imaging of Shape Memory Polymers

A potential application of the MRI and X-ray visible polymers is for use after cancer biopsies of the lung or liver. The intent of these devices would be to expand and seal the biopsy tract while also being used as a fiducial for physician follow-ups using MRI and X-ray.

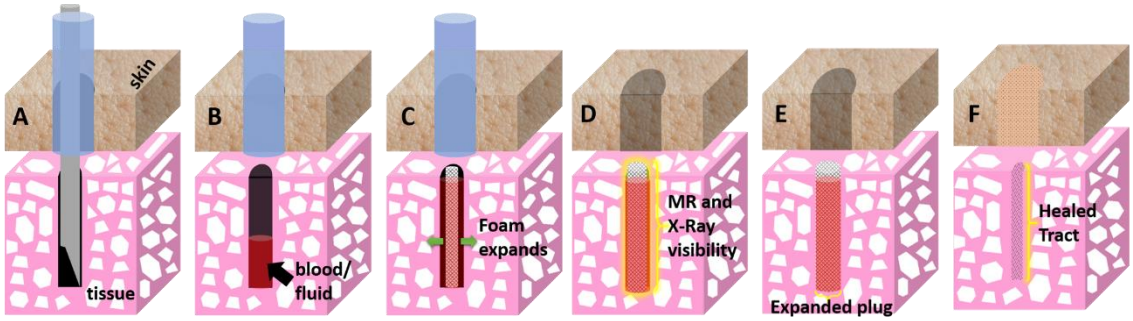

Figure VI-1. Schematic of proposed biopsy tract sealing system. The blood/fluid will drive the expansion of the biopsy sealing device. *Figure courtesy of Lance Graul*

The materials described in this section must be tested for sealing efficacy to be used as a biopsy sealing system in the lungs or liver. Therefore, a benchtop model that tests the device under physiologic air or blood blow is being developed. Optimal pore size must be chosen and it must be determined if a composite material like gelatin or another hydrogel will aid the sealing process. Radial force tests must also be performed to ensure that the devices do not exceed those of predicate devices. MRI imaging *in vivo* needs to be conducted for a range of clinically-relevant parameters in order to determine if the compositions contain adequate gadolinium content for the desired brightening effect.

Drug Delivery Shape Memory Polymer Devices

The current application we are pursuing for the drug-coated SMP devices is the recurrence of breast cancer after a primary resection surgery. A mouse animal model is being developed where MCF-7 breast cancer cells will be injected into the mammary pad of mice. Foams will be placed at tumor excision site and imaged to compare regrowth.

Figure VI-2. Animal model schematic. MCF-7 breast cancer cell line will be injected into the mouse mammary pad to grow a tumor. Tumor will be resected and drug loaded foam will be put into resected space. Resection will be stitched closed and monitored for tumor recurrence. *(Figure created using BioRender.com)*

Application-Specific Modifications of Shape Memory Polymers

The first application of antimicrobial foams has been piloted in traumatic wound models since the beginning of this project.[61] They performed well in these studies and are being explored for use in military applications, specifically gun shot wounds and traumatic liver injuries. Another future direction of these materials is exploring phenolic acids other than cinnamic acid such as benzoic acid, vanillic acid, and tannic acid. The

final embodiments and geometries of these devices for hemorrhagic wounds is something that must be developed and likely tailored to injury type.

Processing Options for TPU

The TPU system described in Chapter III could be processed in two ways moving forward. The first is that molded specimens could be E-beam crosslinked. This will require high levels (kGy) of irradiation by E-beam and may also require the addition of radiation sensitizers prior to molding. The second option is a polymerized high internal phase emulsion (polyHIPE) wherein porosity can be generated in TPU scaffolds. This could be useful for applications such as tissue engineering or small pore occlusion devices.

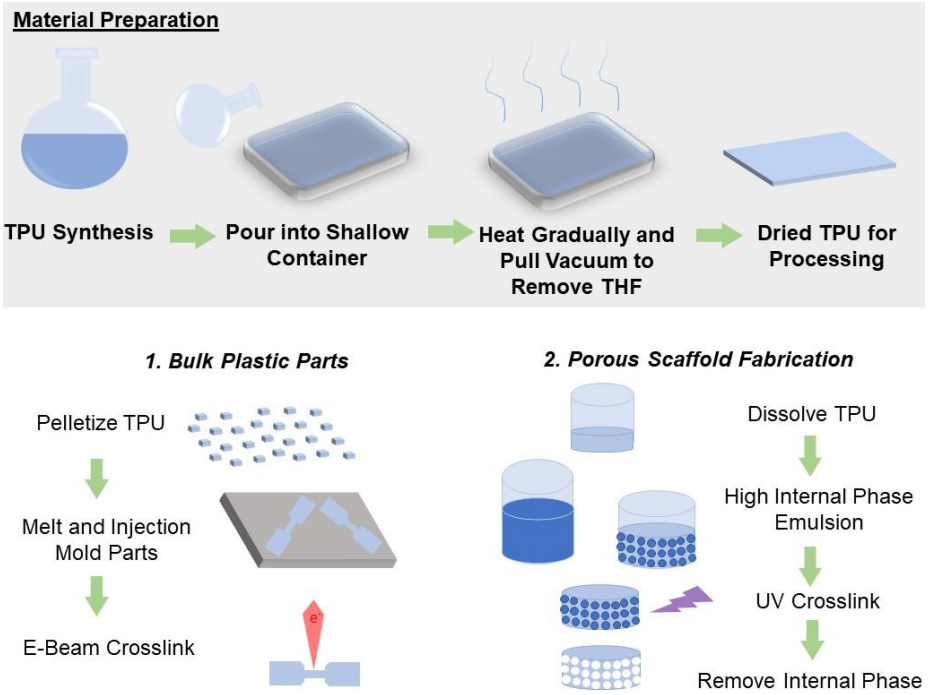

Figure VI-3. Figure showing material preparation and future directions for radiopaque TPU processing. Route 1 shows how bulk plastic parts could be injection molded and

crosslinked post-process via E-beam irradiation. Route 2 shows how a porous scaffold could be fabricated through emulsion templating. A high internal phase emulsion (HIPE) would be UV crosslinked and the internal phase would subsequently be removed.

Injection Molding and Electron Beam Crosslinking

Injection molding relies on a number of process conditions including melt temperature, injection pressure, and flow rate. Lower MW polymers will injection mold better due to their reduced viscosity and melt strength. Lower MW is also beneficial in reducing premature thermal crosslinking that can occur when processing must occur at high temperatures. The process optimization will be guided by characterization of the material including the melting and thermal degradation temperatures of the TPU resin. Once process conditions are optimized, injection molding is a very repeatable process enabling fabrication of parts with complex and precise geometries.

Electron beam crosslinking would enable a high throughput method of crosslinking injection molded parts, but may require sensitizers being added to the polymer mixture prior to molding which can limit process flexibility due to thermal instability. Hearon et al. investigated the effects of C=C sidechains through the incorporation of the commercially-available TMPAE as well as a custom monomer. (cite) This approach was compared to previous TPU formulations with C=C moieties in the backbone (cite) and they concluded that the sidechain approach was better for E-beam crosslinking without sensitizers due to the increased mobility.

Polymerized High Internal Phase Emulsions (polyHIPEs)

PolyHIPEs are typically fabricated in a two-phase emulsion with an aqueous internal phase and a hydrophobic external phase containing macromers. PolyHIPEs offer many advantages to the current gas-blown thermoset foams. The current lower limit for the thermoset foam pore size is 200 microns, but polyHIPEs enable pore sizes the range of 1-100 microns.[62] PolyHIPEs require lower MW chains with appropriate hydrophobicity and solvent interactions for stability, so material optimization will be critical for success.

In our preliminary polyHIPE system, the continuous phase contains the TPU, surfactant, and thiol crosslinker in the diluent chloroform. In order to achieve interconnected porous morphology, radical initiator will be added to the continuous phase.[63] The internal phase will be water or an immiscible solvent and will be removed after polymerization. The hydrophile-lipophile balance (HLB) is critical to emulsion stability. It is possible to combine surfactants and obtain an optimal HLB for the specific material.

Preliminary polyHIPEs were made with 75, 80, and 85% internal phase content (Figure VI-4). This scaffold fabrication technique successfully reduced the average pore size to ~10 μm and below desired for neuroembolic application (Table VI-1). This also extends the potential utility of the TPU material, which has previously only been used in solid part fabrication.

a. 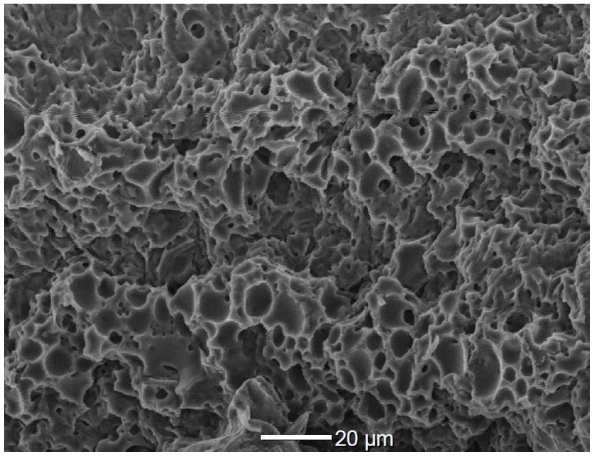

b. 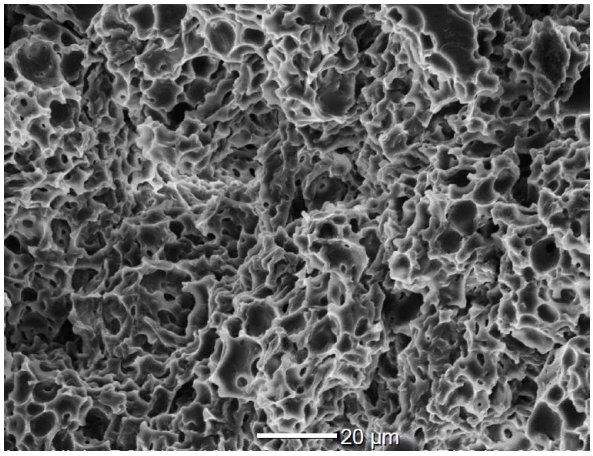

c. 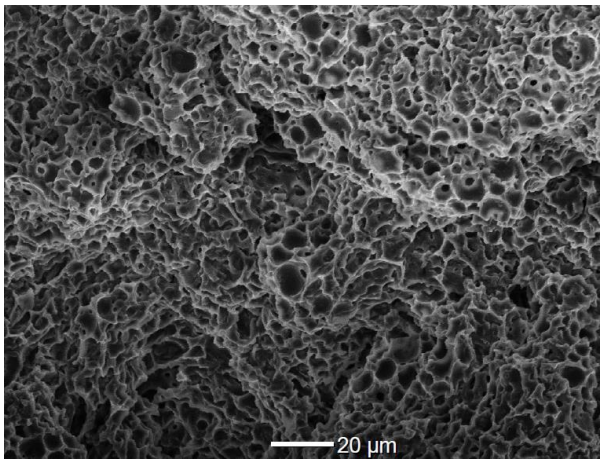

Figure VI-4. SEM images of pilot polyHIPEs with varied internal phase content. a. 75% internal phase, b. 80% internal phase, c. 85% internal phase.

Table VI-1. Pore sizes of preliminary polyHIPEs with varied internal phase content.

polyHIPE	Pore Size (μm)
75% Internal Phase	9.8 ± 2.9
80% Internal Phase	7.3 ± 1.5
85% Internal Phase	6.2 ± 1.2

Summary

The work described in this dissertation can expand the utility of the shape memory polymer systems for medical devices. First, increasing the X-ray and MRI visibility allows for polymer-only devices rather than incorporating metallic components for visibility. Devices that are delivered under fluoroscopy or in a minimally invasive procedure would benefit from enhanced radiopacity. Drug delivery from a shape memory polymer matrix could be explored for many applications, but feasibility was shown for an adjuvant drug delivery device for breast cancer tumor resections. Antimicrobial hemostats could be used in a variety of wound types and the geometry, pore size, thermomechanical behavior, and antimicrobial agent could be varied for different applications. Degradation behavior could be tuned for specific applications, but improving the biostability of the materials helps from a regulatory perspective. The future work section describes exciting applications of these polymers and avenues in which to build upon the work described in this dissertation.

REFERENCES

1. Singhal, P.; Rodriguez, J. N.; Small, W.; Eagleston, S.; Van de Water, J.; Maitland, D. J.; Wilson, T. S., Ultra low density and highly crosslinked biocompatible shape memory polyurethane foams. *Journal of Polymer Science Part B: Polymer Physics* **2012,** *50* (10), 724-737.

2. Rodriguez, J. N.; Yu, Y.-J.; Miller, M. W.; Wilson, T. S.; Hartman, J.; Clubb, F. J.; Gentry, B.; Maitland, D. J., Opacification of Shape Memory Polymer Foam Designed for Treatment of Intracranial Aneurysms. *Annals of Biomedical Engineering* **2012,** *40* (4), 883-897.

3. Singhal, P.; Boyle, A.; Brooks, M. L.; Infanger, S.; Letts, S.; Small, W.; Maitland, D. J.; Wilson, T. S., Controlling the Actuation Rate of Low-Density Shape-Memory Polymer Foams in Water. *Macromolecular Chemistry and Physics* **2013,** *214* (11), 1204-1214.

4. Singhal, P.; Small, W.; Cosgriff-Hernandez, E.; Maitland, D. J.; Wilson, T. S., Low density biodegradable shape memory polyurethane foams for embolic biomedical applications. *Acta biomaterialia* **2014,** *10* (1), 67-76.

5. Hasan, S. M.; Thompson, R. S.; Emery, H.; Nathan, A. L.; Weems, A. C.; Zhou, F.; Monroe, M. B. B.; Maitland, D. J., Modification of shape memory polymer foams using tungsten, aluminum oxide, and silicon dioxide nanoparticles. *RSC Advances* **2016,** *6* (2), 918-927.

6. Hasan, S. M.; Raymond, J. E.; Wilson, T. S.; Keller, B. K.; Maitland, D. J., Effects of Isophorone Diisocyanate on the Thermal and Mechanical Properties of Shape-

Memory Polyurethane Foams. *Macromolecular Chemistry and Physics* **2014,** *215* (24), 2420-2429.

7. Hasan, S.; Harmon, G.; Zhou, F.; Raymond, J.; Gustafson, T.; Wilson, T.; Maitland, D., Tungsten-loaded SMP foam nanocomposites with inherent radiopacity and tunable thermo-mechanical properties. *Polymers for Advanced Technologies* **2016,** *27* (2), 195-203.

8. Nash, D. L.; Browning Monroe, B. M.; Ding, Y.-H.; Ezell, P. K.; Boyle, J. A.; Kadirvel, R.; Kallmes, F. D.; Maitland, J. D., Increased X-ray Visualization of Shape Memory Polymer Foams by Chemical Incorporation of Iodine Motifs. *Polymers* **2017,** *9* (8).

9. Weems, A. C.; Raymond, J. E.; Easley, A. D.; Wierzbicki, M. A.; Gustafson, T.; Monroe, M. B. B.; Maitland, D. J., Shape memory polymers with visible and near-infrared imaging modalities: synthesis, characterization and in vitro analysis. *RSC Advances* **2017,** *7* (32), 19742-19753.

10. Monroe, M. B. B.; Easley, A. D.; Grant, K.; Fletcher, G. K.; Boyer, C.; Maitland, D. J., Multifunctional Shape-Memory Polymer Foams with Bio-inspired Antimicrobials. *ChemPhysChem* **2017**.

11. Landsman, T. L.; Weems, A. C.; Hasan, S. M.; Thompson, R. S.; Wilson, T. S.; Maitland, D. J., 20 - Embolic applications of shape memory polyurethane scaffolds. In *Advances in Polyurethane Biomaterials*, Woodhead Publishing: 2016; pp 561-597.

12. Boyle, A. J.; Landsman, T. L.; Wierzbicki, M. A.; Nash, L. D.; Hwang, W.; Miller, M. W.; Tuzun, E.; Hasan, S. M.; Maitland, D. J., In vitro and in vivo evaluation

of a shape memory polymer foam-over-wire embolization device delivered in saccular aneurysm models. *Journal of Biomedical Materials Research Part B: Applied Biomaterials* **2016,** *104* (7), 1407-1415.

13. Landsman, T. L.; Bush, R. L.; Glowczwski, A.; Horn, J.; Jessen, S. L.; Ungchusri, E.; Diguette, K.; Smith, H. R.; Hasan, S. M.; Nash, D.; Clubb, F. J.; Maitland, D. J., Design and verification of a shape memory polymer peripheral occlusion device. *Journal of the Mechanical Behavior of Biomedical Materials* **2016,** *63*, 195-206.

14. Hearon, K.; Wierzbicki, M. A.; Nash, L. D.; Landsman, T. L.; Laramy, C.; Lonnecker, A. T.; Gibbons, M. C.; Ur, S.; Cardinal, K. O.; Wilson, T. S.; Wooley, K. L.; Maitland, D. J., A Processable Shape Memory Polymer System for Biomedical Applications. *Advanced Healthcare Materials* **2015,** *4* (9), 1386-1398.

15. Hearon, K.; Nash, L. D.; Volk, B. L.; Ware, T.; Lewicki, J. P.; Voit, W. E.; Wilson, T. S.; Maitland, D. J., Electron Beam Crosslinked Polyurethane Shape Memory Polymers with Tunable Mechanical Properties. *Macromolecular chemistry and physics* **2013,** *214* (11), 1258-1272.

16. Hearon, K.; Besset, C. J.; Lonnecker, A. T.; Ware, T.; Voit, W. E.; Wilson, T. S.; Wooley, K. L.; Maitland, D. J., A Structural Approach to Establishing a Platform Chemistry for the Tunable, Bulk Electron Beam Cross-Linking of Shape Memory Polymer Systems. *Macromolecules* **2013,** *46* (22), 8905-8916.

17. Liang, C.; Rogers, C. A.; Malafeew, E., Investigation of Shape Memory Polymers and Their Hybrid Composites. *Journal of Intelligent Material Systems and Structures* **1997,** *8* (4), 380-386.

18. Nail, L. N.; Zhang, D.; Reinhard, J. L.; Grunlan, M. A., Fabrication of a Bioactive, PCL-based "Self-fitting" Shape Memory Polymer Scaffold. *JoVE* **2015,** (104), e52981.

19. Small, W.; Singhal, P.; Wilson, T. S.; Maitland, D. J., Biomedical applications of thermally activated shape memory polymers. *Journal of materials chemistry* **2010,** *20* (18), 3356-3366.

20. Landsman, T. L.; Touchet, T.; Hasan, S. M.; Smith, C.; Russell, B.; Rivera, J.; Maitland, D. J.; Cosgriff-Hernandez, E., A shape memory foam composite with enhanced fluid uptake and bactericidal properties as a hemostatic agent. *Acta Biomater* **2017,** *47*, 91-99.

21. Lendlein, A.; Behl, M.; Hiebl, B.; Wischke, C., Shape-memory polymers as a technology platform for biomedical applications. *Expert Review of Medical Devices* **2010,** *7* (3), 357-379.

22. Kolb, H. C.; Finn, M. G.; Sharpless, K. B., Click Chemistry: Diverse Chemical Function from a Few Good Reactions. *Angewandte Chemie International Edition* **2001,** *40* (11), 2004-2021.

23. Hoyle, C. E.; Bowman, C. N., Thiol–Ene Click Chemistry. *Angewandte Chemie International Edition* **2010,** *49* (9), 1540-1573.

24. Jivan, F.; Yegappan, R.; Pearce, H.; Carrow, J. K.; McShane, M.; Gaharwar, A. K.; Alge, D. L., Sequential Thiol–Ene and Tetrazine Click Reactions for the Polymerization and Functionalization of Hydrogel Microparticles. *Biomacromolecules* **2016,** *17* (11), 3516-3523.

25. Grim, J. C.; Marozas, I. A.; Anseth, K. S., Thiol-ene and photo-cleavage chemistry for controlled presentation of biomolecules in hydrogels. *Journal of Controlled Release* **2015,** *219*, 95-106.

26. Chen, G.; Amajjahe, S.; Stenzel, M. H., Synthesis of thiol-linked neoglycopolymers and thermo-responsive glycomicelles as potential drug carrier. *Chemical Communications* **2009,** (10), 1198-1200.

27. McCall, J. D.; Anseth, K. S., Thiol–Ene Photopolymerizations Provide a Facile Method To Encapsulate Proteins and Maintain Their Bioactivity. *Biomacromolecules* **2012,** *13* (8), 2410-2417.

28. Murray, K. A.; Kennedy, J. E.; McEvoy, B.; Vrain, O.; Ryan, D.; Cowman, R.; Higginbotham, C. L., The influence of electron beam irradiation conducted in air on the thermal, chemical, structural and surface properties of medical grade polyurethane. *European Polymer Journal* **2013,** *49* (7), 1782-1795.

29. Hong, S.; Carlson, J.; Lee, H.; Weissleder, R., Bioorthogonal radiopaque hydrogel for endoscopic delivery and universal tissue marking. *Advanced healthcare materials* **2016,** *5* (4), 421-426.

30. Dawlee, S.; Jayabalan, M., Intrinsically radiopaque polyurethanes with chain extender 4,4′-isopropylidenebis [2-(2,6-diiodophenoxy)ethanol] for biomedical applications. *Journal of Biomaterials Applications* **2014,** *29* (10), 1329-1342.

31. Wang, Q.; Qian, K.; Liu, S.; Yang, Y.; Liang, B.; Zheng, C.; Yang, X.; Xu, H.; Shen, A. Q., X-ray Visible and Uniform Alginate Microspheres Loaded with in Situ Synthesized BaSO4 Nanoparticles for in Vivo Transcatheter Arterial Embolization. *Biomacromolecules* **2015,** *16* (4), 1240-1246.

32. Nathan, A. L.; Fletcher, G. K.; Monroe, M. B. B.; Hwang, W.; Herting, S. M.; Hasan, S. M.; Keller, B. K.; Maitland, D. J., Particulate Release From Nanoparticle-Loaded Shape Memory Polymer Foams. *Journal of Medical Devices* **2017,** *11* (1), 0110091-0110099.

33. Weems, A. C.; Raymond, J. E.; Wacker, K. T.; Gustafson, T.; Keller, B.; Wooley, K. L.; Maitland, D. J., Examination of radio-opacity enhancing additives in shape memory polyurethane foams. *Journal of Applied Polymer Science* **2015,** *132* (23).

34. Lu, G.; Kalyon, D. M.; Yilgör, I.; Yilgör, E., Rheology and processing of BaSO4-filled medical-grade thermoplastic polyurethane. *Polymer Engineering & Science* **2004,** *44* (10), 1941-1948.

35. Romero-Ibarra, I. C.; Bonilla-Blancas, E.; Sánchez-Solís, A.; Manero, O., Influence of the morphology of barium sulfate nanofibers and nanospheres on the physical properties of polyurethane nanocomposites. *European Polymer Journal* **2012,** *48* (4), 670-676.

36. Weems, A. C.; Szafron, J. M.; Easley, A. D.; Herting, S.; Smolen, J.; Maitland, D. J., Shape memory polymers with enhanced visibility for magnetic resonance- and X-ray imaging modalities. *Acta biomaterialia* **2017,** *54*, 45-57.

37. FDA Drug Safety Communication: FDA warns that gadolinium-based contrast agents (GBCAs) are retained in the body; requires new class warnings. https://www.fda.gov/drugs/drug-safety-and-availability/fda-drug-safety-communication-fda-warns-gadolinium-based-contrast-agents-gbcas-are-retained-body.

38. Shapira-Furman, T.; Serra, R.; Gorelick, N.; Doglioli, M.; Tagliaferri, V.; Cecia, A.; Peters, M.; Kumar, A.; Rottenberg, Y.; Langer, R.; Brem, H.; Tyler, B.; Domb, A. J., Biodegradable wafers releasing Temozolomide and Carmustine for the treatment of brain cancer. *Journal of Controlled Release* **2019,** *295*, 93-101.

39. Weinberg, B. D.; Blanco, E.; Gao, J., Polymer Implants for Intratumoral Drug Delivery and Cancer Therapy. *Journal of Pharmaceutical Sciences* **2008,** *97* (5), 1681-1702.

40. Peppas, N. A.; Mongia, N. K., Ultrapure poly(vinyl alcohol) hydrogels with mucoadhesive drug delivery characteristics. *European Journal of Pharmaceutics and Biopharmaceutics* **1997,** *43* (1), 51-58.

41. Jang, L. K.; Fletcher, G. K.; Monroe, M. B. B.; Maitland, D. J., Biodegradable shape memory polymer foams with appropriate thermal properties for hemostatic applications. *Journal of Biomedical Materials Research Part A* **2020,** *108* (6), 1281-1294.

42. Weems, A. C.; Wacker, K. T.; Carrow, J. K.; Boyle, A. J.; Maitland, D. J., Shape memory polyurethanes with oxidation-induced degradation: In vivo and in vitro correlations for endovascular material applications. *Acta Biomaterialia* **2017,** *59*, 33-44.

43. Wilson, T. S.; Bearinger, J. P.; Herberg, J. L.; Marion III, J. E.; Wright, W. J.; Evans, C. L.; Maitland, D. J., Shape memory polymers based on uniform aliphatic urethane networks. *Journal of Applied Polymer Science* **2007,** *106* (1), 540-551.

44. Hasan, S. M.; Nash, L. D.; Maitland, D. J., Porous shape memory polymers: Design and applications. *Journal of Polymer Science Part B: Polymer Physics* **2016,** *54* (14), 1300-1318.

45. Lex, T. R.; Brummel, B. R.; Attia, M. F.; Giambalvo, L. N.; Lee, K. G.; Van Horn, B. A.; Whitehead, D. C.; Alexis, F., Iodinated Polyesters with Enhanced X-ray Contrast Properties for Biomedical Imaging. *Scientific Reports* **2020,** *10* (1), 1508.

46. Unal, O.; Li, J.; Cheng, W.; Yu, H.; Strother, C. M., MR-visible coatings for endovascular device visualization. *Journal of Magnetic Resonance Imaging* **2006,** *23* (5), 763-769.

47. Kurita, T.; Kagayaki, K.; Takeo, O., Gd-DTPA-based MR-visible Polymer for Direct Visualization of Interventional Devices. *Magnetic Resonance in Medical Sciences* **2011,** *10* (4), 263-267.

48. Younis, M.; Darcos, V.; Paniagua, C.; Ronjat, P.; Lemaire, L.; Nottelet, B.; Garric, X.; Bakkour, Y.; El Nakat, J. H.; Coudane, J., MRI-visible polymer based on poly(methyl methacrylate) for imaging applications. *RSC Advances* **2016,** *6* (7), 5754-5760.

49. Brocker, K. A.; Lippus, F.; Alt, C. D.; Hallscheidt, P.; Zsolt, F.; Soljanik, I.; Lenz, F.; Bock, M.; Sohn, C., Magnetic Resonance-Visible Polypropylene Mesh for Pelvic Organ Prolapse Repair. *Gynecologic and Obstetric Investigation* **2015,** *79* (2), 101-106.

50. Lauffer, R. B., Paramagnetic metal complexes as water proton relaxation agents for NMR imaging: theory and design. *Chemical Reviews* **1987,** *87* (5), 901-927.

51. Weinmann, H. J.; Brasch, R. C.; Press, W. R.; Wesbey, G. E., Characteristics of gadolinium-DTPA complex: a potential NMR contrast agent. *AJR. American journal of roentgenology* **1984,** *142* (3), 619-24.

52. Goodfriend, A. C.; Welch, T. R.; Nguyen, K. T.; Wang, J.; Johnson, R. F.; Nugent, A.; Forbess, J. M., Poly(gadodiamide fumaric acid): A Bioresorbable, Radiopaque, and MRI-Visible Polymer for Biomedical Applications. *ACS Biomaterials Science & Engineering* **2015,** *1* (8), 677-684.

53. Ionita, C. N.; Loughran, B.; Jain, A.; Swetadri Vasan, S. N.; Bednarek, D. R.; Levy, E.; Siddiqui, A. H.; Snyder, K. V.; Hopkins, L. N.; Rudin, S., New head equivalent phantom for task and image performance evaluation representative for neurovascular procedures occurring in the Circle of Willis. *Proceedings of SPIE--the International Society for Optical Engineering* **2012,** *8313*, 83130q.

54. Rogosnitzky, M.; Branch, S., Gadolinium-based contrast agent toxicity: a review of known and proposed mechanisms. *Biometals* **2016,** *29* (3), 365-376.

55. Jang, L. K.; Nash, L. D.; Fletcher, G. K.; Cheung, T.; Soewito, A.; Maitland, D. J., Enhanced X-ray Visibility of Shape Memory Polymer Foam Using Iodine Motifs and Tantalum Microparticles. *Journal of Composites Science* **2021,** *5* (1).

56. Muschalek, R.; Nash, L.; Jones, R.; Hasan, S. M.; Keller, B. K.; Monroe, M. B. B.; Maitland, D. J., Effects of Sterilization on Shape Memory Polyurethane Embolic Foam Devices. *Journal of medical devices* **2017,** *11* (3), 0310111-310119.

57. Boyle, A. J.; Weems, A. C.; Hasan, S. M.; Nash, L. D.; Monroe, M. B. B.; Maitland, D. J., Solvent stimulated actuation of polyurethane-based shape memory polymer foams using dimethyl sulfoxide and ethanol. *Smart materials & structures* **2016,** *25*.

58. Paszel-Jaworska, A.; Totoń, E.; Dettlaff, K.; Kaczmarek, A.; Bednarski, W.; Oszczapowicz, I.; Jelińska, A.; Rybczyńska, M., Increased proapoptotic activity of electron beam irradiated doxorubicin and epirubicin in multidrug-resistant human leukemic cells. *Chemico-Biological Interactions* **2016,** *258*, 69-78.

59. Monroe, M. B. B.; Easley, A. D.; Grant, K.; Fletcher, G. K.; Boyer, C.; Maitland, D. J., Multifunctional Shape-Memory Polymer Foams with Bio-inspired Antimicrobials. *ChemPhysChem* **2018,** *19* (16), 1999-2008.

60. Hasan, S. M.; Fletcher, G. K.; Monroe, M. B. B.; Wierzbicki, M. A.; Nash, L. D.; Maitland, D. J., Shape Memory Polymer Foams Synthesized Using Glycerol and Hexanetriol for Enhanced Degradation Resistance. *Polymers* **2020,** *12* (10), 2290.

61. Christmas, N.; Vakil, A. U.; Hatch, C. J.; Dong, S.; Fikhman, D.; Beaman, H. T.; Monroe, M. B. B., Characterization of shape memory polymer foam hemostats in in

vitro hemorrhagic wound models. *Journal of Biomedical Materials Research Part B: Applied Biomaterials* **2021,** *109* (5), 681-692.

62. Moglia, R. S.; Holm, J. L.; Sears, N. A.; Wilson, C. J.; Harrison, D. M.; Cosgriff-Hernandez, E., Injectable PolyHIPEs as High Porosity Bone Grafts. *Biomacromolecules* **2011,** *12* (10), 3621-3628.

63. Robinson, J. L.; McEnery, M. A. P.; Pearce, H.; Whitely, M. E.; Munoz-Pinto, D. J.; Hahn, M. S.; Li, H.; Sears, N. A.; Cosgriff-Hernandez, E., Osteoinductive PolyHIPE Foams as Injectable Bone Grafts. *Tissue Engineering. Part A* **2016,** *22* (5-6), 403-414.

APPENDIX A

ADDITION OF CELL OPENER

For the ATIPA/GPA thermoset foams described in Chapter II, cell opener was required to address the shrinkage seen in the post-cure stage of the materials developed by Nash et al. This information and rationale was not included in the publication (other than the final wt% of cell opener added), but it was the starting point for re-optimization of the ATIPA foaming protocol prior to expanding the system's use through GPA for MR imaging and tantalum for enhanced radiopacity.

The initial ATIPA foam was closed-pore and had issues with collapsing as shown in the picture below. Additionally, the lower figure shows SEM images of how the collapsed pore morphology improved after the addition of cell opener.

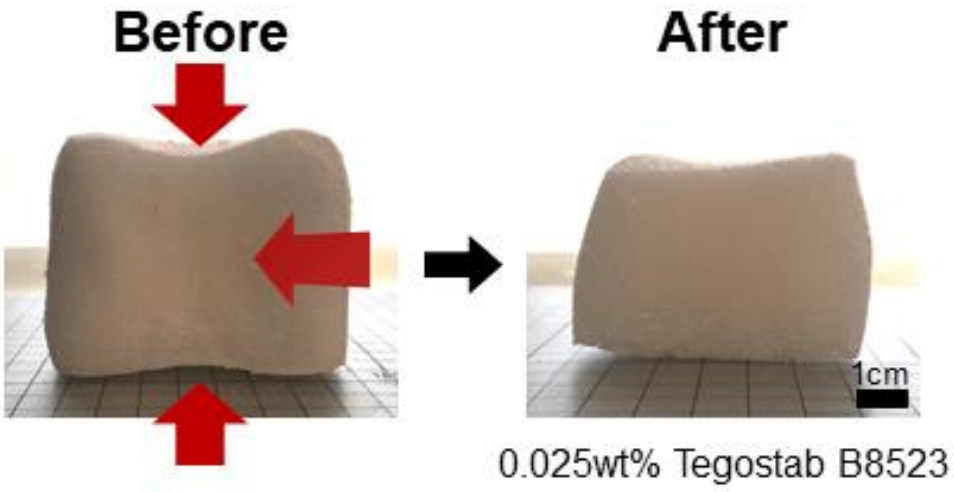

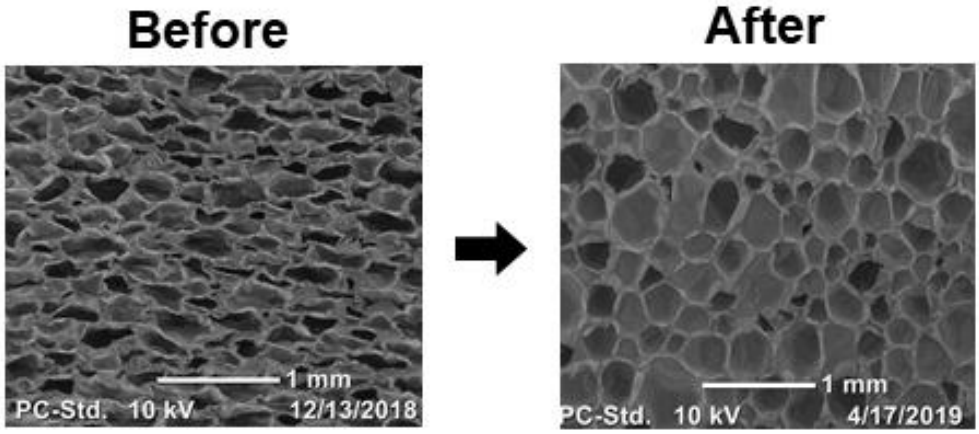
Before
After
1 mm
PC-Std. 10 kV 12/13/2018
1 mm
PC-Std. 10 kV 4/17/2019

APPENDIX B

PILOT X-RAY VISIBLE THERMOPLASTIC COMPOSITIONS

Pilot compositions were imaged before any other characterization to ensure that the primary criterion of radiopacity was achieved. Originally, 1, 2.5, and 5% TIP compositions were synthesized for pilot injection molding and imaging. The 5% TIP composition was not pursued further since it had lower radiopacity relative to the 2.5% TIP composition in the rod mold. This is likely due to the lower molecular weight making it more difficult to mold. Additionally, the TPU in these runs was molded at 150°C, which was lower than what was used in the following studies.

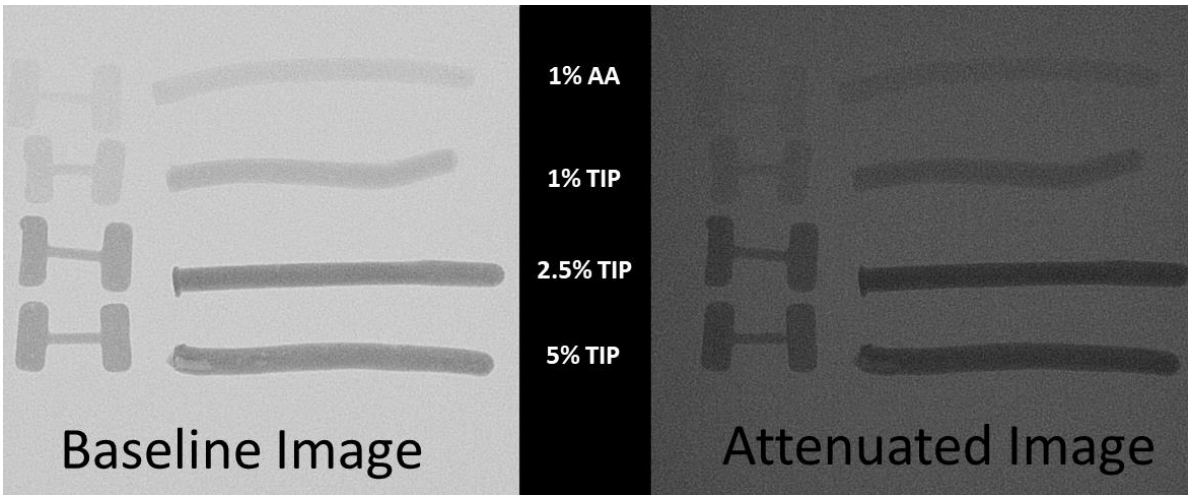

APPENDIX C

INJECTION MOLD COMPOSITION SHRINKING

This is a picture of the 2.5% TIP 20% TMPAE 1-6 HD composition (bottom) compared to the control HDPE (top) that was taken approximately 30 days after injection molding. The shrinkage in the length is about 33% and it looks to be similar shrinkage in height. The molded TPU likely has residual stresses. It is likely that the temperature for molding was not optimized for this polymer.